Imperial College London

Dissertation submitted in partial fulfilment
of the

Quantum Fields and Fundamental Forces MSc

Primordial Black Holes

Author
Simone Gordon

Supervisor
Prof. Carlo Contaldi

September 25, 2020

This dissertation reviews the current literature on primordial black holes (PBHs) regarding their possible formation from overdensities in the early Universe and how they may contribute to the evolution of the Universe. Key concepts from cosmology are introduced to supplement the derivation of the power spectrum of initial fluctuations from inflation. A brief historical account of the development of the theoretical underpinnings of PBHs in the latter half of the 20^{th} century is provided. Various forms of the PBH mass function are discussed and their merits are compared in the context of physical viability and usefulness in modelling. Particular emphasis is placed on the critical collapse formation mechanism in the standard slow roll inflationary scenario, but the modified models of hybrid and running-mass inflation are also conducive to PBH formation in principle. These models are used in section three to demonstrate how certain assumptions about the mass function can impact the form of the power spectrum in the case of critical collapse. The ability of PBHs to help explain two outstanding problems in cosmology- the nature of dark matter and aspects of structure formation- is covered in the final sections. An overview of observational constraints on the monochromatic PBH mass function is provided in the case of dark matter and constraints on the extended mass function are discussed in relation to two mass ranges currently favoured to provide a large fraction of dark matter. The potential role of PBHs in structure formation and as the seeds of supermassive black holes at the centre of galaxies is briefly outlined.

Contents

1 Introduction

1.1 Cosmology

The Copernican principle forms the lynchpin of modern cosmology. It asserts that our position on earth is in no way 'special', and from it one can make two important assumptions about the geometry of the Universe; *homogeneity* and *isotropy*. Homogeneity implies that the Universe looks the same at all points in space and time, whilst isotropy requires uniformity in all directions from a given vantage point in spacetime. Naturally, the usefulness of this assumption is scale-dependent. It describes the appearance of the Universe in the regime of intergalactic space (or more precisely, on the order of the Hubble volume, a sphere with a radius of roughly 13 Giga-light-years at present) as opposed to small scales, for example, within our solar system [1].

The most general metric with homogeneous and isotropic spatial sections is the Friedmann-Lemaître- Robertson-Walker (FLRW) metric, first developed in the early 20^{th} century by the Russian, Belgian and American physicists who make up its name [2]. The metric allows one to choose the curvature of the space in question; flat (Euclidean space), positive curvature (closed, spherical) or negative curvature (open, saddle-shaped). It is often written in polar coordinates as

$$\mathrm{d}s^2 = \frac{1}{1-\kappa r^2}\,\mathrm{d}r^2 + r^2\,\mathrm{d}\theta^2 + r^2\sin\theta^2\,\mathrm{d}\phi^2, \tag{1.1}$$

where κ equals 0, $+1$ or -1 for flat, open and closed Universes respectively. Based on observational results from the Wilkinson Microwave Anisotropy Probe (WMAP) amongst other instruments, one can assume the Universe to be flat to within a margin of error of 0.4% [3]. Therefore, we can specialise to the flat space, smooth FLRW metric which takes the form of the Minkowski metric with a quantity called the scale factor multiplying the spatial components,

$$\mathrm{d}s^2 = -\,\mathrm{d}t^2 + a(t)^2\delta_{ij}\,\mathrm{d}x^i\,\mathrm{d}x^j. \tag{1.2}$$

The scale factor $a(t)$ incorporates the observed expansion of the Universe. This metric is often referred to as the comoving gauge, since the scale factor relates the physical separation of two points $\vec{r}$ to the comoving distance between them $\vec{x}$ by $\vec{r} = a(t)\vec{x}$. The homogeneity property ensures that the scale factor is a function of time only and informs us of how physical separations evolve in time, since the

comoving coordinates are fixed by definition. For example, if the scale factor doubles between times t_1 and t_2, this means the Universe has doubled in size and it will take a particle twice as long to travel between two points. The metric evolves according to the Einstein equations

$$G^{\mu}_{\nu} = 8\pi G T^{\mu}_{\nu}, \tag{1.3}$$

where $T_{\mu\nu}$ is the energy-momentum tensor given by $T_{\mu\nu} = \mathrm{diag}(-\rho, P, P, P)$ for a comoving observer in flat space (as per metric (1.2)) where ρ is the energy density and P is the pressure. The LHS of (1.3) can be expanded as

$$G^{\mu}_{\nu} = g^{\mu\nu}\left(R_{\mu\nu} - \frac{1}{2}g_{\mu\nu}R\right) \tag{1.4}$$

where $R_{\mu\nu}$ the Ricci tensor and R is the Ricci scalar. These equations describe the curvature of spacetime ($R_{\mu\nu}$ and R) due to the effect of a distribution of mass-energy (T^{μ}_{ν}). These quantities can be expanded in terms of the Christoffel symbol

$$\Gamma^{\rho}_{\mu\nu} = \frac{1}{2}\, g^{\mu\alpha}\left(\partial_{\mu} g_{\alpha\nu} + \partial_{\nu} g_{\mu\alpha} - \partial_{\alpha} g_{\mu\nu}\right). \tag{1.5}$$

The Ricci tensor is given as

$$R_{\mu\nu} = \partial_{\rho}\Gamma^{\rho}_{\mu\nu} - \partial_{\nu}\Gamma^{\rho}_{\mu\rho} + \Gamma^{\sigma}_{\mu\nu}\Gamma^{\rho}_{\rho\sigma} - \Gamma^{\sigma}_{\mu\rho}\Gamma^{\rho}_{\nu\sigma}, \tag{1.6}$$

and the Ricci scalar is the trace of this, $R = g^{\mu\nu}R_{\mu\nu}$. The non-zero Christoffel symbols for this metric (1.2) are

$$\begin{aligned} \Gamma^{0}_{ij} &= \delta_{ij} H a^2, \\ \Gamma^{i}_{0j} &= \delta_{ij} H, \end{aligned} \tag{1.7}$$

where $H = (\mathrm{d}a/\,\mathrm{d}t)/a$ is the Hubble parameter. One can calculate the first and second components of the covariant Einstein tensor $G_{\mu\nu}$ by inserting these expressions into (1.4) to find

$$\begin{aligned} G_{00} &= 3\left(\frac{\mathrm{d}a}{\mathrm{d}t}\frac{1}{a}\right)^2, \\ G_{11} &= 2a\frac{\mathrm{d}^2 a}{\mathrm{d}a^2} + \left(\frac{\mathrm{d}a}{\mathrm{d}t}\right)^2. \end{aligned} \tag{1.8}$$

However, the Universe we observe today is not smooth in the way described by equation 1.2. Structure formation points to a clear deviation from homogeneity on smaller scales. The perturbations to the gravitational field caused by overdensities in matter can be accounted for in the so-called conformal Newtonian gauge,

$$ds^2 = g_{\mu\nu}dx^\mu dx^\nu = -\left(1+2\Psi(\vec{x},t)\right)dt^2 + a^2\delta_{ij}\left(1+2\Phi(\vec{x},t)\right)dx^i dx^j, \tag{1.9}$$

which describes scalar perturbations to the flat FLRW metric. The scalar fields Ψ and Φ are treated as small quantities, for which linear order terms are kept only. Ψ corresponds to the perturbations of the metric, whist Φ gives the perturbations to the spatial curvature. It is useful to note that $g^{00} = -1 + 2\Psi(\vec{x},t)$ which arises from imposing the relation $g^{\mu\sigma}g_{\sigma\nu} = \delta^\mu_\nu$ to first order. We use the metric signature typical in cosmology $(-,+,+,+)$. This metric also evolves according to the Einstein equations 1.3 and 1.4. The non-zero Christoffel symbols at first order are

$$\begin{aligned}
\delta\Gamma^0_{00} &= \partial_0\Psi(\vec{x},t),\\
\delta\Gamma^0_{0i} &= \Gamma^0_{i0} = \partial_i\Psi(\vec{x},t) = ik_i\tilde{\Psi},\\
\delta\Gamma^0_{ij} &= \Gamma^0_{ji} = \delta_{ij}a^2\left(H + 2H(\Phi-\Psi) + \partial_0\Phi\right),\\
\delta\Gamma^i_{00} &= \frac{ik^i}{a^2}\Psi,\\
\delta\Gamma^i_{0j} &= \Gamma^i_{j0} = \delta_{ij}(H + \partial\Phi),\\
\delta\Gamma^i_{jm} &= i\Phi\left(\delta_{ij}k_m + \delta_{im}k_j - \delta_{jm}k_i\right),
\end{aligned} \tag{1.10}$$

where, for the second symbol, we have used the convention prevalent in cosmology $\tilde{\Psi} = \Psi$, i.e. the tilde distinguishing the Fourier-transformed field is dropped. Note that the delta symbols in front of the first order Christoffel symbols may not always be included in the literature, but it should be obvious from the appearance of the perturbation fields which order of Christoffel symbols are being used. Inserting these terms into (1.6), we obtain the two perturbed Ricci tensor components

$$\delta R_{00} = -\frac{3}{a}\frac{\partial^2 a}{\partial t^2} - \frac{k^2}{a^2}\Psi - 3\partial^0\partial_0\Psi + 3H\left(\partial_0\Psi - 2\partial_0\Psi\right), \tag{1.11}$$

and

$$\begin{aligned}\delta R_{ij} = \delta_{ij}\left[\left(2a^2H^2 + a\frac{d^2a}{dt^2}\right)(1+2\Phi-2\Psi) + a^2H(6\partial_0\Phi - \partial_0\Psi)\right] \\ +\delta_{ij}\left[a^2\partial^0\partial_0 + a^2\partial^0\partial_0\Phi + k^2\Phi\right] + k_ik_j(\Phi+\Psi),\end{aligned} \tag{1.12}$$

which will henceforth be referred to as the time-time and space-space Ricci tensor components respectively. The perturbed Ricci scalar is

$$\delta R = -12\left(H^2 + \frac{1}{a}\frac{d^2a}{dt^2}\right) + \frac{2k^2}{a^2} + 6\partial^0\partial_0\Phi - 6H\left(\partial_0 - 4\partial_0\Phi\right) + \frac{4k^2\Phi}{a^2}. \tag{1.13}$$

The first order time-time component of the Einstein tensor is

$$\delta G^0_0 = -6H\left(\partial_0\Phi\right) + 6H^2\Psi - 2\frac{k^2}{a^2}\Phi, \tag{1.14}$$

However, the space-space component is more complicated and it is not necessary to write out the explicit expression for our purposes. It has the form

$$G^i_j = \delta^{ik}\frac{(1-2\Phi)}{a^2}R_{kj} - \frac{1}{2}\delta^{ij}R. \tag{1.15}$$

Friedmann not only contributed to finding the FLRW metric, but also used the fundamental principles of cosmology and general relativity to write down an equation which links together key cosmological parameters. While Friedmann used the full power of general relativity in 1922 to do so, it is possible to derive his equation in a Newtonian framework and then state what must be altered to generalise it.

Firstly, consider a homogeneous sphere of matter with total mass M. The sphere is expanding and contracting isotropically so that its radius $R(t)$ is varying with time. The gravitational force F experienced by a test mass m at the centre of the sphere will be

$$F = -\frac{GMm}{R(t)^2}. \tag{1.16}$$

The gravitational acceleration at the surface of the sphere will be

$$\frac{\mathrm{d}^2R}{\mathrm{d}t^2} = -\frac{GM}{R(t)^2}. \tag{1.17}$$

Multiply each side of the equation by $\mathrm{d}R/\,\mathrm{d}t$ and integrate to find

$$\frac{1}{2}\left(\frac{\mathrm{d}R}{\mathrm{d}t}\right)^2 = \frac{GM}{R(t)} + U, \tag{1.18}$$

where U is a constant of integration. Since the mass of the sphere is constant as it expands or contracts, we may write

$$M = \frac{4\pi}{3}\rho(t)R(t)^3. \tag{1.19}$$

Since the expansion is isotropic about the sphere's centre, we may write the radius *R(t)* in the form

$$R(t) = a(t)r, \tag{1.20}$$

where $a(t)$ is the scale factor and r is the comoving radius of the sphere. In terms of $\rho(t)$ and $a(t)$, the energy conservation equation 1.18 can be rewritten in the form

$$\frac{1}{2}r^2\dot{a}^2 = \frac{4\pi}{3}Gr^2\rho(t)a(t)^2 + U \tag{1.21}$$

where $\dot{a}$ denotes the $\mathrm{d}a/\,\mathrm{d}t$. Dividing each side of this equation by $r^2a^2/2$ yields the equation

$$\left(\frac{\dot{a}}{a}\right)^2 = \frac{8\pi G}{3}\rho(t) + \frac{2U}{r^2}\frac{1}{a(t)^2}, \tag{1.22}$$

which is the Friedmann equation in its Newtonian form. Taking the case of an expanding sphere ($\dot{a} > 0$), we can deduce from the above equation that it has three possible fates: $U > 0$, in which the expansion never ceases; $U < 0$, for which expansion ceases at the point $a_{\max} = -GM/Ur$ and since $\ddot{a}$ becomes negative, the sphere will contract; and finally, $U = 0$ is the boundary case in which $\dot{a} \to 0$ as $t \to \infty$and $\rho \to 0$. However, one must be careful when mapping this information to the real Universe. Firstly, a spherical volume of finite radius is not homogeneous and isotropic. The centre of the sphere is a 'special location' and at any point there exists a special direction (towards the centre of the sphere). Instead, one can take the perspective that the sphere of radius R is carved out of an infinite, homogeneous and isotropic Universe. Newtonian dynamics informs us that the gravitational acceleration inside a hollow spherically-symmetric shell is equal to zero. We divide up the region outside the sphere into concentric shells and conclude that the test mass m at R experiences

no net acceleration from matter outside the sphere. However, this argument assumes that the space is Euclidean. One must incorporate the possibility of spatial curvature in order to have an accurate Friedmann equation for the Universe. This is done by replacing the mass density $\rho(t)$ by the total energy density $\epsilon(t)/c^2$, which includes rest mass energy and other forms of energy (e.g., energy of photons, or thermal energy of atoms). Additionally, the potential energy term is intimately tied to the curvature of space. One makes the substitution

$$\frac{2U}{r^2} = -\frac{\kappa c^2}{R^2}, \tag{1.23}$$

where κ is the curvature. The case $U < 0$ corresponds to positive curvature $\kappa = +1$, $U > 0$ corresponds to negative curvature $\kappa = -1$ and $U = 0$ corresponds to a flat Euclidean spacetime $\kappa = 0$. A full derivation of the Friedmann equation involves inserting the FLRW metric of equation 1.1 into the Einstein field equations 1.3. However, the substitutions made above make pedagogical sense if one considers mass-energy equivalence for the first and the Einsteinian worldview that energy density manifests itself as curvature in spacetime for the second.

The Friedmann equation is often written in terms of the *Hubble parameter* $H(t) \equiv \dot{a}/a$, an observable property. Using the relation between $H(t)$, recession speed ν and proper distance d,

$$\nu(t) = H(t)d(t), \tag{1.24}$$

the Friedmann equation can be rewritten in the form

$$H(t)^2 = \frac{8\pi G}{3c^2}\epsilon(t) - \frac{\kappa c^2}{R_0^2\, a(t)^2}. \tag{1.25}$$

For a spatially flat Universe, the Friedmann equation is simplified to

$$H(t)^2 = \frac{8\pi G}{3c^2}\epsilon(t). \tag{1.26}$$

Thus, for a given value of the Hubble parameter, there is a *critical density*,

$$\epsilon_c(t) \approx \frac{3c^2}{8\pi G}H(t)^2. \tag{1.27}$$

If the energy density $\epsilon(t)$ is greater than this value, the Universe is positively curved ($\kappa = +1$) and if it is less than this value, the Universe is negatively curved ($\kappa = -1$). The critical density is often written in the literature as the equivalent mass density and this figure will be used more frequently in this paper, $\rho_{c,0} \equiv \epsilon_{c,0}/c^2$. When discussing the energy density of the Universe, the dimensionless *density parameter* is usually employed

$$\Omega(t) \equiv \frac{\epsilon(t)}{\epsilon_c(t)}. \tag{1.28}$$

In addition to the Friedmann equation, the fluid and acceleration equations make up the fundamental equations of cosmology which can tell us how the scale factor $a(t)$ evolves in time. We will make use of the first law of thermodynamics

$$\mathrm{d}Q = \mathrm{d}E + P\,\mathrm{d}V, \tag{1.29}$$

where $\mathrm{d}Q$ is the heat flow into or out of a region, $\mathrm{d}E$ is the change in internal energy, P is the pressure and $\mathrm{d}V$ is the change in the volume of the region. $\mathrm{d}Q = 0$ for a comoving volume in an expanding Universe, that is, there is no bulk flow of heat. As such, we have the simplified equation

$$\dot{E} + P\dot{V} = 0. \tag{1.30}$$

Now, consider a sphere of comoving radius r so that it's proper radius is $R(t) = a(t)r$. The volume of the sphere is

$$V(t) = \frac{4\pi}{3} r^3 a(t)^3, \tag{1.31}$$

and the rate of change of volume is

$$\dot{V} = \frac{4\pi}{3} r^3 \left(3a^2\dot{a}\right) = V\left(3\frac{\dot{a}}{a}\right). \tag{1.32}$$

The internal energy of the sphere is $E(t) = V(t)\epsilon(t)$, so the rate of change of the sphere's internal energy is

$$\dot{E} = V\dot{\epsilon} + \dot{V}\epsilon = V\left(\dot{\epsilon} + 3\frac{\dot{a}}{a}\epsilon\right). \tag{1.33}$$

Combining equations 1.30, 1.32, 1.33 and dividing across by V, we find the *fluid equation*

$$\dot{\epsilon} + 3\frac{\dot{a}}{a}(\epsilon + P) = 0. \tag{1.34}$$

If we multiply equation the Friedmann equation 1.25 by a^2 and take the time derivative, we obtain

$$2\dot{a}\ddot{a} = \frac{8\pi G}{3c^2}(\dot{\epsilon}a^2 + 2\epsilon a\dot{a}). \tag{1.35}$$

Then dividing by $2\dot{a}a$ and using the fluid equation 1.34 to make the substitution,

$$\dot{\epsilon}\frac{a}{\dot{a}} = -3(\epsilon + P), \tag{1.36}$$

we derive the *acceleration equation*

$$\frac{\ddot{a}}{a} = -\frac{4\pi G}{3c^2}(\epsilon + 3P). \tag{1.37}$$

Together the Friedmann equation 1.25, the fluid equation 1.34 and the acceleration equation 1.37 describe how the Universe expands. They lay the groundwork for all further discussion of cosmology and will be referenced liberally in this work.

1.2 Dark matter

The idea of dark matter arose in the early 20^{th} when astronomers were trying to ascertain the mass density of the Universe from stellar mass in galaxies. Stars primarily emit light in the infrared, visible and ultraviolet range of the electromagnetic spectrum. One can make a simple order-of-magnitude calculation of stellar mass density from the luminosity density. We follow the approach outlined in [4]. If one installs a B-band filter on the telescope, then only blue and violet light will be allowed through. We know that the Sun's luminosity in the B band is $\mathrm{L}_{\odot,B} = 4.7 \times 10^{25}$ watts. We also know that the total luminosity density of stars within a few hundred megaparsecs of our galaxy is $j_{*,B} = 1.2 \times 10^8\, \mathrm{L}_{\odot,B}\, \mathrm{Mpc}^{-3}$. To convert this into a mass density ρ_*, we need to know the *mass-to-light ratio* for the stars; that is, the average mass of star it takes to produce one watt of starlight in the B band. The scale is based on our Sun's ratio which is set to 1. One assumes a standard mixture of stars in the 1 kpc vicinity of the Sun, so that the mass-to-light ratio is $[M/L_B] \approx 4\,\mathrm{M}_\odot/L_{\odot,B} \approx 170,000$ kg watt^{-1}. If the mass-to-light ratio within a kiloparsec of our solar system is not unusually high or

low, than the mass density of stars in the Universe is

$$\rho_{*,0} = \langle M/M_\odot \rangle j_{*,B} \approx 5 \times 10^8 \mathrm{M}_\odot \mathrm{pc}^{-3}. \tag{1.38}$$

We can use the current known critical density of the Universe $\rho_{c,0}$ to determine the current density parameter of stars,

$$\Omega_{*,0} = \frac{\rho_{*,0}}{\rho_{c,0}} \approx \frac{5 \times 10^8 \mathrm{M}_\odot \mathrm{pc}^{-3}}{1.4 \times 10^{11} \mathrm{M}_\odot \mathrm{pc}^{-3}} \approx 0.004. \tag{1.39}$$

$\Omega_{*,0} \approx 0.004$ is by no means a precise figure due to the uncertainty around the number of low-mass, low-luminosity stars in galaxies. Additionally, galaxies contain non-stellar baryonic matter in the form of free gas within the interstellar medium. Likewise, the intergalactic medium contains a significant amount of gas. Thus, $\Omega_{*,0}$ is not a good measure of the baryonic mass density of the Universe.

The best current limits on the baryon density of the Universe emerge from the predictions of primordial nucleosynthesis which posits that the density of protons and neutrons in the early Universe affects the efficiency with which fusion takes place. Studies of the amounts of deuterium and other elements present in primordial gas clouds indicate that the density parameter of baryonic matter is

$$\Omega_{bary,0} = 0.04 \pm 0.01, \tag{1.40}$$

which is an order of magnitude larger than the density parameter of stars equation 1.39.

However, the overall mass density of the Universe is larger still. This is because most of the density in the Universe is contained in an elusive, potentially non-baryonic mass called *dark matter* which is defined by its properties of not absorbing, emitting or scattering light. Fritz Zwicky was the first astronomer to argue for the existence of dark matter in the 1930s [5]. When studying the Coma cluster of galaxies, he noticed that the dispersion in the radial velocity of the cluster's galaxies was very large at around $1000\,\mathrm{km\,s^{-1}}$. The stars and gas visible within the galaxies did not provide enough gravitational attraction to hold the cluster together. Finding dark matter by looking for its gravitational influence on visible matter in this way is a classic detection method.

We will now work towards obtaining the mass density parameter of a cluster of galaxies mathematically, following Zwicky's reasoning. Suppose that a cluster of galaxies is comprised of N galaxies, each of which can be approximated as a point mass m_i, a position $\vec{x}_i$ and a velocity $\dot{\vec{x}}_i$. We can

treat the dynamics of clusters as Newtonian based on three of their properties: clusters of galaxies are gravitationally bound objects and do not expand with the Hubble flow which causes galaxies to recede from each other due to the expansion of the Universe; they are small compared to the horizon size, with the Coma cluster being about 6 Mpc in diameter which is 0.0004% of the horizon size; and finally, the galaxies within a cluster move at non-relativistic speeds with the Coma velocity dispersion being less than 1% the speed of light. Thus, the acceleration of the i^{th} galaxy in the cluster is given by the Newtonian formula

$$\ddot{\vec{x}}_i = G \sum_{j \neq i} m_j \frac{\vec{x}_j - \vec{x}_i}{|\vec{x}_j - \vec{x}_i|^3}. \tag{1.41}$$

The gravitational potential energy of the system of N galaxies is

$$W = -\frac{G}{2} \sum_{j \neq i} \frac{m_i m_j}{|\vec{x}_j - \vec{x}_i|}, \tag{1.42}$$

which is the energy required to pull the N galaxies away from each other to infinite distance. The potential energy can also be written as

$$W = -\alpha \frac{GM^2}{r_h}, \tag{1.43}$$

where $M = \sum_i m_i$ is the total mass of all the galaxies in the cluster, α is a numerical factor which depends on the density profile of the cluster (from observation, $\alpha \approx 0.4$) and r_h is the half-mass radius of the cluster (the radius of a sphere around the cluster containing $M/2$).

The kinetic energy associated with the relative motion of galaxies in the cluster is

$$K = \frac{1}{2} \sum_i m_i |\dot{\vec{x}}_i|^2. \tag{1.44}$$

The kinetic energy associated with the relative motion of the galaxies in the cluster is

$$K = \frac{1}{2} M \langle \nu^2 \rangle, \tag{1.45}$$

where ν is the mean square velocity (weighted by galaxy mass) of all the galaxies in the cluster and is

defined as

$$\langle \nu^2 \rangle \equiv \frac{1}{M} \sum_i m_i |\dot{\vec{x}}_i|^2. \tag{1.46}$$

It is also useful to define the moment of inertia of the cluster as $I \equiv \sum_i m_i |\vec{x}_i|^2$. This can be linked to the kinetic and potential energies by taking the second derivative of I,

$$\ddot{I} = 2 \sum_i m_i (\vec{x}_i \cdot \ddot{\vec{x}}_i + \dot{\vec{x}}_i \cdot \dot{\vec{x}}_i). \tag{1.47}$$

Using equation 1.44, we can rewrite this as

$$\ddot{I} = 2 \sum_i m_i (\vec{x}_i \cdot \ddot{\vec{x}}_i) + 4K. \tag{1.48}$$

To introduce the potential energy W, we can write equation 1.41 to write

$$\sum_i m_i (\vec{x}_i \cdot \ddot{\vec{x}}_i) = G \sum_{j \neq i} m_i m_j \frac{\vec{x}_i \cdot (\vec{x_j} - \vec{x}_i)}{|\vec{x}_j - \vec{x}_i|^3}. \tag{1.49}$$

Since equation is invariant under $j \leftrightarrow i$, we have

$$\begin{aligned} \sum_i m_i (\vec{x}_i \cdot \ddot{\vec{x}}_i) &= \frac{1}{2} \left[\sum_i m_i (\vec{x}_i \cdot \ddot{\vec{x}}_i) + \sum_j m_j (\vec{x}_j \cdot \ddot{\vec{x}}_j) \right] \\ &= -\frac{G}{2} \sum_{j \neq i} \frac{m_i m_j}{|\vec{x}_j - \vec{x}_i|} = W. \end{aligned}$$

We can substitute this into equation 1.47 to obtain the relation

$$\ddot{I} = 2W + 4K, \tag{1.50}$$

which is called the *viral theorem*. If the system has a constant moment of inertia, we get a useful relation between the kinetic and potential energies:

$$K = -W/2. \tag{1.51}$$

Inserting equations 1.43, 1.44 into 1.51, we find

$$\frac{1}{2}M\langle\nu^2\rangle = \frac{\alpha}{2}\frac{GM^2}{r_h}. \tag{1.52}$$

Thus, we can make use of the virial theorem to estimate the mass of a cluster of galaxies (or indeed any other self-gravitating steady-state system):

$$M = \frac{\langle\nu^2\rangle r_h}{\alpha G}. \tag{1.53}$$

We now need to ascertain the values of $\langle\nu^2\rangle$ and r_h. The velocity dispersion along the line of sight can be found from the mean redshift of the Coma cluster $\langle z\rangle = 0.0232$ as

$$c\langle z\rangle = \langle\nu_r\rangle = 6960\mathrm{km\,s^{-1}}, \tag{1.54}$$

where ν_r is the radial velocity, and so we have

$$\sigma_r = \langle(\nu_r - \langle\nu_r\rangle)^2\rangle^{1/2} = 880\mathrm{km\,s^{-1}}. \tag{1.55}$$

If we assume that the velocity dispersion is isotropic, then the three-dimensional mean square velocity $\langle\nu^2\rangle$ will be equal to thrice the one-dimensional mean square velocity σ_r^2, yielding

$$\langle\nu^2\rangle = 3(880)^2\,\mathrm{km^2 s^{-2}} = 2.32\times10^{12}\,\mathrm{m^2 s^{-2}}. \tag{1.56}$$

Estimating the half-mass radius r_h of the Coma cluster is more complex without knowing the dark matter distribution a priori, so we must make the assumption that the mass-to-light ratio is constant with radius. This means that the sphere containing half the mass of the cluster will be the same as the sphere containing half the luminosity of the cluster. Also assuming sphericity, we have that the observed distribution of galaxies within the Coma cluster indicates a half-mass radius

$$r_h \approx 1.5\mathrm{Mpc} \approx 4.6\times10^{22}\,\mathrm{m}. \tag{1.57}$$

We may now estimate the mass of the Coma cluster using equation 1.53 and $M_\odot = 1.988 \times 10^{30}$ kg,

$$\begin{aligned} M_{\text{Coma}} = \frac{\langle \nu^2 \rangle r_h}{\alpha G} &\approx \frac{(2.32 \times 10^{12})(4.6 \times 10^{22})}{(0.4)(6.7 \times 10^{-11}} \text{kg} \\ &\approx 4 \times 10^{45} \text{kg} \approx 2 \times 10^{15}\, \text{M}_\odot. \end{aligned} \tag{1.58}$$

Thus, less than two percent of the mass of the Coma cluster lies in stars as $M_{Coma,*} \approx 3 \times 10^{13} \text{M}_\odot$. Combined with the luminosity of the Coma cluster, $L_{\text{Coma},B} = 8 \times 10^{12} \text{L}_{\odot,B}$, the total mass of the Coma cluster implies a mass-to-light ratio of

$$\langle M/L_B \rangle_{\text{Coma}} \approx 250\, \text{M}_\odot/\text{L}_{\odot,B}. \tag{1.59}$$

The presence of a vast amount of dark matter in the Coma cluster is confirmed by the fact that the hot, X-ray emitting intracluster gas is still in place; if there were no dark matter to anchor the gas gravitationally, it would have expanded beyond the cluster on time scales much shorter than the Hubble time. Other galaxy clusters have been found to have mass-to-light ratios in the range $\langle M/L_B \rangle = 250 \pm 50 \text{M}_\odot/\text{L}_{\odot,B}$, so the Coma cluster is quite typical for the amount of dark matter it contains. If the masses of all the clusters of galaxies are added together, it is found that their density parameter is

$$\Omega_{\text{clus},0} \approx 0.2, \tag{1.60}$$

which acts as the lower limit of the mass density of the Universe since it does not include any matter in the intracluster voids. The actual mass density of the Universe is around 30% and dark matter is responsible for most of that with a density parameter of $\Omega_{\text{DM}} \approx 0.25$ [6]. These figures can be derived from a dark matter detection technique called *gravitational lensing*. General relativity asserts that mass affects the trajectory of photons, thus dark matter can bend and focus light, acting as a gravitational lens [7].

While we are certain that dark matter exists, its elusive properties (potentially non-baryonic, interacting weakly with the electromagnetic force) make it fiendish task to figure out its precise nature. There are two broad categories of dark matter candidates; WIMPs, Weakly Interacting Massive Particles, and MACHOs, Massive Compact Halo Objects. WIMPs arise naturally in various theories beyond the Standard Model; as the lightest supersymmetric particle in supersymmetric theories, which

in many models is the neutralino [8], or as the lightest Kaluza-Klein particle in theories with extra spacetime dimensions [9]. However, there has been scant experimental evidence for such particles [10]. Many have hoped that with each upgrade of the Large Hadron Collider (LHC), there would be a detection [11], but this has not come to pass at the time of writing. As such, physicists have turned to other possibilities, including MACHOs, the category to which black holes (and primordial black holes), brown dwarfs, neutron stars and other such macroscopic bodies belong. These objects emit very little radiation and drift through galaxies unattached to planetary systems. Primordial black holes (PBHs) are the only non-baryonic MACHO of current interest. There is quite a lot of evidence that at least some of the dark matter must be non-baryonic [12], with significant constraints coming from the theory of Big Bang nucleosynthesis (BBN)[1] and from observations of the cosmic microwave background (CMB) [2] [13]. For this and other reasons, PBHs have attracted more attention in recent years for their potential in answering the dark matter question by providing all or some of the matter.

1.3 Primordial black holes

By the 1970s, the theory of stellar black hole formation was well established in the literature. When a sufficiently massive star of at least $3M_\odot$ undergoes gravitational collapse at the end of its lifetime and contracts to a size less than its Schwarszchild radius, a black hole is formed. The Schwarzschild radius is defined as

$$r_s = \frac{2GM}{c^2}, \tag{1.61}$$

where G is the gravitational constant, c is the speed of light and M is the mass of the collapsing object. This result was derived around 1916 by Karl Schwarzchild who obtained the first exact solution to the Einstein's equations which described the gravitational field surrounding a non-rotating, spherically symmetric mass M. The corresponding metric is

$$\mathrm{d}s^2 = -\left(1 - \frac{r_s}{r}\right) c^2\,\mathrm{d}t^2 + \left(1 - \frac{r_s}{r}\right)^{-1} \mathrm{d}r^2 + r^2(\mathrm{d}\theta^2 + \sin^2\theta\,\mathrm{d}\phi^2), \tag{1.62}$$

which becomes singular at $r_s = 0$ and when r_s is equal to the Schwarzchild radius. The lower bound of $3M_\odot$ emerges from the physics of gravitational collapse; in particular, there exists strong internal

[1] Big Bang nucleosynthesis is a theory of nuclei formation in the early Universe which predicts the observed abundance of the chemical elements.

[2] The Cosmic Microwave Background is a faint glow of radiation that fills the Universe, falling on Earth from every direction with nearly uniform intensity. It is the residual energy from the early stages of the Universe and is an important source of information about this era.

degeneracy pressure at high densities which counteracts the collapse, and this must be overcome in order for the mass to form a black hole.

Despite this solution being found so early on in the last century, the term 'black hole' did not enter the scientific lexicon until the 1960s, when Stephen Hawking, Roger Penrose, Roy Kerr, David Finkelstein and Martin Kruskal amongst others began to investigate its physical interpretation more precisely. The observation of pulsars by Jocelyn Bell-Burnell in 1968 invigorated research into compact bodies generally, as previously there had been little validation that such bodies were physical [14]. The development of black hole thermodynamics by Hawking, Berkenstein and Bardeen in the early 1970s and the eventual prediction of thermal radiation from black holes played a crucial role in the emergence of primordial black holes as a field of study [15]. The rate at which black holes emit radiation is inversely proportional to their mass, and stellar mass black holes are predicted to radiate too weakly to be able to detect a loss in mass from Earth. This led Hawking to consider an alternative formation mechanism which could produce black holes of mass small enough for thermal radiation to be appreciable, namely, the collapse of fluctuations in the very early Universe, less than one second after the Big Bang [16]. It should be noted that Novikov and Zel'dovich are often credited as the pioneers in the field of primordial black holes due to a 1966 paper in which they consider the implications of a hot cosmological model on the accretion of matter in the early Universe [17]. While they mentioned the possibility of PBHs, it was Hawking who cultivated the theory and brought it into mainstream debate (although they did contribute more during the 70s based on Hawking's work [18]).

The theoretically large mass range of PBHs is one of the primary reasons they are such promising objects to study. There could exist black holes as small as 10^{-5}g and as large as $10^{5}M_{\odot}$ [19]. Imposing constraints on the PBH mass spectrum is an ongoing endeavour and crucial to progressing the field. Many theorists are enthusiastic about the possibility of PBHs being dark matter and/or the seeds for supermassive black holes observed in the centre of galaxies. There are particular mass ranges for which one or both of these hypotheses could be true. Understanding the formation mechanism behind PBHs is key goal of the field and may have a significant influence on the mass spectrum. This topic will be explored in chapter 4. While this work focuses on the dark matter role of PBHs, there is some discussion of other possible functions in the final sections. Furthermore, an up-to-date overview of constraints on the PBH mass spectrum will be provided in section 5.1.1.

2 Evolution of the Universe

As mentioned in the previous section, *primordial* black holes imply formation in the very early Universe. However, it will benefit our discussion to contextualise this in terms of the cosmic timeline of the Universe. More precisely, term 'primordial' usually refers to a time much earlier than one second after the Big Bang; roughly less than 10^{-11} seconds [20]. This is called the Quark epoch, in which baryogenesis may have taken place with matter gaining the upper hand over anti-matter as baryon to anti-baryon constituencies were established.

Before the Quark epoch, there was the Electroweak epoch, during which the Universe undergoes cosmic inflation, expanding by a magnitude of order 10^{26} between 10^{-33}and10^{-32} seconds after the Big Bang. At 10^{-32}s, inflation ends and elementary particles form as a primordial soup of hot ionised gas called quark-gluon plasma. Since the temperature of the Universe is still too high, this plasma persists during the Quark epoch. At 10^{-12}s, matter particles can interact with the Higgs field and acquire mass due the Electroweak phase transition, when the four fundamental interactions operate as distinct forces.

After the Quark epoch, the Hadron, Lepton and Photon epochs follow respectively. After the first 20 minutes, normal matter has formed (75% hydrogen nuclei and 25% helium nuclei), dark matter halos begin to form and the Universe is hot, glowing and opaque as it is radiation-dominated ($\omega = 1/3$ in the equation of state). 47,000 years post-Big Bang (z = 3600) heralds the epoch of matter-radiation equality, after which matter dominates the Universe ($\omega = 0$). During the era of recombination, (z = 1100), free electrons became bound to protons (hydrogen nuclei) to form neutral hydrogen atoms. Photon decoupling also happened during this time; photons ceased to interact with electrons, and the Universe becomes transparent. These photons reach present-day observers as the cosmic microwave background radiation (CMB). This radiation appears to come from a spherical surface around the observer such that the radius of the shell is the distance each photon has travelled since it was last scattered at the epoch of recombination. This surface is called the surface of last scattering.

After decoupling, the Universe experienced its first Dark Age, during which the cosmic background radiation cooled from 4000K to about 60K. The epoch of Reionisation occured between redshifts $6 < z < 20$ and ended the Dark Age with the formation of the first stars (Population III stars) and quasars, followed by large scale structures such as galaxies and clusters. The Universe remained matter-dominated until it was about 9.8 billion years old, after which time it became dark-energy-

dominated [4].

The era of most interest in this chapter is the radiation-dominated era, before $z = 3600$. Through calculating the Boltzmann equations for photons, we can see many important aspects of the evolution of the early Universe when it was dominated by radiation. We will eventually obtain a value for the energy density of photons from which we can derive the perturbed energy density fluctuations which in turn will be used to find the power spectrum of initial density fluctuations due to inflation. This is important for our discussion of primordial black holes as their mass spectrum and mechanism of formation is dependent on these primordial fluctuations. We will begin by discussing inflation and specifically slow roll inflation as this is the most basic inflationary model and will inform the discussion in section 4.6 of how other inflationary models constrain the mass spectrum of PBHs. We follow the approach taken by Dodelson [21].

2.1 Inflation

Inflation was proposed as the solution to the so-called *horizon problem*. An outline of this problem follows. Consider two antipodal points on the surface of last scattering (LSS). The current proper distance to this surface is

$$d(t_0) = c \int_{t_{\rm ls}}^{t_0} \frac{\mathrm{d}t}{a(t)}. \tag{2.1}$$

Since the last scattering of CMB photons occurred when $t_{\rm ls} \ll t_0$, the current proper distance to the LSS is only slightly smaller than the current horizon distance. For the standard Hot Big Bang scenario [3], the current proper distance to the LSS is $d(t_0) = 0.98 d_{\rm hor}(t_0)$. Thus, two antipodal points on the LSS, separated by 180 degrees as seen by an observer on Earth, are currently separated by a proper distance of $1.96 d_{\rm hor}(t_0)$. Since the two points are farther apart than the horizon distance, they are causally disconnected i.e., they can't exchange information and crucially cannot reach thermal equilibrium together. However, we know from observations of the CMB today that these two points have almost the same temperature; in fact, the CMB is close to isotropic. So the question begs; how can two points, having never been in causal contact, possess nearly identical properties? See figure 1 for an illustration of the problem.

The theory of inflation proposes that the Universe underwent a period of accelerated expansion

[3]The Hot Big Bang model is the standard model of cosmology and posits that the observable Universe was initially dense and hot and has since been expanding and cooling.

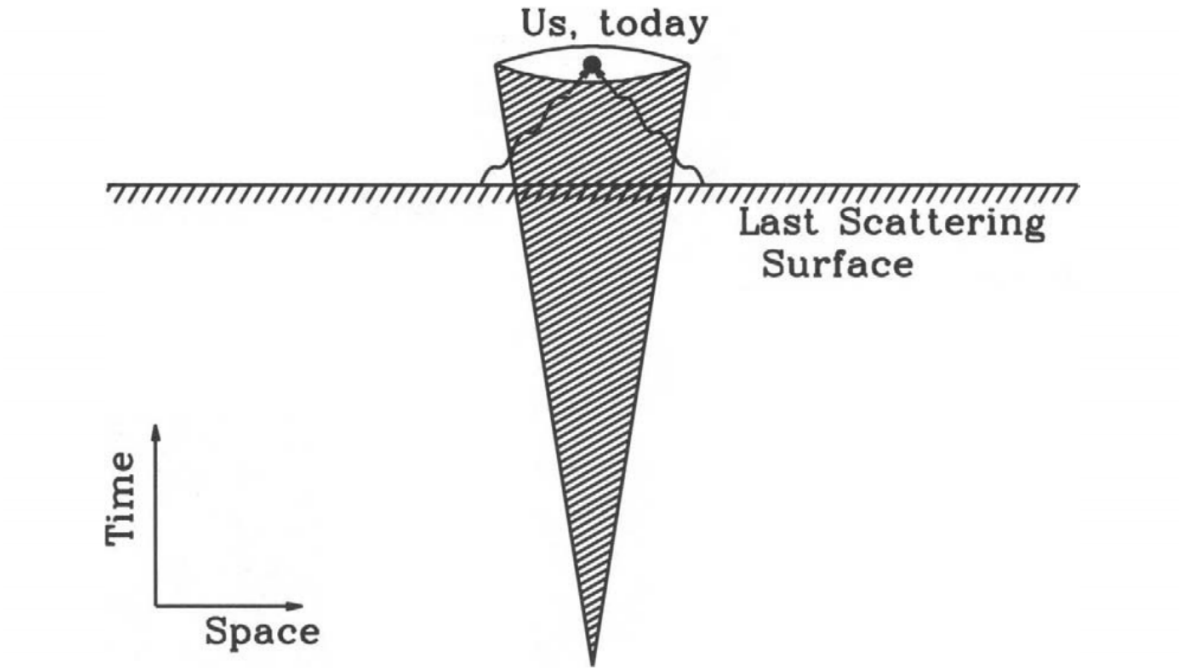

Figure 1. A representation of the horizon problem. The region inside the cone is causally connected to us, at the centre of the cone. Photons emitted from the last scattering surface (LSS) started outside of this region. Therefore, at the LSS, they were not in causal contact with us and certainly not with each other. Taken from [21].

soon after the Big Bang, during which the scale factor grew exponentially with time,

$$a(t) \propto e^{H_i t}. \tag{2.2}$$

Suppose that the exponential growth began at a time t_i and lasted until t_f, when the expansion was switched off and the Universe returned to its radiation-dominated state of expansion. In this toy model, we can write the scale factor as

$$a(t) = \begin{cases} a_i (t/t_i)^{1/2} & t < t_i \\ a_i e^{H_i (t - t_i)} & t_i < t < t_f \\ a_i e^{H_i (t_f - t_i)(t/t_f)^{1/2}} & t > t_f. \end{cases} \tag{2.3}$$

Thus, between time t_i, when the exponential inflation began and the time t_f when the inflation

stopped, the scale factor increased by a factor

$$\frac{a(t_f)}{a(t_i)} = e^N, \tag{2.4}$$

where N, the number of e-foldings of inflation, was

$$N = H_i(t_f - t_i). \tag{2.5}$$

If the duration of inflation $t_f - t_i$ was long compared to the Hubble time during inflation, H_i^{-1}, then N was large, and the growth in the scale factor during inflation was enormous.

To see how inflation solves the horizon problem, consider again the region bounded by the surface of last scattering. We use a model for inflation which has a growth in scale factor of

$$\frac{a(t_f)}{a(t_i)} \sim e^{100} \sim 10^{43}. \tag{2.6}$$

Currently, the proper distance to the surface of last scattering is $d_p(t_0) \approx 1.4 \times 10^4$ Mpc. If inflation ended at $t_f \approx 10^{-34}s$, that corresponds to a scale factor $a_f \sim d_p(t_f) = a_f d_p(t_0) \sim 3 \times 10^{-23}$Mpc ~ 0.9 m. Immediately after inflation, in this model, all the mass-energy destined to become the hundreds of billions of galaxies we see today was enclosed within a sphere only six feet across. If there were N = 100 e-foldings of inflation, then immediately prior to the inflationary epoch, the currently visible Universe was enclosed within a sphere of proper radius $d_p(t_i) = e^{-N} d_p(t_f) \sim 3 \times 10^{-44}$ m. Note that this distance is 16 orders of magnitude smaller than the horizon size immediately prior to inflation ($d_h or(t_i) \sim 6 \times 10^{-28}$ m.) Thus, the portion of the Universe which we can see today had plenty of time to achieve thermal uniformity before inflation began [4].

The most basic model of inflation is the slow roll paradigm. Inflation is represented by a scalar field, sometimes referred to as the inflaton field. We begin by writing the effective energy density and pressure of a homogeneous scalar inflaton field ϕ,

$$\rho_\phi = \frac{1}{2}\dot{\phi}^2 + V(\phi), P_\phi = \frac{1}{2}\dot{\phi}^2 - V(\phi). \tag{2.7}$$

One can think of the first term in each as a kinetic energy and the second as a potential energy. The potential energy $V(\phi)$ can be thought of as a form of 'binding' energy; it measures how much

internal energy is associated with a particular field value. The equations for an expanding Universe are easily obtained by substituting equations 2.7 in the flat-space Friedmann equation with 1.26(with $\epsilon(t)/c^2 = \rho(t)$ and the fluid 1.34 equation, giving

$$H^2 = \frac{8\pi}{3m_{\rm Pl}^2}\left(V(\phi) + \frac{1}{2}\dot{\phi}^2\right), \tag{2.8}$$

$$\ddot{\phi} + 3H\dot{\phi} = -V'(\phi), \tag{2.9}$$

where prime indicates differentiation with respect to ϕ and $m_{\rm Pl}^2 = \hbar c/G$ is the Planck mass. Since $\ddot{a} > 0$ implies $P < -\rho/3$, we have that $\dot{\phi}^2 < V(\phi)$. Hence, inflation will occur whenever the potential energy dominates. This is possible provided the potential is flat enough and has a minimum. The standard strategy for solving these equations is the slow roll approximation. This assumes that a term can be neglected in each of the equations of motion since the potential dominates; the $\dot{\phi}^2$ term in the first and the $\ddot{\phi}$ term in the second. We're left with

$$H^2 \approx \frac{8\pi}{3m_{\rm Pl}^2}V, \tag{2.10}$$

$$3H\dot{\phi} \approx -V'. \tag{2.11}$$

If we then define the slow roll parameters

$$\begin{aligned} \epsilon(\phi) &= \frac{m_{\rm Pl}^2}{2}\left(\frac{V'}{V}\right)^2, \\ \eta_\nu(\phi) &= m_{\rm Pl}^2\frac{V''}{V}, \end{aligned} \tag{2.12}$$

where the first measures the slope of the potential and the second measures the curvature, then the necessary conditions for the slow roll approximation to hold are $\epsilon \ll 1$ and $\mod \eta_\nu \ll 1$. Be aware that ϵ was employed in section 1.1 for the total energy density. This is clearly distinct from the slow roll parameter ϵ. The use of one or the other will be clear from context henceforth. These parameters will be referred to in subsequent discussions of inflation in chapter 3 and in section 4.6, where other models of inflation are discussed. However, the factors of the slow roll parameters may deviate from what is written here for the purposes of simplification. Consider this treatment as an illustration of how the slow roll parameters emerge from the effective energy density and pressure of

a homogeneous scalar field.

2.2 Boltzmann equations for photons and cold dark matter

In the Universe today, we observe anisotropies in the distribution of photons in the CMB and inhomogeneities in the distribution of matter with structure formation. We wish to calculate these perturbations in the early Universe to derive a spectrum for initial fluctuations in the radiation due to inflation, from which PBHs may have formed. However, these perturbations interact with each other and the metric, which complicate matters. The Boltzmann equations provides a way of dealing with these couplings by relating the rate of change of the distribution function $f(t, \vec{x}, \vec{p})$ with all possible collision terms $C[f]$,

$$\frac{df}{dt} = C[f]. \tag{2.13}$$

It will be useful to note that at equilibrium temperature T, photons have the Bose-Einstein distribution

$$f_{\text{BE}} = \frac{1}{e^{(E-\mu)T} - 1}. \tag{2.14}$$

We would like to decompose the LHS of equation 2.13 for massless photons as a sum of partial derivatives. To do so, we define the momentum vector

$$P^{\mu} = \frac{dx^{\mu}}{d\lambda}, \tag{2.15}$$

where λ is an affine parameter, i.e. it satisifes the geodesic equation. The massless photon implies that $ds^2 = 0$ for the metric of equation 1.9, which constrains the momentum tensor to just three independent components. Let the magnitude of momentum be defined over the spatial components $p^2 = g_{ij}P^iP^j$, with which we can define the time component

$$P^0 = \frac{P}{\sqrt{1+2\Psi}} = p(1-\Psi), \tag{2.16}$$

where we have used the binomial expansion $(1+2\Psi)^{-1/2} = 1 - \Psi + \mathcal{O}(\Psi^2)$ since $\Psi \ll 1$. With our sign convention**, an overdense region has $\Psi < 0$, therefore the RHS of equation 2.16 is greater than one. This implies that photons lose energy (redshift) as they move out of a potential well. We

can now omit dependence on the time component of the momentum in our decomposition of df/dt

$$\frac{df}{dt} = \frac{\partial f}{\partial t} + \frac{\partial f}{\partial x^i}\frac{dx^i}{dt} + \frac{\partial f}{\partial p}\frac{dp}{dt} + \frac{\partial f}{\partial \hat{p}^i}\frac{d\hat{p}^i}{dt}, \tag{2.17}$$

where $\hat{p}^i$ is the angular direction vector of momentum as p is the magnitude. The last term with direction vector $\hat{p}^i$ does not contribute to first order in perturbation theory. This arises from the fact that the zeroth order distribution function for photons is equation 2.14, which depends on p (corresponding to energy E) and not the direction vector. Therefore, $df/d\hat{p}^i$ is only non-zero at first order in f. However, $df/d\hat{p}^i$ is itself at first order as the direction of a photon only changes in the presence of perturbations, so the final term in equation 2.17 is a second order term and can be neglected.

Let us now compute the coefficients for the remaining partial derivatives. Firstly, note that by chain rule

$$\frac{dx^i}{dt} = \frac{dx^i}{d\lambda}\frac{d\lambda}{dt} = \frac{P^i}{P^0}. \tag{2.18}$$

To express P^ii in terms of p, let $P = C\hat{p}^i$ for some constant C. Then

$$p^2 = a^2(1+2\Phi)C^2\delta_{ij}\hat{p}^i\hat{p}^j. \tag{2.19}$$

Since the direction vector is a unit vector, its inner product is 1. Therefore, after obtaining an expression for C, we obtain

$$P^i = C\hat{p}^i = p\hat{p}^i\frac{(1-\Phi)}{a}. \tag{2.20}$$

Inserting this expression and equation 2.16 into equation 2.18 gives

$$\frac{dx^i}{dt} = \frac{\hat{p}^i}{a}(1+\Psi-\Phi) \tag{2.21}$$

An overdense region has $\Psi < 0$ and $\Phi > 0$, so the RHS is less than one**. This equation implies that a photon slows down (dx/dt decreases) when permeating an overdense region.

Now, to calculate the second coefficient dp/dt, we consider that it equivalent to the term $-kx$ for the classical harmonic oscillator which describes the decrease in momentum. In general relativity, the

analogue of this is the geodesic equation for affine parameter λ

$$0 = \frac{dP^\sigma}{d\lambda} + \Gamma^\sigma_{\mu\nu} P^\mu P^\nu. \tag{2.22}$$

Consider this equation for $\sigma = 0$. Since $P^0 = dt/d\lambda$, we have

$$0 = P^0 \frac{dP^0}{dt} + \Gamma^0_{\mu\nu} P^\mu P^\nu. \tag{2.23}$$

Expanding terms and rearranging,

$$\frac{dp}{dt}(1-\Psi) = p\frac{d\Psi}{dt} - \Gamma^0_{\mu\nu}\frac{P^\mu P^\nu}{p}(1+\Psi). \tag{2.24}$$

Multiply both sides by $(1+\Psi)$, keeping only linear terms and expressing the total time derivative of Ψ in terms of partial derivatives,

$$\frac{dp}{dt} = p\left[\frac{\partial\Psi(\vec{x},t)}{\partial t} + \frac{\hat{p}^i}{a}\frac{\partial\Psi}{\partial x^i}\right] - \Gamma^0_{\mu\nu}\frac{P^\mu P^\nu}{p}(1+2\Psi). \tag{2.25}$$

We will calculate explicitly the final term using the perturbed Christoffel symbols of equation 1.10, being careful about taking terms of linear order only in all scalar fields,

$$\begin{aligned}
&= \Gamma^0_{00}\frac{P^0P^0}{p} + \Gamma^0_{ij}\frac{P^iP^j}{p} + 2\Gamma^0_{i0}\frac{P^iP^0}{p}, \\
&= \partial_0\Psi p(1-\Psi)^2 + \delta_{ij}\left(H + 2H(\Phi-\Psi) + \partial_0\Phi\right)p\hat{p}^i\hat{p}^j(1-\Phi)^2 \\
&+ 2\partial_i\Psi p\frac{\hat{p}^i}{a}(1-\Phi)(1-\Psi). \\
&= p\left(\partial_0\Psi + 2\frac{\hat{p}^i}{a}\partial_i\Psi + H - 2H\Psi + \partial_0\Phi\right).
\end{aligned} \tag{2.26}$$

Inserting this into (2.25),

$$\begin{aligned}
\frac{dp}{dt} &= p\,\partial_0\Psi + p\frac{\hat{p}^i}{a}\partial_i\Psi \\
&\quad - p\left(\partial_0\Psi + 2\frac{\hat{p}^i}{a}\partial_i\Psi + H - 2H\Psi + \partial_0\Phi\right)(1+2\Psi).
\end{aligned} \tag{2.27}$$

Finally, taking all terms to first order and dividing by p gives

$$\frac{1}{p}\frac{dp}{dt} = -H - \frac{\partial \Phi}{\partial t} - \frac{\hat{p}^i}{a}\frac{\partial \Psi}{\partial x^i}. \tag{2.28}$$

This equation describes the change in momentum of the photon as it travels through a perturbed FLRW Universe. The first term corresponds to the loss of momentum due to Hubble expansion, the second can be interpreted as the photon redshifting in a deepening gravitational well and the third describes the energy gain ('blueshifting') as a photon is falling into a potential well.

Substituting terms of equations 2.21 and 2.28 into equation 2.17 with the final term omitted, we obtain the LHS Boltzmann equation for photons

$$\frac{df}{dt} = \frac{\partial f}{\partial t} + \frac{\hat{p}^i}{a}\frac{\partial f}{\partial x^i} - p\frac{\partial f}{\partial p}\left(H + \frac{\partial \phi}{\partial t} + \frac{\hat{p}^i}{a}\frac{\partial \Psi}{\partial x^i}\right). \tag{2.29}$$

The first two terms give the continuity and Euler equations when integrated, the third terms tell us that photons lose energy in an expanding Universe (which we expect from inflation) and the final two terms describe the effects of overdense regions on the photon distribution.

We will now introduce a perturbation to the photon distribution function denoted by $\Theta = \delta T/T$ where T is the equilibrium temperature. i.e.... By expanding $f^{(0)}$, the zeroth order Bose-Einstein equation of 2.14, we obtain

$$f(\vec{x}, p, \hat{p}, t) = \left[exp\left(\frac{p}{T(t)\left[1 + \Theta(\vec{x}, \hat{p}, t)\right]}\right) - 1\right]^{-1}. \tag{2.30}$$

The dependency of the terms in this expression are deduced from the definition of the background metric. Homogeneity and isotropy imply that T is independent of $\vec{x}$ and $\hat{p}$ respectively. On the other hand, Θ is dependent on both these variables as it takes into account perturbations of the photon distribution called inhomogeneities and anisotropies (non-uniformity in all directions). Θ does not depend on the magnitude of momentum p as this is hardly disturbed by Compton scattering. It is also small, so we can expand to linear order,

$$\begin{aligned} f &\simeq \frac{1}{e^{p/T} - 1} + \left(\frac{\partial}{\partial T}\left[e^{p/T} - 1\right]^{-1}\right) T\Theta, \\ &= f^{(0)} - \frac{1}{T^2} p\Theta f^{(0)}, \end{aligned} \tag{2.31}$$

and using the fact that $T(\partial f^{(0)}/\partial t) = -p(\partial f^{(0)}/\partial p)$ **(Why?),

$$f \simeq f^{(0)} - p\,\Theta\frac{\partial f^{(0)}}{\partial p}. \tag{2.32}$$

We can now derive the zeroth order expression of equation 2.29, which does not include any perturbative terms. Since the distributions functions are at their equilibrium value, so the rate for the reaction precisely cancels out the rate for its inverse reaction, collision terms (the RHS of the Boltzmann equation) vanish. Therefore, we can write

$$\frac{df}{dt} = \frac{\partial f^{(0)}}{\partial t} - Hp\frac{\partial f^{(0)}}{\partial p} = 0. \tag{2.33}$$

The Bose-Einstein distribution implies that photons were highly coupled to electrons sometime in the early Universe.** By chain rule, we have

$$\frac{\partial f^{(0)}}{\partial t} = \frac{\partial f^{(0)}}{\partial T}\frac{dT}{dt} = -p\,\frac{dT/dt}{T}\frac{\partial f^{(0)}}{\partial p}, \tag{2.34}$$

so that the zeroth order equation becomes

$$\left.\frac{df}{dt}\right|_{0^{th}} = \left(-p\frac{dT/dt}{T} - pH\right)\frac{\partial f^{(0)}}{\partial p} = 0, \tag{2.35}$$

from which we can derive the relationship

$$\frac{dT}{da} = -\frac{T}{a} \Rightarrow T \propto \frac{1}{a}, \tag{2.36}$$

which suggests that the wavelength of photons gets stretched ($\lambda \propto 1/T$) as the Universe expands. To calculate the first order equation, we insert expression 2.32 into equation 2.29, carefully keeping all terms at first order in Θ, Φ and Ψ,

$$\begin{aligned}\left.\frac{df}{dt}\right|_{1^{st}} = &- p\frac{\partial}{\partial t}\left(\frac{\partial f((0)}{\partial p}\Theta\right) - p\frac{\hat{p}^i}{a}\frac{\partial\Theta}{\partial x^i}\frac{\partial f^{(0)}}{\partial p} \\ &+ pH\Theta\frac{\partial}{\partial p}\left[p\frac{\partial f^{(0)}}{\partial p}\right] - p\frac{\partial f^{(0)}}{\partial p}\left[\frac{\partial\Phi}{\partial t} + \frac{\hat{p}_i}{a}\frac{\partial\Psi}{\partial x^i}\right].\end{aligned} \tag{2.37}$$

Consider the first term on the RHS. The time derivative can be written as a temperature derivative

by chain rule,

$$-p\frac{\partial}{\partial t}\left[\frac{\partial f^{(0)}}{\partial p}\Theta\right] = -p\frac{\partial f^{(0)}}{\partial p}\frac{\partial \Theta}{\partial t} - p\,\Theta\frac{dT}{dt}\frac{\partial^2 f^{(0)}}{\partial T \partial p}, \tag{2.38}$$

and since $f^{(0)}/\partial T = -(p/T)\,\partial f^{(0)}/\partial p$,

$$-p\frac{\partial}{\partial t}\left[\frac{\partial f^{(0)}}{\partial p}\Theta\right] = -p\frac{\partial f^{(0)}}{\partial p}\frac{\partial \Theta}{\partial t} + p\,\Theta\frac{dT/dt}{T}\frac{\partial}{\partial p}\left(p\frac{\partial f^{(0)}}{\partial p}\right). \tag{2.39}$$

Using equation 2.36, we have that $(dT/Tdt) = -H$, so this term cancels with the third term in equation 2.37 and we're left with

$$\left.\frac{df}{dt}\right|_{1^{st}} = -p\frac{\partial f^{(0)}}{\partial p}\left[\frac{\partial \Theta}{\partial t} + \frac{\hat{p}^i}{a}\frac{\partial \Theta}{\partial x^i} + \frac{\partial \Phi}{\partial t} + \frac{\hat{p}^i}{a}\frac{\partial \Psi}{\partial x^i}\right]. \tag{2.40}$$

The first two terms describe the free streaming of photons (not scattering) and the last two terms correspond to the effect of gravity on the distribution.

In order to obtain the full Boltzmann equation for photons, the collision terms on the RHS of equation 2.13 must also be calculated. This requires calculating the influence of photons scattering with charged particles (Compton scattering) on the distribution function. For our purposes, we simply quote the result, but a full derivation can be found in [21],

$$C\left[f(\vec{p})\right] = -p\frac{\partial f^{(0)}}{\partial p}n_e\sigma_T\left[\Theta_0 - \Theta(\vec{p}) + \hat{p}\cdot\bar{\nu}_b\right]. \tag{2.41}$$

The new terms here denote the following: σ_T is the Thomson (elastic) scattering cross section, $\bar{\nu}_b$ is the bulk velocity of electrons, n_e is the number density of free electrons and Θ_0 is the monopole part of the perturbation, i.e. it does not depend on the direction vector $\hat{p}$. This equation can tell us incisive information about our Universe. In particular, it confirms our observation of the uniformity of the CMB. Heuristically, the argument is as follows; when Compton scattering is very efficient (as it is taken to be in the early Universe when electrons and photons are strongly coupled), the mean free path of a photon is very small as it is scattering off electrons very close to it. These electrons likely have a very similar temperature and can efficiently transfer energy back to the photon. The fact that the photon gives energy to the electron and vice versa allows Compton scattering to generate thermal equilibrium in the Thomson limit of elastic scattering. So photons have the same temperature in all directions, and this near isotropy is what we observe in the CMB today. This is typical of a monopole

distribution, and indeed we see that if $\bar{\nu}_b$ is very small, the monopole term dominates. If the bulk velocity were non-zero, we would obtain a dipole moment of the perturbation (which is not included in equation 2.41), with all higher terms vanishing as in the monopole case. These properties of the photon background are conducive to the behaviour of a fluid.

We are now ready to write down the full expression of the Boltzmann equation for photons by equating expressions 2.29 and 2.41, converting to conformal time denoted by a dot by letting $dt = a\, d\eta$,

$$\dot{\Theta} + \hat{p}^i \frac{\partial \Theta}{\partial x^i} + \frac{\partial \Phi}{\partial t} + \hat{p}^i \frac{\partial \Psi}{\partial x^i} = a n_e \sigma_T \left[\Theta_0 - \Theta + \hat{p} \cdot \bar{\nu}_b\right]. \tag{2.42}$$

This expression can be further simplified by Fourier transforming, which has two important effects: it converts it into an ODE, which is easier to solve than the PDE in position space, and allows one to solve each mode independently. We will define the Fourier transformed version of equation 2.42 in terms of two new variables. The first is quantity $\mu = \cos\theta$, where θ is the angle between the wavenumber $\vec{k}$ and photon direction $\hat{p}$ which describes the direction of photon propagation,

$$\mu = \frac{\vec{k} \cdot \hat{p}}{k}. \tag{2.43}$$

If $\mu = 1$, the photon is travelling in the direction along which the temperature is changing. If $\mu = 0$, the photon is travelling orthogonally to the varying wavenumber, so the temperature is constant. It is assumed that the velocity is irrotational, so $\bar{\nu}_b \cdot \hat{p} = \bar{\nu}_b \cdot \mu$. The second new quantity is optical depth $\tau(\eta)$

$$\tau(\eta) = \int_{\eta}^{\eta_0} d\eta'\, n_e \sigma_T a. \tag{2.44}$$

At late times, the free electron density n_e is small, so $\tau \ll 1$. Conversely, at early times, the Universe is dense with photons and electrons, so $\tau \gg 1$. Thus τ decreases over time and therefore has a negative rate of change. Using the definition of the Fourier transform

$$\Theta(\vec{x}) = \int \frac{d^3k}{(2\pi)^3}\, e^{i\vec{k}.\vec{x}}\, \tilde{\Theta}(\vec{k}), \tag{2.45}$$

we can now write the more useful form of the Boltzmann equation in momentum space,

$$\dot{\tilde{\Theta}} + ik\mu\tilde{\Theta} + \dot{\tilde{\Phi}} + ik\mu\tilde{\Psi} = -\dot{\tau}\left[\tilde{\Theta_0} - \tilde{\Theta} + \mu\tilde{\nu_b}\right]. \tag{2.46}$$

Note that it is a common convention in cosmology to set $\Theta = \tilde{\Theta}$, which will be followed in this paper.

We now work towards obtaining expressions for the evolution of the perturbation variables Φ and Ψ using the time-time 1.14 and space-space 1.15 components of Einstein equations. The RHS will require expressions for the energy momentum tensor in terms of the distribution function f. The first component is

$$T_0^0(\vec{x}, t) = -g_i \sum_i \frac{d^3}{(2\pi)^3} E_i(p) f_i(\vec{p}, \vec{x}, t). \tag{2.47}$$

To obtain this in terms of the perturbation variables for photons, the expansion to the distribution function 2.32 is used. Recalling that $E = p$ and $g_i = 2$ for photons,

$$T_0^0(\vec{x}, t) = -\rho = -2 \int \frac{d^3p}{(2\pi)^3}\, p \left[f^{(0)} - p\, \Theta \frac{\partial f^{(0)}}{\partial p} \right]. \tag{2.48}$$

The first term is the zeroth order photon energy

$$\rho_{rad} = -2 \int \frac{d^3p}{(2\pi)^3}\, p f^{(0)}. \tag{2.49}$$

To solve the second term, we require the definition of the monopole part of the photon perturbation,

$$\Theta_0(\vec{x}, t) = \frac{1}{4\pi} \int d\Omega'\, \hat{\Theta}(\hat{p}', \vec{x}, t), \tag{2.50}$$

where Ω represents the solid angle. Letting $d^3p = p^2 dp\, d\Omega$,

$$2 \int \frac{d^3p}{(2\pi)^3}\, p^2\, \Theta \frac{\partial f^{(0)}}{\partial p} = 2 \int \frac{dp}{(2\pi)^3}\, p^4 \frac{\partial f^{(0)}}{\partial p} \int d\Omega\, \Theta. \tag{2.51}$$

Inserting equation 2.50 and then integrating by parts over the p integral,

$$-2 \int \frac{dp}{4\pi^2} 4p^3 f^{(0)} \Theta_0 = -4\Theta_0 \left[2 \int \frac{dp}{(4\pi)^2} p^3 f^{(0)} \right] = -4\Theta_0 \rho_{rad}. \tag{2.52}$$

Hence, the energy momentum tensor for photons is

$$T_0^0 = -\rho_{rad} \left[1 + 4\Theta_0 \right], \tag{2.53}$$

which is what one would expect, considering $\rho \propto T^4$ and $(\delta\rho/\rho) = (4\delta T/T)$. The first order

contribution from massless neutrinos takes the same form, with $\mathcal{N}_0$ replacing Θ_0. We also note that the perturbations to matter of species i (dark matter and baryons) takes the simple form

$$T_0^0 = -\rho_i(1+\delta_i). \tag{2.54}$$

Thus, altogether we have at first order

$$\delta T_0^0 = -4\rho_{rad}\Theta_0 - 4\rho_{rad}\mathcal{N}_0 - \rho_{dm}\delta - \rho_b\delta_b. \tag{2.55}$$

Inserting this into the RHS of 1.3 and equation 1.14 into the LHS, we obtain the first evolution equations for photons

$$k^2\Phi + 3\frac{\dot{a}}{a}\left(\dot{\Phi} - \Psi\frac{\dot{a}}{a}\right) = 4\pi a^2\left[4\rho_{rad}\Theta_0 + 4\rho_\nu\mathcal{N}_0 + \rho_{dm}\delta + \rho_b\delta_b\right]. \tag{2.56}$$

The second evolution equation is obtained from the space-space components

$$G_j^i = \delta^{ik}\frac{(1-2\Phi)}{a^2}R_{kj} - \frac{1}{2}\delta^{ij}R. \tag{2.57}$$

From the expression for R_{ij} in equation 1.12, we can see that most of these terms are proportional to δ_{kj}, which when contracted with δ^{ik}, will produce many terms $\propto \delta_{ij}$. Therefore, G_j^i takes the form

$$G_j^i = A\,\delta_{ij} + \frac{k_ik_j(\Phi+\Psi)}{a^2} \tag{2.58}$$

where A has close to a dozen terms. The projection operator $\hat{P} = \hat{k}_i\hat{k}^j - (1/3)\delta_i^j$ can be applied to this to extract the longitudinal traceless part of the Einstein tensor G_L,

$$(G_j^i)_L = \hat{P}G_j^i = \left(\hat{k}_i\hat{k}^j - (1/3)\delta_i^j\right)\left(\frac{k^ik_j(\Phi+\Psi)}{a^2}\right) = \frac{2k^2}{3a^2}(\Phi+\Psi), \tag{2.59}$$

using that $\hat{k}_ik^i = k$ and $\delta_i^jk^ik_j = k^2$. The same operation can be carried out on the space-space component of the energy-momentum tensor which is

$$T_j^i = 3P_i = \int\frac{d^3p}{(2\pi)^3}p^2\frac{f_i(\vec{x},\vec{p})}{E(\vec{p})}. \tag{2.60}$$

We have the integral

$$\left(\hat{k}_i\hat{k}^j - (1/3)\delta_i^j\right) T_j^i = \sum g_i \int \frac{d^3p}{(2\pi)^2} \frac{p^2(\mu^2 - 1/3)}{E_i(p)} f_i(p), \tag{2.61}$$

and the term $\mu^2 - 1/3 = (2/3)\mathcal{P}_2(\mu)$, i.e. the second Legendre polynomial and the zero-order part of the distribution function has no quadrupole, so the source term is first order. The longitudinal part of the energy-momentum tensor, which is called anisotropic stress, is

$$(T_j^i)_L = -\frac{8\rho^{(0)}\Theta_2}{3}. \tag{2.62}$$

Therefore, the second evolution equation is obtained from

$$8\pi(T_j^i)_L^2 = (G_j^i)_L^2. \tag{2.63}$$

Expanding $\rho^{(0)}\Theta_2$ for photons and neutrinos (as only these species contribute at quadrupole moment),

$$-32\pi a^2(\rho_\gamma\Theta_2 + \rho_\nu\mathcal{N}_2) = k^2(\Phi + \Psi). \tag{2.64}$$

Since the quadrupole moments do not contribute significantly at early times when Compton scattering is strong, we can take $\Psi = -\Phi$ (this equality will be useful in the following sections when obtaining the power spectrum for initial fluctuations).

We now turn to deriving the Boltzmann equations for cold dark matter (CDM). Dark matter plays an important role in structure formation in most cosmological models and it is pertinent for our discussion of PBHs to understand the evolution of CDM. By definition, dark matter does not interact with any other particles in the Universe so there are no collision terms. Additionally, CDM is non-relativistic in contrast to photons. Thus equation 2.22 becomes

$$g_{\mu\nu}P^\mu P^\nu = -m^2, \tag{2.65}$$

where $E = \sqrt{p^2 + m^2}$ by the dispersion relation. We can now write down the equations for CDM analogous to equations 2.16 to 2.20 in the photons case for a massive particle with $p = E$ being the

only difference for now, so

$$P^\mu = (P^0, P^i) = \left(E(1-\Psi),\ p\hat{p}^i \frac{(1-\phi)}{a} \right). \tag{2.66}$$

Similarly, replacing p with E gives the total time derivative of the dark matter distribution function $f\,\mathrm{d}m$,

$$\frac{\mathrm{d}f_{\mathrm{dm}}}{\mathrm{d}t} = \frac{\partial f_{\mathrm{dm}}}{\partial t} + \frac{\partial f_{\mathrm{dm}}}{\partial x^i}\frac{\mathrm{d}x^i}{\mathrm{d}t} + \frac{\partial f_{\mathrm{dm}}}{\partial E}\frac{\mathrm{d}E}{\mathrm{d}t} + \frac{\partial f_{\mathrm{dm}}}{\partial \hat{p}^i}\frac{\mathrm{d}\hat{p}^i}{\mathrm{d}t}. \tag{2.67}$$

Again, after performing the same procedure as in the photon case, one obtains the collisionless Boltzmann equation for non-relativistic matter

$$\frac{\partial f_{\mathrm{dm}}}{\partial t} + \frac{\hat{p}^i}{a}\frac{p}{E}\frac{\partial f_{\mathrm{dm}}}{\partial x^i} - \frac{\partial f_{\mathrm{dm}}}{\partial E}\left[\frac{\mathrm{d}a/\,\mathrm{d}t}{a}\frac{p^2}{E} + \frac{p^2}{E}\frac{\partial \Phi}{\partial t} + \frac{\hat{p}^i p}{a}\frac{\partial \Psi}{\partial x^i} \right] = 0. \tag{2.68}$$

The key difference between this and equation 2.29 is the p/E factor which corresponds to velocity. Since for photons $p = E$ it does not appear in its Boltzmann equation. Since dark matter is non-relativistic, one can neglect its thermal motion and as such we do not have a fermionic or bosonic distribution function to perturb around as before. However, density perturbations induce velocity flows in the dark matter via the continuity equation which give rise to $p/M \sim \nu$ terms and these must be retained to linear order. Instead of assuming a form for $f\,\mathrm{d}m$, we take moments of equation 2.29. Firstly, multiply across by the phase space volume $d^3p/(2\pi)^3$ and integrate. This leads to

$$\begin{aligned} 0 = &\frac{\partial}{\partial t}\int \frac{\mathrm{d}^3p}{(2\pi)^3} f\,\mathrm{d}m + \frac{1}{a}\frac{\partial}{\partial x^i}\int \frac{\mathrm{d}^3p}{(2\pi)^3} f\,\mathrm{d}m \frac{p\hat{p}^i}{E} \\ &- \left[\frac{\mathrm{d}a/\,\mathrm{d}t}{a} + \frac{\partial \phi}{\partial t} \right] \int \frac{\mathrm{d}^3p}{(2\pi)^3} f\,\mathrm{d}m \frac{p^2}{E} - \frac{1}{a}\frac{\partial \Psi}{\partial x^i}\int \frac{\mathrm{d}^3p}{(2\pi)^3}\frac{\partial f_{\mathrm{dm}}}{\partial E}\hat{p}^i p. \end{aligned} \tag{2.69}$$

The last term can be neglected since the integral over the direction vector is non-zero only for the perturbed part of $f\,\mathrm{d}m$. This results in a product of two first order terms which constitutes a second order term. We now makes some substitutions to simplify the expression. The dark matter number density is defined as

$$n_{\mathrm{dm}} = \int \frac{\mathrm{d}^3p}{(2\pi)^3} f_{\mathrm{dm}}, \tag{2.70}$$

and the velocity is

$$\nu^i = \frac{1}{n_{\mathrm{dm}}}\int \frac{\mathrm{d}^3p}{(2\pi)^3} f_{\mathrm{dm}} \frac{p\hat{p}^i}{E}, \tag{2.71}$$

the first two terms in equation 2.69 can then be expressed in terms of these variables. In order to relate the third term to the density, we use the fact that $\mathrm{d}E/\,\mathrm{d}p = p/E$, so that

$$\int \frac{\mathrm{d}^3p}{(2\pi)^3}\frac{\partial f_{\rm dm}}{\partial E}\frac{p^2}{E} = \int \frac{\mathrm{d}^3p}{(2\pi)^3}\frac{\partial f_{\rm dm}}{\partial E}\frac{\mathrm{d}E}{\mathrm{d}p}p = \int \frac{\mathrm{d}^3p}{(2\pi)^3}\,p\frac{\partial f_{\rm dm}}{\partial E}. \tag{2.72}$$

We then perform an integration by parts,

$$\begin{aligned}\int \frac{\mathrm{d}^3p}{(2\pi)^3}\,p\frac{\partial f_{\rm dm}}{\partial E} &= \int_0^\infty \frac{\mathrm{d}p}{(2\pi)^3}(4\pi p^2)p\,\frac{\partial f_{\rm dm}}{\partial p} = \frac{4\pi}{(2\pi)^3}\int_0^\infty \mathrm{d}p\,p^3\frac{\partial f_{\rm dm}}{\partial p},\\ &= -3\left(\frac{4\pi}{(2\pi)^3}\right)\int_0^\infty \mathrm{d}p\,p^2 f_{\rm dm} = -3\,n_{\rm dm}.\end{aligned} \tag{2.73}$$

So, putting these together into equation 2.69 gives

$$0 = \frac{\partial n_{\rm dm}}{\partial t} = \frac{1}{a}\frac{\partial(n_{\rm dm}\nu^i)}{\partial x^i} + 3\left[\frac{\mathrm{d}a/\,\mathrm{d}t}{a} + \frac{\partial\Phi}{\partial t}\right]n_{\rm dm}. \tag{2.74}$$

The first two terms correspond to the standard continuity equation for fluid mechanics and the final term arises due to our use of the FLRW metric and its perturbations. We now collect the zero order and first order terms of equation 2.74. The velocity is first order, as is Φ, so the only zero order terms are

$$\frac{\partial n^{(0)}_{\rm dm}}{\partial t} + 3\frac{\mathrm{d}a/\,\mathrm{d}t}{a}n^{(0)}_{\rm dm} = 0 \tag{2.75}$$

where, as usual, the subscript (0) denotes homogeneous zeroth order terms. An aside is that this can be written equivalently as

$$\frac{\mathrm{d}}{\mathrm{d}t}\left(n^{(0)}_{\rm dm}a^3\right) = 0 \implies n^{(0)}_{\rm dm} \propto a^{-3}, \tag{2.76}$$

which is an expected property of the expanding Universe.

Now, we extract the first order part of equation 2.74. All factors of $n_{\rm dm}$ multiplying the first order quantities ν and Φ may be set to $n^{(0)}_{\rm dm}$. Everywhere else, we need to expand $n_{\rm dm}$ out to include a first order perturbation. In particular, we set $n_{\rm dm} = n^{(0)}_{\rm dm}\,[1+\delta(\vec{x},t)]$ which defines the first order piece as $n^{(0)}_{\rm dm}\delta$. Since the energy density of matter is equal to mass $\times n$, δ is also the fractional overdensity, i.e. $\delta\rho/\rho = \delta$. The first order equation becomes

$$0 = n^{(0)}_{\rm dm}\frac{\partial\delta}{\partial t} + \frac{1}{a}\frac{\partial(n_{\rm dm}\nu^i)}{\partial x^i} + {n^{(0)}_{\rm dm}}^3\frac{\partial\Phi}{\partial t}. \tag{2.77}$$

then dividing across by $n^{(0)}_{\rm dm}$ we obtain the first evolution equation

$$0 = \frac{\partial \delta}{\partial t} + \frac{1}{a}\frac{\partial \nu^i}{\partial t} + 3\frac{\partial \Phi}{\partial t}. \tag{2.78}$$

To obtain a second evolution equation, we now take the second moment of equation 2.68. This is done by multiplying equation 2.68 across by

$$\int \frac{\mathrm{d}^3 p}{(2\pi)^3}\frac{p}{E}\hat{p}^i, \tag{2.79}$$

which gives the first moment equation,

$$\begin{aligned} 0 =& \frac{\partial}{\partial t}\int \frac{\mathrm{d}^3 p}{(2\pi)^3}\, f_{\rm dm}\frac{p\hat{p}^j}{E} + \frac{1}{a}\frac{\partial}{\partial x^i}\int \frac{\mathrm{d}^3 p}{(2\pi)^3}\, f_{\rm dm}\frac{\hat{p}^i\hat{p}^j}{E^2} \\ &- \left[\frac{\mathrm{d}a/\,\mathrm{d}t}{a} + \frac{\partial \Phi}{\partial t}\right]\int \frac{\mathrm{d}^3 p}{(2\pi)^3}\frac{\partial f_{\rm dm}}{\partial E}\frac{p^3\hat{p}^j}{E^2} \\ &- \frac{1}{a}\frac{\partial \Psi}{\partial x^i}\int \frac{\mathrm{d}^3 p}{(2\pi)^3}\frac{\partial f_{\rm dm}}{\partial E}\frac{p^2\hat{p}^i\hat{p}^j}{E}. \end{aligned} \tag{2.80}$$

By inspection, one can see that the first term corresponds to the time derivative of $n^{(0)}_{\rm dm}\nu^i$, while the second term can be neglected since it is second order in p/E. We take more care in simplifying the final three terms. Using that $p\partial/E\partial E = \partial/\partial p$, one can see that the third term is of order $p^2\partial/E\partial p \sim p/E$ and the last term is independent of velocity $p/E \sim \nu$. We perform the integration by parts explicitly in the third term,

$$\begin{aligned} \int \frac{\mathrm{d}^3 p}{(2\pi)^3}\,\frac{\partial f_{\rm dm}}{\partial p}\frac{p^2\hat{p}^j}{E} &= \int \frac{\mathrm{d}\Omega}{(2\pi)^3}\,\hat{p}^j\int_0^\infty \mathrm{d}p\frac{p^4}{E}\frac{\partial f_{\rm dm}}{\partial p} \\ &= -\int \frac{\mathrm{d}\Omega\hat{p}^j}{(2\pi)^3}\int_0^\infty \mathrm{d}p\, f_{\rm dm}\left(\frac{4p^3}{E} - \frac{p^5}{E^3}\right). \end{aligned} \tag{2.81}$$

The p^5/E^3 is negligible since it is higher than first order, therefore,

$$\begin{aligned} &= -\int \frac{\mathrm{d}\Omega\hat{p}^j}{(2\pi)^3}\int_0^\infty \mathrm{d}p\, f_{\rm dm}\frac{4p^3}{E} \\ &= -4\int \frac{\mathrm{d}\Omega}{(2\pi)^3}\int_0^\infty \mathrm{d}p\, f_{\rm dm}\frac{p^3}{E} = -4\int \frac{\mathrm{d}\Omega}{(2\pi)^3}\int_0^\infty \mathrm{d}p\, f_{\rm dm}p^2\left(\frac{\hat{p}^j p}{E}\right) \\ &= -4\int \frac{\mathrm{d}\Omega}{(2\pi)^3} f_{\rm dm}\nu^j = -4n_{\rm dm}\nu^j. \end{aligned} \tag{2.82}$$

The same steps carry through for the last term in equation 2.80. We also note that

$$\int \mathrm{d}\Omega\, \hat{p}^i \hat{p}^j = \delta^{ij} \frac{4\pi}{3}. \tag{2.83}$$

So considering all these terms, we write the first moment of the Boltzmann equation

$$0 = \frac{\partial (n_{\mathrm{dm}} \nu^j)}{\partial t} + 4 \frac{\mathrm{d}a/\,\mathrm{d}t}{a} n_{\mathrm{dm}} \nu^j + \frac{n_{\mathrm{dm}}}{a} \frac{\partial \Psi}{\partial x^j}. \tag{2.84}$$

This equation has no zero-order terms, which allows us to set $n_{\mathrm{dm}} \to n_{\mathrm{dm}^{(0)}}$ everywhere. Using that $\mathrm{d}(n^{(0)}_{\mathrm{dm}} a^3)/\,\mathrm{d}t = 0$ can divide across by $n^{(0)}_{\mathrm{dm}}$ to find

$$0 = \frac{\partial \nu^j}{\partial t} + 4 \frac{\mathrm{d}a/\,\mathrm{d}t}{a} \nu^j + \frac{1}{a} \frac{\partial \Psi}{\partial x^j}. \tag{2.85}$$

So we have that equations 2.80 and 2.85 govern the evolution of the density and velocity of CDM. Note that the equation for density depends on the next highest moment, the velocity. This is general: the integrated Boltzmann equation for the l^{th} moment depends on the $l+1$ moment. In principle, this process leads to a hierarchy of equations for the moments of the distribution function. By this reasoning, one might expect that the velocity equation would depend on the next highest moment, the quadrupole, of the dark matter distribution. However, it doesn't, and the reasons are grounded in the fact that dark matter is cold. We have explicitly dropped all terms of order $(p/E)^2$ and higher. These terms correspond to the higher moments of the distribution, but since we are dealing with cold, dark matter, they are irrelevant. If we were interested in dark matter particles with much smaller masses such as massive neutrinos, we would need to keep these higher moments.

Writing equations 2.80 and 2.85 in terms of conformal time η and Fourier transforming: the density equation becomes

$$\dot{\tilde{\delta}} + ik\tilde{\nu} + 3\dot{\tilde{\Phi}} = 0, \tag{2.86}$$

where one assumes the velocity is irrotational so that $\tilde{\nu}^i = (k^i/k)\tilde{\nu}$. The velocity equation is

$$\dot{\tilde{\nu}} + \frac{\dot{a}}{a}\tilde{\nu} + ik\tilde{\Psi} = 0 \tag{2.87}$$

The final components of the Universe which require a set of Boltzmann equations are electrons

and protons. Despite electrons being leptons, these particles are grouped together for their evolution equations and called baryons. Since e^- and p^+ are tightly coupled by Coulomb scattering, their overdensities have the common value

$$\frac{\rho_e - \rho_e^{(0)}}{\rho_e^{(0)}} = \frac{\rho_p - \rho_p^{(0)}}{\rho_p^{(0)}} \equiv \delta_b. \tag{2.88}$$

We will not derive the Boltzmann equations for baryons here, but only state the two resulting evolution equations:

$$\begin{aligned} \dot{\tilde{\delta}}_b + ik\tilde{\nu}_b + 3\dot{\tilde{\Phi}} &= 0 \\ \dot{\tilde{\nu}}_b + \frac{\dot{a}}{a}\tilde{\nu}_b + ik\tilde{\Psi} &= \dot{\tau}\frac{4\rho_\gamma}{3\rho_b}\left[3\tilde{\Theta}_i + \tilde{\nu}_b\right]. \end{aligned} \tag{2.89}$$

2.3 Boltzmann equations in the early Universe

Consider slightly different versions of the Einstein-Boltzmann equations for photons we have derived:

$$\dot{\Theta} + ik\mu\Theta = -\dot{\Phi} - ik_\mu\Psi + \dot{\tau}\left[\Theta_0 - \Theta + \mu\nu_b - \frac{1}{2}P_2(\mu)\Pi\right], \tag{2.90a}$$

$$\Pi = \Theta_2 + \Theta_{P_2} + \Theta_{P_0}, \tag{2.90b}$$

$$\dot{\Theta}_p + ik\mu\Theta_p = -\dot{\tau}\left[-\Theta_p + \frac{1}{2}\left(1 - P_2(\mu)\right)\Pi\right], \tag{2.90c}$$

$$\dot{\delta} + ik\nu = -3\dot{\Phi}. \tag{2.90d}$$

Note that Θ_p represents the strength of the polarisation field, sourced by Θ_2 only which is the quadrupole moment of polarisation. The term $P_2(\mu) = (3\mu^2 - 1)/2$ is proportional to the second Legendre polynomial. One of the new terms, $P_2\Theta_2/2$, accounts for the angular dependence of Compton scattering, which we was previously ignored. The monopole and dipole moments do not completely characterise the photon distribution, so one generalises to

$$\Theta_l = \frac{1}{(-i)^l}\int_{-1}^{1}\frac{\mathrm{d}\mu}{2}P_l(\mu)\Theta(\mu), \tag{2.91}$$

where $\mu = \hat{p}\cdot\hat{k}$. We now consider these equations at very early times, so that for any k-mode the wavelength ($\lambda \propto 1/k$) of the perturbation is much larger than the comoving horizon η i.e. $k\eta \ll 1$. The comoving horizon corresponds to the distance over which events can be causally connected. This

condition has the effect of simplifying the Einstein-Boltzmann equations. Consider the LHS of equation 2.90a: we have that $\dot{\Theta} \propto \Theta/\eta$ and $ik\mu\Theta \propto k\Theta$. Since $1/\eta \gg k$, it is clear that the $\dot{\Theta}$ term dominates. Therefore, we can extend this and say that all terms multiplied by k in the Boltzmann equation can be neglected at early times. Higher multipoles of the photon temperature (past the monopole) can also be ignored. The reason for this is that higher moments pertain to the small scale structure of the temperature field, however, since the perturbation wavelengths we are considering are beyond the causal horizon, the temperature field for a given observer will appear uniform, which corresponds to a monopole distribution.

Accounting for these two approximations, the perturbations to the photon temperature evolves according to

$$\dot{\Theta}_0 + \dot{\Phi} = 0, \tag{2.92}$$

which is much simpler than 2.90a. The same assumption can be made to reduce the matter overdensities equation for dark matter to

$$\dot{\delta} = -3\Phi. \tag{2.93}$$

Consider the first evolution equation for ϕ and ψ 2.56. Note that for massless neutrinos, the T_0^0 is identical inform to T_0^0 for photons

$$T_0^0 = -\rho_{\text{rad}} \left[1 + 4\Theta_0\right] = -\rho_\nu \left[1 + 4\mathcal{N}_0\right]. \tag{2.94}$$

The first term in equation 2.56 is $\propto k^2$, so it can be neglected. The two matter terms on the RHS can be ignored since the early Universe is radiation-dominated. So we're left with,

$$3\frac{\dot{a}}{a}\left(\dot{\Phi} - \frac{\dot{a}}{a}\Psi\right) = 16\pi a^2 \left(\rho_{\text{rad}}\Theta_0 + \rho_\nu \mathcal{N}_0\right). \tag{2.95}$$

In a radiation-dominated Universe $a \propto \eta$. This arises from considering the Friedmann equation for a perfect fluid as the early Universe can be approximated to behave in this way. For equation of state $P = w\rho$, $w = 1/3$ for radiation-domination and we have that in the flat Friedmann metric

$$a(t) = a_0\, t^{2/3(w+1)^{-1}} = a_0\, t^{2/3(w+1)^{-1}} = a_0\, t^{1/2} \propto \eta = \frac{a}{\dot{a}}. \tag{2.96}$$

Furthermore, considering the time-time component of the Einstein equations at zeroth order (equation 1.14), we can make write

$$\frac{16\pi\rho a^2}{3} = \frac{2}{\eta^2}. \tag{2.97}$$

Making these two substitutions, we can write

$$\frac{\dot{\Phi}}{\eta} - \frac{\Psi}{\eta^2} = \frac{2}{\eta^2}\left(\frac{\rho_{\rm rad}}{\rho}\Theta_0 + \frac{\rho_\nu}{\rho}\right)\mathcal{N}_0. \tag{2.98}$$

To simplify further, we can define the ration of neutrino energy density to the total radiation density to be

$$f_\nu = \frac{\rho_\nu}{\rho_{\rm rad} + \rho_\nu}. \tag{2.99}$$

Multiplying equation 2.98 by η^2 gives

$$\dot{\Phi}\eta - \Psi = 2\left([1 - f_\nu]\Theta_0 + f_\nu\mathcal{N}_0\right). \tag{2.100}$$

We can now eliminate both monopoles by differentiating both sides with respect to η,

$$\ddot{\Phi}\eta + \dot{\Phi} - \dot{\Psi} = -2\left(\dot{\Theta}_0 + \dot{\mathcal{N}_0}\right) = -2\dot{\Phi}, \tag{2.101}$$

since $\dot{\Theta}_0 = \dot{\mathcal{N}_0} = -\dot{\Phi}$ for these large-scale modes, as discussed after the second evolution equation 2.64. If we neglect higher order moments and let $\Phi = -\Psi$, the previous equation becomes

$$\ddot{\Phi}\eta + 4\dot{\Phi} = 0. \tag{2.102}$$

Now, setting $\Phi = \eta^p$ leads to the algebraic expression $p(p-1) + 4p = 0$, which has two solutions: $p = 0$ or $p = -3$. The latter mode is the decaying mode. If it is excited early on, it will quickly die out and have no impact on evolution. However, the $p = 0$ mode does not decay if excited and is the mode of interest here. If some mechanism can be found which excites this mode, then equation 2.101 relates the gravitational potential to the neutrino and photon overdensities,

$$\Phi = 2\left([1 - f_\nu]\Theta_0 + f_\nu\mathcal{N}_0\right). \tag{2.103}$$

Both Θ_0 and $\mathcal{N}_0$ are constant in time. In most models of structure formation, they are equal since whatever causes the perturbations tends not to distinguish between photons and neutrinos. Therefore, it is possible to set $\Theta_0(k,\eta_i) = \mathcal{N}_0(k,\eta_i)$, which leads to

$$\Phi(k,\eta_i) = -2\Theta_0(k,\eta_i), \tag{2.104}$$

where η_i is some early conformal time.

The initial conditions for matter $(\delta_{dm} + \delta_b)$ depend on the nature of primordial perturbations. Combining the derived equalities $\dot{\Phi} = \dot{\Theta}_0$ and $\dot{\delta} = -3\dot{\Phi}$ leads to

$$\delta = 3\Theta_0 + \text{constant}, \tag{2.105}$$

and for adiabatic perturbations this constant $= 0$, otherwise they are called isocurvature perturbation. Adiabatic perturbations are defined by their constant matter-to-radiation ratio everywhere, since

$$\frac{n_{\rm dm}}{n_\gamma} = \frac{n_{\rm dm}^{(0)}}{n_\gamma^{(0)}} \left[\frac{1+\delta}{1+3\Theta_0}\right]. \tag{2.106}$$

The prefactor (i.e. the ratio of zero-order number densities) is a constant in both space and time. For the ratio of matter for radiation density to be uniform, therefore, the combination inside the brackets which linearises to $1 + \delta - 3\Theta_0$ must be independent of space. So the perturbations must sum to zero,

$$\delta = 3\Theta_0 \quad \text{for adiabatic perturbations.} \tag{2.107}$$

By and large, velocities and dipole moments are negligibly small in the very early Universe. We note however that their initial conditions are

$$\Theta_1 = \mathcal{N}_1 = \frac{i\nu_b}{3} = \frac{-k\Phi}{6aH}. \tag{2.108}$$

3 Cosmological Perturbation Theory

3.1 The scalar field driving inflation and slow roll parameters

The source for inflation is taken to be a generic scalar field, $\phi(\vec{x}, t)$. A condition imposed on this field from the observed accelerating expansion of the Universe is that it must have negative pressure as the acceleration equation 1.37 tells us that $\ddot{a} > 0$ when $P < -\epsilon/3$. This is not a feature conducive to normal matter or radiation, and so the precise nature of the inflationary field remains a mystery. We will explore further the implications of negative pressure in this section. Firstly, consider the energy-momentum tensor for ϕ

$$T^{\mu}_{\nu} = g^{\mu}_{\alpha} g^{\beta}_{\nu} \frac{\partial \phi}{\partial x^{\alpha}} \frac{\partial \phi}{\partial x^{\beta}} - g^{\mu}_{\nu} \left(\frac{1}{2} g^{\alpha\beta} \frac{\partial \phi}{\partial x^{\alpha}} \frac{\partial \phi}{\partial x^{\alpha}} + V(\phi) \right), \tag{3.1}$$

where $V(\phi)$ is the potential for the field. We can decompose the scalar field into a zeroth-order homogeneous part (independent of position) and a perturbation,

$$\phi(\vec{x}, t) = \phi^{(0)}(t) + \delta\phi(\vec{x}, t). \tag{3.2}$$

We will only discuss properties of the $\phi^{(0)}$ field and will address the perturbed part in the next section. Only the time derivatives are relevant for the homogeneous part, and so we set $\alpha = \beta = 0$ in equation 3.1 and obtain

$$T^{(0)\mu}_{\nu} = -g^{\mu}_{0} g^{0}_{\nu} \left(\frac{d\phi^{(0)}}{dt} \right)^2 + g^{\mu}_{\nu} \left(\frac{1}{2} g^{\alpha\beta} \left(\frac{\partial \phi^{(0)}}{\partial t} \right)^2 - V(\phi^{(0)}) \right). \tag{3.3}$$

Using that $T^{0}_{0} = -\rho$, we obtain the expression for energy density

$$\rho = \frac{1}{2} \left(\frac{d\phi^{(0)}}{dt} \right)^2 + V(\phi^{(0)}), \tag{3.4}$$

which we note resembles that of the single particle moving in a potential. The pressure for the homogeneous field is given by the space-space components of equation 3.3,

$$P = \frac{1}{2} \left(\frac{d\phi^{(0)}}{dt} \right)^2 - V(\phi^{(0)}). \tag{3.5}$$

By inspection, we see that negative pressure implies the potential energy exceeds the kinetic energy

of the field configuration. The field can find itself trapped in a false (local) minimum of the potential (Mexican hat shaped curve). This also suggests another strange feature of the inflationary field; its energy density remains constant in time since it is effectively the potential. In contrast, the densities of ordinary matter decrease quickly as the Universe expands. Therefore, considering the time-time component of the zeroth-order Einstein equations, we can obtain an expression for the evolution of the scale factor,

$$\frac{1}{a}\frac{da}{dt} = \sqrt{\frac{8\pi\rho}{3}} = \text{constant}, \tag{3.6}$$

which defines the Hubble constant H. We can use this to write an expression for the primordial comoving horizon generated between the beginning of inflation t_b and the end of inflation t_e,

$$\eta_{\text{prim}} = \int_{t_b}^{t_e} dt \frac{H}{H_e a_e} e^{-H(t-t_e)} = \frac{1}{H_e a_e}\left(e^{H(t_e-t_b)} - 1\right). \tag{3.7}$$

The only way for the field to reach its true minimum (i.e. the global vacuum state) is to tunnel quantum mechanically through the potential barrier. Initially small localised regions tunnel from the false to the true vacuum, forming bubbles of the true vacuum state. For the Universe to move to the true vacuum state, these bubbles would have to coalesce. However, it has been shown that this would not happen, and that the regions of false vacuum would expand rapidly and remain, so that the true vacuum state of the Universe would never be attained. To avoid the problem of the vacuum never reaching its ground state, the requirement that the scalar field rolls slowly towards the true vacuum was imposed. The energy density of such a field is also very close to being constant, so it quickly dominates.

To determine the evolution of the homogeneous part of the field $\phi^{(0)}$ when the field is not trapped we use the zeroth order time-time and space-space components of the Einstein equations

$$\left(\frac{da/dt}{a}\right)^2 = \frac{8\pi\rho}{3} \tag{3.8}$$

$$\frac{d^2a/dt^2}{a} + \frac{1}{2}\left(\frac{da/dt}{a}\right)^2 = -4\pi P. \tag{3.9}$$

Consider the former equation. If the dominant component in the Universe is ϕ, then the energy density on the RHS becomes that of equation 3.4. Substituting this into the expression 3.8 and differentiating,

we obtain

$$2\frac{da/dt}{a}\left[\frac{d^2a/dt^2}{a}-\left(\frac{da/dt}{a}\right)^2\right]=\frac{8\pi}{3}\left[\left(\frac{d\phi^{(0)}}{dt}\right)\frac{d^2\phi^{(0)}}{dt^2}+V'\frac{d\phi^{(0)}}{dt}\right], \tag{3.10}$$

where V' is defined as the derivative of V with respect to the zeroth order scalar field. Subtracting equation 3.8 multiplied by a factor of two from equation 3.9 gives

$$\frac{d^2a/dt^2}{a}=-4\pi\left(\frac{\rho}{3}+P\right), \tag{3.11}$$

which can replace the corresponding first term on the LHS of equation 3.10, whilst the second term can be replaced by equation 3.8. Therefore, we have

$$\frac{da/dt}{a}8\pi\left(-\frac{\rho}{3}-P-\frac{2\rho}{3}\right)=-8\pi H\left(\frac{d\phi^{(0)}}{dt}\right)^2. \tag{3.12}$$

Equating this to the RHS and converting to conformal time $dt = ad\eta$ gives the evolution equation for the homogeneous scalar field in an expanding Universe

$$0=\ddot{\phi}^{(0)}+2aH\dot{\phi}^{(0)}+a^2V' \tag{3.13}$$

The most popular models of inflation are called slow roll models in which the zeroth order field (and hence the Hubble rate), vary slowly. Therefore, during inflation, we can approximate H to be a constant. This leads to the comoving horizon being defined as

$$\eta\simeq\frac{1}{H}\int_{a_e}^{a}\frac{da}{a^2}\simeq-\frac{1}{aH}, \tag{3.14}$$

where the final term arises from the fact that the scale factor is much bigger at the end of inflation than in the middle, $a_e \gg a$. As discussed in section 2.1, slow roll inflation is parametrised by two variables which vanish in the limit that ϕ is constant and are both much less than one. Analogous to equations 2.12, we can write the first slow roll parameter in terms of the Hubble parameter,

$$\epsilon_v\equiv-\frac{\dot{H}}{aH^2}. \tag{3.15}$$

Since H is always decreasing, ϵ_v is always positive. During inflation, ϵ is small, whereas during the

radiation era it has a value of 2. The other slow roll parameter is

$$\eta_v \equiv -\frac{1}{H}\left(\dot{\phi}^{(0)}\right)^{-1}\left[aH\dot{\phi}^{(0)} - \ddot{\phi}^{(0)}\right], \tag{3.16}$$

which, after using equation 3.13, becomes

$$\eta_v = \frac{1}{H}\left(\dot{\phi}^{(0)}\right)^{-1}\left[3aH\dot{\phi}^{(0)} + a^2V'\right]. \tag{3.17}$$

3.2 Power spectrum of initial fluctuations

We work towards providing an expression for the perturbation spectrum of Ψ, the perturbation to the time-time component of the flat FLRW metric. In this section, we assume Φ and Ψ are of the same order of magnitude. Firstly, the perturbation spectrum for the generic scalar field ϕ driving inflation is calculated, neglecting Ψ. This $\delta\phi$ spectrum will be used to produce the spectrum for Ψ; the justifications for doing so will be given in due course.

We aim to find an equation for the perturbation $\delta\phi$ of equation 3.2 in the presence of a flat, smoothly expanding Universe,

$$ds^2 = -dt^2 + a(t)^2\delta_{ij}dx^i dx^j. \tag{3.18}$$

Consider the conservation equations for the stress-energy tensor T^μ_ν,

$$\nabla_\mu T^\mu_\nu = \partial_\mu T^\mu_\nu + \Gamma^\mu_{\alpha\mu}T^\alpha_\nu - \Gamma^\alpha_{\nu\mu}T^\mu_\alpha. \tag{3.19}$$

The $\nu = 0$ components of this equation to linear order give us an expression for $\delta\phi$. Since we are assuming a smooth metric, the only contributions are from the perturbed stress-energy tensor, not the metric curvature. Therefore, we use the Christoffel symbols for the flat FLRW metric,

$$\begin{aligned}\Gamma^0_{ij} &= \delta_{ij}a^2H \\ \Gamma^i_{0j} &= \Gamma^i_{0j} = \delta_{ij}H\end{aligned} \tag{3.20}$$

with all other components being zero. Expanding out equation 3.19 with $\nu = 0$ (including terms

only with non-zero Christoffel symbols),

$$\begin{aligned}\nabla_\mu T_0^\mu &= \frac{\partial}{\partial x^\mu}\left(\delta T_0^\mu\right) + \Gamma_{0i}^i T_0^0 + \Gamma_{0i}^0 T_0^i - \Gamma_{0i}^i T_i^i - \Gamma_{0i}^0 T_0^i, \\ &= \frac{\partial}{\partial t}\left(\delta T_0^0\right) + \frac{\partial}{\partial x^i}\left(\delta T_0^i\right) + \Gamma_{0i}^i T_0^0 - \Gamma_{0i}^i T_i^i,\end{aligned} \tag{3.21}$$

and substituting the partial derivative with respect to x^i with the Fourier space equivalent, using the convention that $\Psi(\vec{x}) = \tilde{\Psi}(\vec{k})$, and using equation 3.20,

$$0 = \partial_t\left(\delta T_0^0\right) + ik_i\left(\delta T_0^i\right) + 3H\delta T_0^0 - H\delta T_i^i. \tag{3.22}$$

Now we compute each of the perturbed stress-energy tensor components. Considering T_ν^μ for the full scalar field

$$T_\nu^\mu = g^{\mu\alpha}\partial_\alpha\phi\,\partial_\nu\phi - g_\nu^\mu\left(\frac{1}{2}g^{\alpha\beta}\partial_\alpha\phi\,\partial_\beta\phi + V(\phi)\right), \tag{3.23}$$

we can calculate the T_0^i components using the fact that the time-space components are zero for the metric, so

$$\begin{aligned}T_0^i &= g^{i\nu}\partial_\nu\,\partial_0\phi - g_0^i\left(\frac{1}{2}g^{\alpha\beta}\partial_\alpha\beta + V(\phi)\right), \\ T_0^i &= g^{ij}\partial_j\,\partial_0\phi,\end{aligned} \tag{3.24}$$

where $g^{ij} = \delta^{ij}a^{-2}$. Letting $\phi = \phi^{(0)}(t) + \delta\phi(\vec{x},t)$, we have $\partial_i\phi^{(0)}(t) = 0$ and

$$\partial_i\phi = \partial_i\left(\delta\phi(\vec{x},t)\right) = ik_i\delta\phi. \tag{3.25}$$

By setting all other factors to their zero-order values and noting that $\partial_0\phi = \partial_0\phi^{(0)} = \dot{\phi}^{(0)}/a$, where the dot denotes differentiating with respect to conformal time η, we obtain the expression for δT_0^i

$$\delta T_0^i = \frac{ik_i}{a^3}\dot{\phi}^{(0)}\delta\phi. \tag{3.26}$$

Now, to calculate δT_0^0, expand equation 3.23 for $\mu = \nu = 0$,

$$T_0^0 = g^{00}\left(\partial_0\phi\right)^2 - \frac{1}{2}g_0^0 g^{\alpha\beta}\partial_\alpha\phi\partial_\beta\phi - g_0^0 V, \tag{3.27}$$

where $g_0^0 = g^{00}g_{00} = (-1)(-1) = 1$. Expanding the scalar field into its components,

$$T_0^0 = -\frac{1}{2}\left(\partial_0\phi^{(0)} + \partial_0(\delta\phi)\right)^2 - \frac{1}{2a^2}\partial_i(\delta\phi)\partial_i(\delta\phi) + V\left(\partial_0\phi^{(0)} + \partial_0(\delta\phi)\right). \tag{3.28}$$

Keeping terms of first order in $\delta\phi$ and Taylor expanding the potential as a zero-order term plus a first-order correction,

$$V = V(\phi^{(0)}) + V'\delta\phi, \tag{3.29}$$

where the dash represents differentiation with respect to coordinate time t, we obtain,

$$\delta T_0^0 = -\frac{1}{2}\left(2\,\partial_0\,\phi^{(0)}\,(\partial_0(\delta\phi))\right) - V'\delta\phi, \tag{3.30}$$

substituting $\partial_0 = 1/a\,d\eta$,

$$\delta T_0^0 = -\frac{\dot{\phi}^{(0)}\delta\dot{\phi}}{a^2} - V'\delta\phi. \tag{3.31}$$

We compute δT_j^i in a similar manner,

$$T_j^i = g^{ik}(\partial_k\phi)(\partial_j\phi) - g_j^i\left(\frac{1}{2}g^{\mu\nu}\partial_\mu\partial_\nu + V(\phi)\right), \tag{3.32}$$

where $g^{ik} = \delta^{ik}a^{-2}$ and $g_j^i = g^{ik}g_{kj} = \delta_j^i$. Inserting the expansion for the scalar field, keeping terms to first order in $\delta\phi$ and Taylor expanding the potential as before, we obtain

$$\delta T_j^i = \delta_{ij}\left(\frac{\dot{\phi}^{(0)}\delta\dot{\phi}}{a^2} - V'\delta\phi\right). \tag{3.33}$$

Substituting equations 3.26, 3.30 and 3.33 into equation 3.22 gives

$$\begin{aligned} 0 = {} & \frac{\partial}{\partial t}\left(-\frac{\dot{\phi}^{(0)}\delta\dot{\phi}}{a^2} - V'\delta\phi\right) + ik_i\left(\frac{ik_i}{a^3}\dot{\phi}^{(0)}\delta\phi\right) \\ & + 3H\left(-\frac{\dot{\phi}^{(0)}\delta\dot{\phi}}{a^2} - V'\delta\phi\right) - H\left(\frac{\dot{\phi}^{(0)}\delta\dot{\phi}}{a^2} - 3V'\delta\phi\right). \end{aligned} \tag{3.34}$$

Transferring from coordinate to conformal time, multiplying by a^3 and noting that since $V' = V'(\phi^{(0)})$,

$\partial_\eta V' = V''\dot{\phi}^{(0)}$,

$$\begin{aligned} 0 = a^3 \left(\frac{\phi^{(0)}\delta\dot{\phi} + \dot{\phi}^{(0)}\delta\ddot{\phi}}{a^3} - \frac{V''}{a}\dot{\phi}^{(0)}\delta\phi - \frac{V'}{a}\delta\dot{\phi} \right) + (k_i)^2\dot{\phi}^{(0)}\delta\phi \\ - 3Ha\dot{\phi}^{(0)}\delta\dot{\phi} - 3Ha^3V'\delta\phi - Ha\dot{\phi}^{(0)}\delta\dot{\phi} + 3Ha^3V'\delta\phi. \end{aligned} \tag{3.35}$$

Collecting terms,

$$\begin{aligned} 0 = -\dot{\phi}^{(0)}\delta\ddot{\phi} + \delta\dot{\phi}\left(-\ddot{\phi}^{(0)} - a^2V' - 4aH\dot{\phi}^{(0)}\right) \\ + \delta\phi\left(-a^2V''\dot{\phi}^{(0)} - k^2\dot{\phi}^{(0)}\right). \end{aligned} \tag{3.36}$$

The V'' term is typically small (same order of magnitude as slow roll inflation parameters), so it can be neglected. The second set of terms with coefficient $\delta\dot{\phi}$ can be decomposed into the evolution equation for $\phi^{(0)}$ in an expanding Universe

$$\begin{aligned} -\ddot{\phi}^{(0)} - a^2V' - 4aH\dot{\phi}^{(0)} &= -\left(\ddot{\phi}^{(0)} + a^2V' + 4aH\dot{\phi}^{(0)}\right) - 2aH\dot{\phi}^{(0)}, \\ &= -2aH\dot{\phi}^{(0)}, \end{aligned} \tag{3.37}$$

as the evolution equation in brackets is equal to zero. After these considerations, factoring out $-\dot{\phi}^{(0)}$ and letting $H = \dot{a}/a$, we obtain

$$0 = \delta\ddot{\phi} + 2\dot{a}\delta\dot{\phi} + k^2\delta\phi. \tag{3.38}$$

In order to derive the power spectrum of fluctuations for $\delta\phi$, we must quantise the field and get this equation in the form of the harmonic oscillator by making the change of variables

$$h = \delta\phi,\ \tilde{h} = ah. \tag{3.39}$$

Taking the first and second derivatives

$$\begin{aligned} \dot{h} &= \frac{\dot{\tilde{h}}}{a} - \frac{\dot{a}}{a^2}\tilde{h}, \\ \ddot{h} &= \frac{\ddot{\tilde{h}}}{a} - 2\frac{\dot{a}}{a^2}\dot{\tilde{h}} - \frac{\ddot{a}}{a^2}\tilde{h} + 2\frac{\dot{a}^2}{a^3}\tilde{h}, \end{aligned} \tag{3.40}$$

and inserting these into equation 3.38, we obtain the typical form of the harmonic oscillator without

a damping term

$$0 = \frac{1}{a}\left[\ddot{\tilde{h}} + \left(k^2 - \frac{\ddot{a}}{a}\right)\tilde{h}\right], \tag{3.41}$$

for which we can write down an expression for the quantum operator

$$\hat{\tilde{h}}(\vec{k},\eta) = \nu(\vec{k},\eta)\hat{a}_{\vec{k}} + \nu^*(\vec{k},\eta)\hat{a}^\dagger_{\vec{k}} \tag{3.42}$$

where the coefficients of the creation and annihilation operators satisfy

$$0 = \ddot{\nu} + \left(k^2 - \frac{\ddot{a}}{a}\right)\nu. \tag{3.43}$$

The variance of perturbations in the field $\tilde{h}$ can be written as

$$\langle \hat{\tilde{h}}^\dagger(\vec{k},\eta)\hat{\tilde{h}}(\vec{k'},\eta)\rangle = |\nu(\vec{k},\eta)|^2(2\pi)^3\delta^3(\vec{k}-\vec{k'}) \tag{3.44}$$

where we have used that $\hat{a}_{\vec{k}}|0\rangle = 0$ and $\langle 0|\hat{a}^\dagger_{\vec{k}} = 0$ and the commutator relation between the annihilation and creation operators with $\langle 0|0\rangle = 1$. Recalling that $\tilde{h} = ah$,

$$\langle \hat{h}^\dagger(\vec{k},\eta)\hat{h}(\vec{k'},\eta)\rangle = |\nu(\vec{k},\eta)|^2(2\pi)^3\delta^3(\vec{k}-\vec{k'}), \tag{3.45}$$

from which we define the power spectrum of the primordial density fluctuations

$$P_h(k) = \frac{|\nu(\vec{k},\eta)|^2}{a^2}. \tag{3.46}$$

We aim to find an expression for the numerator of the RHS of equation 3.46 by solving equation 3.43. To simplify matters, we find an alternative linear expression for $\ddot{a}/a$. Recall that in slow roll inflation, the Hubble rate varies slowly, so it can be treated as a constant in certain scenarios. we can then write the conformal time (comoving horizon) as

$$\eta \equiv \int_{a_e}^{a} \frac{da}{Ha^2} \simeq \frac{1}{H}\int_{a_e}^{a}\frac{da}{a^2} \simeq -\frac{1}{aH}, \tag{3.47}$$

where a_e is the scale factor at the end of inflation, where $a_e \gg a$ so $1/a_e \to 0$. Now, using that

$H \simeq -1/a\eta$ we have $\dot{a} = a^2 H \simeq -a/\eta$. Taking the second derivative,

$$\frac{\ddot{a}}{a} \simeq \frac{2}{\eta^2}. \tag{3.48}$$

Substituting this into equation 3.43,

$$0 = \ddot{\nu} + \left(k^2 - \frac{2}{\eta^2}\right)\nu. \tag{3.49}$$

Considering that the initial conditions required to solve this equation come from the very early Universe before inflation, we take $-\eta$ to be very large ($-\eta \simeq \eta_p rim$), so that the k^2 term dominates and we now have the form of a simple harmonic operator:

$$0 = \ddot{\nu} + k^2\nu. \tag{3.50}$$

The properly normalised general solution of the familiar homogeneous PDE in equation 3.49 is

$$\nu_1 = \frac{e^{-ik\eta}}{\sqrt{2k}}, \tag{3.51}$$

to which we can add the peculiar solution $\nu_2 = \nu_1 f(\eta)$ of the non-homogeneous equation where one can work out that $f(\eta) = -i/k\eta$. The full general solution is

$$\nu = \frac{e^{-ik\eta}}{\sqrt{2k}}\left(1 - \frac{i}{k\eta}\right), \tag{3.52}$$

which is accurate for modes well within the horizon, $k|\eta| \gg 1$. After inflation has worked for many e-folds, $k|\eta|$ becomes very small. Since η is normalised, we can calculate its amplitude by taking $(-k\eta) \to 0$ in the equation above,

$$\lim_{-k\eta\to 0} \nu(k,\eta) = \lim_{-k\eta\to 0}\left(\frac{e^{-ik\eta}}{\sqrt{2k}} - \frac{e^{-ik\eta}}{\sqrt{2k}}\frac{i}{k\eta}\right) = \frac{1}{\sqrt{2k}}\frac{-i}{k\eta}. \tag{3.53}$$

Once $(-k\eta) < 1$, the mode leaves the horizon, after which $h = \delta\phi$ remains constant. The primordial power spectrum of equation 3.46 is therefore constant in time after inflation has stretched

the mode to be larger than the horizon. Substituting

$$|\nu(k,\eta)|^2 = \left|\frac{1}{\sqrt{2k}}\frac{-i}{k\eta}\right|^2 = \frac{1}{2k^3\eta^2}, \tag{3.54}$$

into the power spectrum equation 3.46, letting $h = \delta\phi$ once again, we obtain

$$\mathcal{P}_{\delta\phi}(k) = \frac{1}{2k^3\eta^2 a^2} \simeq \frac{H^2}{2k^3}, \tag{3.55}$$

where we have used that $\eta^2 \simeq 1/H^2a^2$ in slow roll inflation. Since H varies very slowly during inflation, the scalar power spectrum is also nearly (but not exactly) scale-invariant. This is a central tenet of observational predictions of inflation.

We must now recognise that to derive this formula, metric perturbations Φ and curvature perturbations Ψ were ignored. To see why this approximation was valid, we include metric perturbations in the perturbed energy conservation of equation 3.22. In order to do so, we require the first order perturbation to the Christoffel symbol $\Gamma^i_{0j} = \delta_{ij}\partial_0\Psi$. Recalling that $T^0_0 = -\rho$ and $T^i_j = \delta^i_j P$, equation 3.21 becomes

$$\begin{aligned} 0 &= -\delta_{ij}(\partial_0\Psi)\rho - (\partial_0\Psi)3P, \\ &= -3(\rho + P)\frac{\partial\Psi}{\partial t}. \end{aligned} \tag{3.56}$$

Equating the above expression with the LHS of equation 3.22,

$$\partial_t\left(\delta T^0_0\right) + ik_i\left(\delta T^i_0\right) + 3H\delta T^0_0 - H\delta T^i_i = -3(P+\rho)\frac{\partial\Psi}{\partial t}, \tag{3.57}$$

where P and ρ are the zero-order pressure and energy density respectively **(from scalar field section). The decision to neglect Ψ in the derivation of $P_{\delta\phi}$ is justified if the individual terms on the RHS are significantly smaller than the terms on the LHS of the above expression. Taking the first term on the LHS as an example, we require that

$$\Psi \ll \frac{\delta T^0_0}{P+\rho}. \tag{3.58}$$

We can prove this by inspecting the time-time component of the Einstein equations 1.14. To simplify matters, we can let $\Phi = -\Psi$ as they are of the same order of magnitude and differ by a sign in the metric. We can also insert dots denoting differentiating with respect to η, where $\partial_\eta = a\,\partial_t$.

Multiplying across by $a^2/2$ and setting $G = 1$, we have

$$k^2\Psi + 3aH(\dot{\Psi} + aH\Psi) = 4\pi a^2 \delta T^0_0. \tag{3.59}$$

Recalling that $k \simeq 1/\eta$ for modes which are crossing the horizon, we can see that for such modes the LHS of the above equation is of leading order $k^2\Psi \sim (aH)^2\Psi$. So by this argument, we have

$$4a^2H^2\Psi + 3aH\dot{\Psi} \sim 4\pi a^2 \delta T^0_0. \tag{3.60}$$

Rearranging and dropping the term $3aH\dot{\Psi} < 4a^2H^2\Psi$, we can write

$$\Psi \sim \frac{\pi \delta T^0_0}{H^2} \sim \frac{\delta T^0_0}{\rho}, \tag{3.61}$$

where the last equality arises from the definition of Ψ. Equivalently, we can write

$$\Psi \sim \frac{P+\rho}{\rho}\left(\frac{\delta T^0_0}{P+\rho}\right). \tag{3.62}$$

By the requirement of equation 3.58, this implies that $(P+\rho)/\rho$ must be small. Indeed, during inflation in the slow roll model $P < -\rho/3$, so that the maximum value of $(P+\rho)/\rho$ is $2/3$.

We were careful to make the preceding argument for modes which had not yet passed outside of the horizon by setting $k \simeq 1/\eta$. Super-horizon modes require a more subtle justification as the condition of equation 3.58 will break down sometime before the end of inflation. This can be seen from recalling the time-time component for the energy-momentum tensor in the radiation-dominated early Universe,

$$T^0_0 = \rho_r(1 + 4\Theta_0) \tag{3.63}$$

which leads to $\delta T^0_0 = -\rho_r\Theta_0$ and $(P+\rho) = 4\rho_r/3$ (from $d\Psi/dt \sim \Theta_0$). Therefore, after inflation, equation 3.58 becomes $\Psi \ll -3\Theta_0$. However, from Einstein-Boltzmann equation at early times 2.104, $\Psi(k,\eta_i) = -2\Theta_0(k,\eta_i)$. This contradicts the previous statement which shows that the requirement on Ψ will break down before the end of inflation; at some point, the perturbations to Ψ must grow in importance relative to those in the energy-momentum tensor. In order deal with this coupling between

perturbations, we introduce the primordial curvature perturbation

$$\zeta = -\frac{ik_i \delta T_i^0 H}{k^2(\rho + P)} - \Psi. \tag{3.64}$$

For sub-horizon modes and those which have just left the horizon, Ψ is negligible, so this can be set to zero. Furthermore, by inserting $\rho + P = (\dot{\phi^{(0)}}/a)^2$ from equation 2.7 (with inclusion of scale factor), and equation 3.26 into ζ for its value at the time of horizon crossing,

$$\zeta = -\frac{aH\delta\phi}{\dot{\phi}^{(0)}}. \tag{3.65}$$

This term is often called the comoving curvature perturbation and can be denoted by $\mathcal{R}$. Since $ik_i\delta T_i^0 = 4ak\rho_r\Theta_1$ which is proportional to the dipole Θ_1 of inflation, and $P = \rho/3$ for radiation, we obtain that after inflation

$$\zeta = -\frac{3aH}{k}\Theta_1 - \Psi = -\frac{3}{2}\Psi, \tag{3.66}$$

where the last term is calculated using $\Theta_1 = k\Psi/6aH$ from equation 2.108. The key feature of the curvature perturbation ζ is that it is conserved when the perturbations pass outside the horizon, i.e. on super-horizon scales. To show this, consider again the conservation equation with metric perturbations from equation 3.57. On large scales, $k_i\delta T_0^i \propto k^2$ and since k is small for super-horizon modes, this term is made negligible. So we're left with

$$\frac{\partial}{\partial t}\left(\delta T_0^0\right) + 3H\delta T_0^0 - H\delta T_i^i = -3(P+\rho)\frac{\partial\Psi}{\partial t}, \tag{3.67}$$

which we want to get in terms of ζ and δT_0^0 only. To obtain an expression for ζ in terms of δT_0^0, we consider the time-time and time-space components of the perturbed Einstein equations 3.24 which imply that

$$\begin{aligned} \delta T_i^0 &= \frac{ik_i}{4\pi}\left(\frac{\dot{\Phi}}{a} - H\Psi\right), \\ \delta T_0^0 &= -\frac{3}{4\pi}H\Phi + \frac{3}{4\pi}H^2\Psi - \frac{k^2\Phi}{4\pi a^2}. \end{aligned} \tag{3.68}$$

Using the former to obtain an expression for Ψ

$$\Psi = \frac{4i\pi\delta T_0^i}{Hk_i} + \frac{\dot{\Phi}}{aH}. \tag{3.69}$$

Inserting this into δT^0_0, rearranging to make δT^0_i the object and taking the large-scale limit (ignoring perturbation fields), we obtain

$$\delta T^0_i = \frac{k^2}{3ik_i H \delta T^0_i}, \tag{3.70}$$

which, when inserted into equation 3.66 gives the expression for Ψ

$$\Psi = -\zeta - \frac{1}{3}\frac{\delta T^0_0}{(\rho + P)}. \tag{3.71}$$

Inserting this into equation 3.67

$$\begin{aligned}\frac{\partial}{\partial t}\left(\delta T^0_0\right) + 3H\delta T^0_0 - H\delta T^i_i = 3(\rho + P)\frac{\partial \zeta}{\partial t} + \frac{\partial}{\partial t}(\delta T^0_0) \\ - \frac{1}{(\rho + P)}\left(\frac{\partial \rho}{\partial t} + \frac{\partial P}{\partial t}\right).\end{aligned} \tag{3.72}$$

We can see the derivatives of δT^0_0 with respect to t cancel. Using the Friedmann equation $\partial\rho/\partial t = -3H(\rho + P)$, more terms cancel and after rearranging, we're left with

$$\frac{\partial \zeta}{\partial t} = \frac{1}{3(\rho + P)^2}\left[\frac{1}{3}\frac{\partial \rho}{\partial t}\delta T^i_i + \frac{\partial P}{\partial t}\delta T^0_0\right]. \tag{3.73}$$

By taking out $d\rho/dt$, the terms in the square brackets take the form

$$\frac{\delta T^i_i}{3} + \frac{dP}{d\rho}\delta T^0_0 = \delta P - \frac{dP}{d\rho}\delta\rho, \tag{3.74}$$

where $\delta T^i_i/3 = \delta P$ is the perturbation to the pressure and $-\delta T^0_0 = \delta\rho$ is the perturbation to the energy density. We expect that, for a given overdensity $\delta\rho$,

$$\delta P \propto \frac{dP}{d\rho}\delta\rho, \tag{3.75}$$

which is the characteristic feature of the adiabatic perturbations of inflation. Thus, ζ is indeed conserved on large scales. Since we know that after inflation $\Psi = -2\zeta/3$ and using equation 3.65, we can write that for $\delta\phi$ at horizon crossing,

$$\Psi = \left(\frac{2}{3}\frac{aH}{\dot{\phi}^{(0)}}\right)\delta\phi. \tag{3.76}$$

The post-inflation power spectrum of Ψ is related to the horizon-crossing spectrum of $\delta\phi$ by the square of the same coefficient. Using equation 3.55, we finally obtain the power spectrum for perturbations to the metric due to inflation

$$\mathcal{P}_\Psi = \frac{2}{k^3}\left(\frac{aH^2}{\dot{\phi}^{(0)}}\right)^2\Bigg|_{aH=k}. \tag{3.77}$$

In the literature, the primordial power spectrum of the comoving curvature perturbation ζ is more often used than 3.77. Since ζ is a metric-invariant variable, we can use it to convert between gauges. We have been working in the conformal Newtonian gauge, however, a convenient gauge involves letting the spacial part of the metric be unperturbed; so-called 'spacially flat slicing'. In this gauge, the power spectrum of $\delta\phi$ of equation 3.55 is the complete power spectrum at horizon crossing. Hence, we have the relation

$$\mathcal{P}_\zeta = \left(\frac{aH}{\dot{\phi}^{(0)}}\right)^2 \mathcal{P}_{\delta\phi} = \left(\frac{H}{\partial_t\phi^{(0)}}\right)^2\left(\frac{H}{2\pi}\right)^2 = \left(\frac{H^2}{2\pi\partial_t\phi^{(0)}}\right)^2\Bigg|_{aH=k} \tag{3.78}$$

The question begs; why is ζ called the curvature perturbation? During inflation, comoving hypersurfaces have the property that they coincide with the hypersurfaces over which the total inflationary field ψ is homogeneous (no $\delta\phi$). However, these hypersurfaces are not the same as the zero curvature surfaces on which $\mathcal{P}_{\delta\phi}$ holds. There is a time delay between them $\delta t = -a\delta\phi/\dot{\phi}^{(0)}$ due to the difference between comoving and conformal time coordinates. The evolution of the background field $\phi^{(0)}$ compensates for the perturbation $\delta\phi$ to give an overall smooth scalar field. The differential background expansion during this time delay means that the comoving curvature perturbation $\mathcal{R}_c$ is equivalent to the curvature perturbation on uniform density hypersurfaces ζ on large scales,

$$\mathcal{R}_c = \zeta|_{aH=k} = H\delta t. \tag{3.79}$$

3.3 Spectral index of the primordial power spectrum

As previously mentioned, the slow variation of H in the slow roll model of inflation implies that the power spectrum of the scalar field is almost scale invariant. In this section, we will derive an expression for a power-law spectrum, which is a convenient way to approximate the dependency of the perturbation spectrum on the wavenumber k, following a treatment similar to [22]. We examine the equation 3.13 and

$$H^2 = \frac{1}{3M_{pl}}\left(V(\phi^{(0)}) + \frac{2}{3}\dot{\phi}^2\right) \tag{3.80}$$

which together constitute the evolution equations of the homogeneous scalar field. Here, $M_{pl} = \sqrt{\hbar c/G}$ is the Planck mass. This equation can be derived from inserting 3.4 and 3.5 into the Friedmann and fluid equations (as in section 2.1, however note that the factors differ here) . During slow roll, the potential energy of the scalar field dominates over the kinetic energy, and so

$$H^2 \simeq \frac{1}{3M_{pl}} V(\phi^{(0)}), \tag{3.81}$$

In addition, the field evolution is limited by friction

$$\partial_t \phi^{(0)} = -\frac{V'(\phi^{(0)})}{3H}, \tag{3.82}$$

where the dash represents differentiation with respect to the homogeneous scalar field. These two equations are considered to be the simplified evolution equations for $\phi^{(0)}$. Substituting 3.82 into the final term of 3.78,

$$\mathcal{P}_\zeta(k) \simeq \left(\frac{3H^2}{2\pi V'}\right)^2 \simeq \frac{(V/M_{pl}^2)^3}{3(2\pi)^2 (V')^2} = \frac{8}{3}\left(\frac{1}{\epsilon_v}\frac{V^{1/4}}{\sqrt{3\pi} M_{pl}}\right)^4, \tag{3.83}$$

where ϵ_v is the slow roll parameter 3.15 with the substitution 3.81. The large angle CMB perturbations constrain $\mathcal{P}_\zeta(k) \sim 2x10^{-9}$ on current Hubble scales. It follows that

$$V^{1/4} \sim 6 \times 10^{16} \epsilon_v \,\text{GeV}. \tag{3.84}$$

Since $\epsilon \ll 1$, the energy scale is at least two orders of magnitude below the Planck scale ($\sim 10^{19}$ GeV), and indeed it is plausible that inflation occured around the GUT (Grand Unified Theory) scale ($\sim 10^{16}$ GeV).

One can quantify small deviations from scale-invariance by defining the scale-dependent spectral index $n_s(k)$

$$n_s(k) - 1 = \frac{\mathrm{d}\ln \mathcal{P}_\zeta}{\mathrm{d}\ln k}, \tag{3.85}$$

where the -1 on the LHS is conventional and means that the scale-free spectrum has $n_s = 1$. For a constant n_s, this definition implies a power-law spectrum

$$\mathcal{P}_\zeta = A_s \left(\frac{k}{k_{\text{pivot}}}\right)^{n_s - 1}, \tag{3.86}$$

for some pivot scale k_{pivot} used for normalisation. We can obtain an expression for n_s by noting that

$$\frac{d}{d\,lnk} = \frac{dt}{d\,lnk}\frac{d\,\phi^{(0)}}{dt}\frac{d}{d\phi^{(0)}}, \tag{3.87}$$

and since $k = aH$ at horizon crossing,

$$\frac{d\,lnk}{dt} = \frac{1}{aH}\left(\partial_t H + a\partial_t H\right) = H\left(1 + \frac{\partial_t H}{H^2}\right). \tag{3.88}$$

Using the Friedmann equation

$$\frac{\ddot{a}}{a} = -\frac{4\pi G}{3}\left(\rho + 3P\right), \tag{3.89}$$

we have that

$$\partial_t H = \frac{\ddot{a}}{a} - H^2 = -\frac{4\pi G}{3}\left(\rho + 3P\right) - H^2. \tag{3.90}$$

Now using that

$$H^2 = \frac{8\pi G}{3}\rho, \tag{3.91}$$

we have

$$\frac{\partial_t H}{H^2} = -\frac{3}{2}\left(\frac{\rho + P}{\rho}\right). \tag{3.92}$$

By the slow roll approximation 3.82, we have

$$\begin{aligned}\frac{\partial_t H}{H^2} &= \left(\frac{9(\partial_t\phi^{(0)})}{(V')^2}\right)^2\left(\frac{V'}{3\partial_t\phi^{(0)}} - \frac{\partial_t V'}{3\partial_t\phi^{(0)}}\right), \\ &\simeq \frac{3\partial_t\phi^{(0)}(V' - \partial_t V')}{V'}\end{aligned} \tag{3.93}$$

which is approximately equivalent to

$$\frac{\partial_t H}{H^2} \simeq -\frac{3}{2}\frac{(\partial_t\phi^{(0)})^2}{V} = -\frac{1}{2}\frac{(3H\partial_t\phi^{(0)})^2}{3H^2V} \simeq -\frac{M_{pl}}{2}\left(\frac{V'}{V}\right)^2 = -\epsilon_v, \tag{3.94}$$

where the last equality arises from equations 3.81 and 3.15. Inserting this into 3.88, we obtain

$$\frac{\mathrm{d}\,lnk}{\mathrm{d}t} = H(1 - \epsilon_v). \tag{3.95}$$

Therefore, to leading order in the slow roll parameters,

$$\begin{aligned}\frac{\mathrm{d}}{\mathrm{d}\,lnk} &\simeq \frac{1}{H}\frac{\mathrm{d}\phi^{(0)}}{\mathrm{d}t}\frac{\mathrm{d}}{\mathrm{d}\phi^{(0)}} \simeq -\frac{V'}{3H^2}\frac{\mathrm{d}}{\mathrm{d}\phi^{(0)}} \simeq -M_{pl}^2\frac{V'}{V}\frac{\mathrm{d}}{\mathrm{d}\phi^{(0)}} \\ &\simeq -M_{pl}\sqrt{2\epsilon_v}\frac{\mathrm{d}}{\mathrm{d}\phi^{(0)}}.\end{aligned} \tag{3.96}$$

Now we can make the convenient replacement

$$\frac{\mathrm{d}\ln\mathcal{P}_\zeta}{\mathrm{d}\,lnk} = -M_{pl}\sqrt{2\epsilon_v}\frac{\mathrm{d}(\ln\mathcal{P}_\zeta)}{\mathrm{d}\phi^{(0)}}. \tag{3.97}$$

From the curvature power spectrum in terms of slow roll parameters, we have that $\ln\mathcal{P}_\zeta = \ln V/\epsilon_v$, therefore

$$\begin{aligned}\frac{\mathrm{d}\ln\mathcal{P}_\zeta}{\mathrm{d}\,lnk} &= -M_{pl}\sqrt{2\epsilon_v}\frac{\mathrm{d}}{\mathrm{d}\phi^{(0)}}(\ln V - \ln\epsilon_v) \\ &= -M_{pl}\sqrt{2\epsilon_v}\left(\frac{V'}{V} - \frac{(\epsilon_v)'}{\epsilon_v}\right).\end{aligned} \tag{3.98}$$

Using that the slow roll parameters in terms of the potential are

$$\begin{aligned}\epsilon_v(V) &= \frac{M_{pl}^2}{2}\left(\frac{V'}{V}\right)^2 \\ \eta_v(V) &= M_{pl}^2\left(\frac{V''}{V}\right),\end{aligned} \tag{3.99}$$

we can write

$$\frac{\mathrm{d}\ln\mathcal{P}_\zeta}{\mathrm{d}\,\ln k} \simeq \frac{\sqrt{2}}{M_{pl}^2}\left(\frac{\eta_v}{\sqrt{\epsilon_v}} - 2\sqrt{\epsilon_v}\right). \tag{3.100}$$

By equating this to the LHS of (3.85), we obtain the following expression for the spectral index in terms of the slow roll parameters at first order

$$n_s(k) - 1 = 2\eta_v(\phi^{(0)}) - 6\epsilon_v(\phi^{(0)}). \tag{3.101}$$

Furthermore, it can be shown that $\mathrm{d}n_s/\,\mathrm{d}k$ is second order in slow roll parameters. Clearly, a power-law primordial density spectrum serves as a relatively good approximation for slow roll inflation. The curvature power spectrum at horizon crossing (3.78) can be written as

$$\mathcal{P}_\zeta(k) \simeq \left.\left(\frac{V^3}{12\pi^2(V^2)'}\right)\right|_{aH=k}. \tag{3.102}$$

The efficiency of this mechanism for producing curvature perturbations depends on both the height of the potential (which determines the expansion rate and hence the size of $\delta\phi$) and the slope of the potential (measured by ϵ_v), which enters through the conversion of the fluctuations to time delays and so to curvature.

4 The PBH Mass Function

4.1 From inhomogeneities to PBHs

We have obtained the power spectrum of primordial fluctuations in the inflationary era (3.77). As the Universe ages, these overdense regions accumulate matter and eventually form structures via gravitational instability. The evolution of cosmological perturbations can be split into various stages; however, we are primarily interested in the radiation era at the end of which modes re-enter the horizon.

The simplest model of PBH formation postulates that for an overdensity $\delta\rho$ to collapse, it must be roughly larger than a scale called the *Jeans length* at maximum expansion ($\sqrt{w}\times$ Horizon size). The Jeans length is defined as the critical oscillation wavelength L_J at which a small perturbation to a self-gravitating medium of uniform density becomes unstable to gravitational collapse,

$$L_J = \sqrt{\frac{\pi c_s^2}{G\rho}}, \tag{4.1}$$

where c_s is the speed of sound of pressure disturbances and $\rho = M/L^3$ is the density of the medium in question. On length scales $L < L_J$, pressure can support the gas against collapse, but when $L > L_J$, gravity overcomes pressure and the body undergoes collapse. One could say that the Jeans length defines the minimum size fragment that a medium(e.g. a cloud) can break up into. It is also the distance a sound wave travels in the collapse time [23]. Hence, at maximum expansion, we have that

$$w \lesssim \left(\frac{M}{M_H}\right)^{2/3} \delta_0 = \delta_H, \tag{4.2}$$

which also defines the density perturbation δ_H at horizon crossing. M_H is the initial mass inside the horizon and M is the mass contained in the initial volume of the overdensity. In the case of radiation-domination, this gives the value $\delta_c \simeq 1/3$. However, a more careful calculation produces the relation [24]

$$\delta_H = \frac{3(1+w)}{5+3w} \sin^2\left(\frac{\pi\sqrt{w}}{1+3w}\right). \tag{4.3}$$

which yields 0.41 in the radiation-dominated case, which is much closer to numerically calculated values. The overdensity then undergoes spherically-symmetric gravitational collapse into black holes upon re-entering the horizon. The fluctuations which formed these overdensities are assumed to have

a Gaussian distribution and form black holes of mass comparable to the horizon mass M_H at the time of formation t_i,

$$M_H \sim \frac{c^3 t}{G} \sim 10^{15} \left(\frac{t_i}{10^{-23} s} \right) g. \tag{4.4}$$

In the following chapters of this paper, we will explore the viability of this model and others to produce a sufficient abundance of black holes so as to appreciably contribute to the dark matter fraction of the Universe. This section begins with a derivation of the matter power spectrum which is then used to obtain an expression for PBH abundance $\Omega_{\rm PBH}$ by the Press-Schechter formalism. We then discuss the two forms the PBH mass function can take- monochromatic and extended- in the context of their physical plausibility and ability to produce the range of masses of interest to be contained in dark matter or to influence structure formation. Constraints imposed by two inflationary models (which deviate from the hitherto discussed slow roll approximation) on the extended mass function are also explored.

4.2 The matter power spectrum

We follow the calculation of the power spectrum of the fractional matter overdensity or density contrast Δ in [25] in the comoving gauge well after Recombination, which is defined $\Delta = \delta\rho/\rho$. The power spectra of fluctuations given so far have dimension $[k]^{-3} = m^3$. It is useful to work with the dimensionless version $\tilde{\mathcal{P}}$ defined by

$$\tilde{\mathcal{P}}_\Delta = \frac{k^3}{2\pi^2} \mathcal{P}_\Delta(k). \tag{4.5}$$

As before, we define the spectrum in terms of the expectation value

$$\tilde{\mathcal{P}} \delta(\vec{k} - \vec{k}') = \frac{k^3}{2\pi^2} \left\langle \Delta(\eta, k) \Delta^*(\eta, k) \right\rangle . \tag{4.6}$$

We also define the real space measure of matter clustering $\sigma_\Delta(R)$, which is defined to be the real space variance of Δ averaged in spheres of radius R [22],

$$\sigma_\Delta^2(R) = \int_0^\infty \frac{dk}{k} \, W^2(kR) \, \tilde{\mathcal{P}}_\Delta(k), \tag{4.7}$$

where $W(kR)$ is the volume-normalised window function which is used to smooth the density

contrast over a scale R, such that we now have smoothed Δ

$$\Delta(R,\vec{x}) = V^{-1}\int d^3\vec{x}\, W\left(\frac{|\vec{x}'-\vec{x}|}{R}\right)\Delta(\vec{x}'). \tag{4.8}$$

where V is the volume of the window function. At every point in $\vec{x}$, the smoothed expression represents the weighted average of the density contrast over a spherical region of radius R centred on $\vec{x}$. The window function is used to deal with the smearing of energy throughout the frequency domains which arises from dealing with discrete units (particle masses) as opposed to a continuum of values, i.e. it is required to compare discrete data with theories based on a fluid-like description of the cosmos. Most of these 'leakages' occur at the extremes of the time interval; the middle has a more accurate form. The window function has the effect of producing a result which ignores the values at either end of the interval and focuses on the central values. We must choose a suitable window function with the property $W(|\vec{x}'-\vec{x}|/R) = 1$ if $|\vec{x}'-\vec{x}| = 0$ and it also must fall off rapidly beyond R. We follow [25] by choosing a Gaussian window function

$$W(kR) = \exp\left(-\frac{k^2R^2}{2}\right). \tag{4.9}$$

If the inital inhomogeneities have a Gaussian perturbation profile, the probability distribution function (PDF) will also be Gaussian,

$$P(\Delta(R)) = \frac{1}{\sqrt{2\pi}\sigma_\Delta(R)}\exp\left(-\frac{\Delta^2(R)}{2\,\sigma_\Delta^2(R)}\right). \tag{4.10}$$

We note that perturbations in quantities such as matter density which are time dependent on the background are hypersurface dependent, even though the physical quantity may be a frame independent scalar in the physical spacetime. We choose to take the comoving hypersurface, on which the momentum density T_i^0 vanishes. Since the perturbation of the scalar field is proportional to T_0^i, this part vanishes and we are left with the homogeneous part $\phi^{(0)}$ only [26]. On these comving hypersurfaces, we can write a simple relation between the density and the comoving curvature perturbations $\mathcal{R}_c$ (which is equivalent to ζ on large scales) [1],

$$\Delta(t,k) = \frac{2(1+\omega)}{5+3\omega}\left(\frac{k}{aH}\right)^2\mathcal{R}_c, \tag{4.11}$$

where $\omega = P/\rho$. In the radiation era, which is of primary interest for PBH formation, $\omega = 1/3$, so we have

$$\Delta(t,k)|_{rad} = \frac{4}{9}\left(\frac{k}{aH}\right)^2 \mathcal{R}_c, \tag{4.12}$$

which we notice has the same proportionality relation as the power spectra of Ψ and ζ after inflation (can be deduced from the discussion before equation (3.77)). Then, at horizon crossing $aH = k$, we have

$$\tilde{\mathcal{P}}_\Delta(\vec{k},\eta) = \frac{4(1+\omega)^2}{(5+3\omega)^2}\tilde{\mathcal{P}}_{\mathcal{R}_c}. \tag{4.13}$$

4.3 PBH abundance

We can now work towards finding an expression for $\Omega_{\rm PBH}(\Delta_{th} > M)$, which is the fraction of the Universe which exceeds the threshold density contrast Δ_{th} for PBH formation at the time at which they form. The threshold density is currently thought to lie between 0.3 and 0.7 based on a variety of analytic and numerical calculations [25]. There are two popular approaches to calculating $\Omega_{\rm PBH}$; the Press-Schechter formalism and the theory of peaks. We shall make use of the former here, in line with [27].

The Press-Schechter prescription has three main assumptions; the mass density field is Gaussian, time evolution is linear such that $\Delta \propto t^{2/3}$ for matter, and an object is said to have collapsed when its density contrast has exceeded the threshold Δ_{th}. First consider a mass at the centre q of a spherical collapsed object of radius R with density contrast Δ. The probability that this mass is greater than the threshold mass is $P(\Delta > \Delta_{th})$. If $\Delta > \Delta_{th}$ on this scale, then there exists a radius larger than R for which $\Delta = \Delta_{th}$. Thus, the mass at the centre of region of size R must also be part of this region of larger mass. The Press-Schechter formalism equates the probability that the mass at q is contained in an object of mass $> M$ and the probability that the fraction of mass in the Universe is contained in objects $> M$,

$$P(>M) = P(\Delta > \Delta_{th}(M)). \tag{4.14}$$

However, an extra factor of two is included (often called the 'fudge' factor), which can be thought of as accounting for the fact that the PBH formation occurs in regions which are overdense with respect to the mean cosmological density [1]. The Press-Schechter prescriptions reads

$$P(>M) = 2P(\Delta > \Delta_{th}(M)). \tag{4.15}$$

In order to calculate the fraction of the Universe which exceeds the threshold for PBH formation (and hence will form a PBH with mass $> M$) one simply integrates the above formula over the relevant range,

$$\begin{aligned}\Omega_{\rm PBH}(\Delta_{th} > M) &= 2\int_{\Delta_{th}}^{\infty} P(\Delta(M))\,{\rm d}\Delta(M), \\ &= {\rm erfc}\left(\frac{\Delta_{th}}{\sqrt{2}\sigma_{\Delta}(M)}\right),\end{aligned} \tag{4.16}$$

where (4.10) is used and erfc is the complementary error function,

$${\rm erfc}(x) = \frac{2}{\sqrt{\pi}}\int_0^x dt\; e^{-t^2}. \tag{4.17}$$

We can define the value of the fraction of the mass of the Universe in PBHs on the horizon mass scale at the time of their formation t_i by $\beta(M)$,

$$\beta(M_H) = \frac{\rho_{\rm PBH}(t_i)}{\rho(t_i)}. \tag{4.18}$$

The dark matter density fraction is$f(M) = \rho(M)/\rho_{\rm CDM}$. We can also define the ratio f of the current PBH dark matter density to the current CDM density as used in [27],

$$f = \frac{\Omega_{\rm PBH}}{\Omega_{\rm CDM}} \simeq 4.8\,\Omega_{\rm PBH}, \tag{4.19}$$

where $\Omega_{\rm CDM} = 0.21$ is the current value for the ratio of the observed density of cold dark matter to the critical density of the Universe.

As an example, we assume the power-law spectrum of (3.86) for PBHs formed from scale-invariant primordial fluctuations, so that the variance

$$\begin{aligned}\sigma_{\Delta}^2 &= \int_0^{\infty} \frac{dk}{k}\, e^{-(kR)^2}\tilde{\mathcal{P}}_{\Delta}(\vec{k}) \\ &= \int_0^{\infty} \frac{dk}{k}\, e^{-(kR)^2} A_s \left(\frac{k}{k_{\rm pivot}}\right)^{n_s-1},\end{aligned} \tag{4.20}$$

for which we can use the gamma function to solve,

$$\Gamma[z] = \int_0^{\infty} {\rm d}x\, e^{-x} x^{z-1}, \tag{4.21}$$

by setting $x = (kR)^2$, becomes

$$\sigma^2_\Delta(M) = \frac{2(1+\omega)^2}{(5+3\omega)^2} A_{\mathcal{R}_c} \frac{\Gamma[(n-1)/2}{(k_0 R)^{n_s-1}}. \tag{4.22}$$

Another useful quantity to define is the function for the number of collapsed objects with mass M,

$$n(M) = M\frac{\mathrm{d}n}{\mathrm{d}M} = \frac{\rho_m}{M}\frac{\partial P}{\partial M}, \tag{4.23}$$

where ρ_m is the mean (baryonic and dark) matter density of the Universe at the time the fluctuation which formed the object had collapsed. Upon substituting the expression for $P(\Delta_{th} > M)$ of (4.10), we obtain

$$M^2 n(M) = \rho_m \nu \sqrt{\frac{2}{\pi}} \exp\left(\frac{-\nu^2}{2}\right) \left|\frac{\partial \ln \sigma_{\Delta_{th}}}{\partial \ln m}\right|, \tag{4.24}$$

where $\nu = \Delta_{th}/\sigma$.

4.4 Extended versus monochromatic mass functions

The derivation of the abundance of PBHs in the last section assumes the most simple model of PBH formation as described in section 4.1, wherein the mass of the PBH at its formation time is assumed to be uniform (about the horizon mass) and the fluctuations which formed it were of constant amplitude at the Horizon epoch. This model produces a so-called monochromatic mass function, which was implicit in the calculations of the preceding two sections. While a precisely monochromatic mass function is obviously unphysical, it serves as a good starting point for considering models which have a narrow spread of mass, such as the axion-curvaton model, and allowed us to write down some simple approximations pertaining to the PBH abundance in the previous section. However, most other (perhaps more realistic) models are not compatible with a nearly-monochromatic mass function.

As such, it is necessary to define an extended mass function which allows for the initial formation of a range of black hole masses. We follow the approach taken in [27], which is to divide the mass function into class intervals (bins) of width M, giving the number density of PBHs in the mass range $(M, 2M)$,

$$n_{\mathrm{PBH}}(M, 2M) = M\frac{\mathrm{d}n}{\mathrm{d}M} = \frac{\mathrm{d}n}{\mathrm{d}\ln M} = \frac{\mathrm{d}N_{\mathrm{PBH}}}{\mathrm{d}\ln M}. \tag{4.25}$$

For a monochromatic mass function, in which all the black holes have a mass M, the cumulative

number density $N_{\rm PBH}$ is written in terms of the Heaviside function Θ,

$$N_{\rm PBH} = n_{\rm PBH}\Theta(M-m), \tag{4.26}$$

Hence, we are essentially splitting up the extended mass function into many monochromatic mass functions. The reason for limiting the bin width to at least size M is based on constraints on mass contribution from PBHs of mass $M_* \simeq 5\times10^{14}g$, which are evaporating in the present epoch. For a monochromatic PBH mass function with initial mass $(1+\mu)M_*$ and $\mu \ll 1$, the current mass is $(3\mu)^{1/3}$, and the Galactic background constrains the fraction of the Universe going into PBHs as a function of μ. However, a precisely monochromatic initial mass function is unphysical and even a small mass range would generate a low-mass tail of PBHs below M_*. This tail would be the main contributor to the Galactic background, so we consider its form and the associated constraints for a variety of scenarios with both extended and nearly-monochromatic initial mass functions. In particular, we consider a scenario in which the PBHs form from critical collapse and have a (extended) mass function which peaks well above M_*. In this case, the largest PBHs could provide the dark matter without the M_* ones exceeding the gamma-ray background limits [28].

4.5 Effect of critical collapse on a nearly-monochromatic mass function

In section 4.3, we calculated the fraction of the mass of the Universe at the time of their formation $\beta(M)$ by assuming that all the masses were the horizon mass. We now consider the scenario wherein the most common black hole mass is that of the horizon, but PBHs of much smaller mass can be formed from spherically-symmetric collapse with the scaling formula

$$M_{\rm PBH} = KM_H(\delta-\delta_c)^\gamma, \tag{4.27}$$

where δ is greater than the threshold δ_c, and K and γ are constants. This scaling formula can be applied to a range of critical phenomena with parameter δ, however here we set it to be the overdensity $\delta\rho/\rho$ [27]. All values are determined by the nature of the fluid containing δ at horizon crossing, however the exponential factor has been shown numerically to have the value $\gamma \simeq 0.35$ for many cases from numerous studies of spherically symmetric collapse [29], and as such can be thought of as a universal parameter. For systems that exhibit universality, the closer the parameter is to its critical value, the

less sensitively the order parameter depends on the details of the system.

The scaling relation (4.27) is generally assumed only to be accurate in the neighbourhood of δ_c. However, since most black holes are expected to form with an initial overdensity δ and the probability distribution function is rapidly decreasing near $\delta = \delta_c$, the probability of having an overdensity $\gg \delta_c$ is exponentially smaller, so the scaling formula is accurate for our purposes. This rapidly declining feature of the PDF has another benefit; it allows one to estimate the mass function independently of the specific form of the PDF of the primoridal density fluctuation or curvature perturbation (which we have hitherto assumed to be Gaussian)[30]. This lack of sensitive dependence of the order parameter δ on the details of the system in question when it approaches its critical value is a result from the studies of critical phenomena [31].

In principle, one should calculate the probability of realising each initial configuration of the perturbed region (over a range of epochs) along with the mass function of the black hole formed in the region (if one forms) and then integrate each probability and mass function pair over all of configuration space to obtain the PBH initial mass function. This would be a tedious calculation. Thankfully, we can exploit the fact that the PBHs are widely considered to form with a typical mass close to the horizon mass (threshold value) to simplify the calculation by allowing it to depend on a single parameter δ as opposed to families of such parameters, as would be the case if the details of the primordial density fluctuations were accounted for.

Following the approach of [30], one can write the rapidly decreasing PDF of δ generally as

$$P(\delta)\,\mathrm{d}\delta = e^{-f(\delta)}\,\mathrm{d}\delta, \tag{4.28}$$

where f is well-behaved around $\delta \simeq \delta_c$. Then the probability $\beta(M)$ that the relevant mass scale has an amplitude of fluctuations exceeding the threshold for collapse as it crosses the horizon is

$$\beta(M) = \int_{\delta_c} P(\delta(M))\,\mathrm{d}\delta(M) = \int_{\delta_c} e^{-f(\delta(M))}\,\mathrm{d}\delta(M), \tag{4.29}$$

which is equivalent to the volume fraction of the region collapsing to a black hole at $t = t_H$. Again, due to the steeply decreasing characteristic of the PDF, the integral is sensitive only to its lower bound

δ_c. Since $\delta_c \ll \delta$, one can Taylor expand $f(\delta)$ around δ_c,

$$f(\delta) = f(\delta_c) + f'(\delta_c)(\delta - \delta_c) + \mathcal{O}((\delta - \delta_c)^2) \simeq f_c + q(\delta - \delta_c), \tag{4.30}$$

so that we can write, for $q = f'(\delta_c)$,

$$\beta(M_H) \simeq \frac{1}{q} e^{-f_c}, \tag{4.31}$$

which is accurate if higher order terms are negligible. If the PDF is Gaussian, as in equation 4.10, this is equivalent to the condition that the variance $\sigma \ll \delta_c$. Then we can express the contribution of PBHs to the density parameter $\Omega_{\rm PBH}$ at the time of formation $t_i \gtrsim t_H$,

$$\Omega_{\rm PBH}(t_i) = \frac{1}{M_H} \int_{\delta_c} M_{\rm PBH}(\delta) P(\delta)\, \mathrm{d}\delta, \tag{4.32}$$

by performing a change of variables $\delta(M) = \delta_c + \left(\frac{M_{\rm PBH}}{K}\right)^{1/\gamma}$ from equation 4.27, and letting $M_{\rm PBH} = M$ for simplicity, we obtain

$$\Omega_{\rm PBH}(t_i) = \frac{1}{M_H} \int_0^\infty M P[\delta(M)] \frac{1}{\gamma} \left(\frac{M}{K}\right)^{\frac{1}{\gamma}} \frac{\mathrm{d}M}{M}. \tag{4.33}$$

Inserting equation 4.28 and the expansion 4.30 into the above integral,

$$\Omega_{\rm PBH}(t_i) = \frac{1}{M_H} \int_0^\infty M \exp\left(-f_c - q\left(\frac{M}{K}\right)^{1/\gamma}\right) \frac{1}{\gamma} \left(\frac{M}{K}\right)^{\frac{1}{\gamma}} \mathrm{d}(\ln M), \tag{4.34}$$

from which we can read off the differential mass spectrum,

$$\frac{\mathrm{d}\Omega_{\rm PBH}(M, t_i)}{\mathrm{d}\ln M} = \frac{M}{\gamma M_H} \left(\frac{M}{K}\right)^{\frac{1}{\gamma}} \exp\left(-f_c - q\left(\frac{M}{K}\right)^{1/\gamma}\right). \tag{4.35}$$

To find the maximum mass reached, one differentiates this expression with respect to M and sets to zero,

$$\begin{aligned} 0 &= \left[\left(1 + \frac{1}{\gamma}\right) \frac{M^{1/\gamma}}{\gamma M_H K^{\frac{1}{\gamma}}} - \frac{M^{1/\gamma+1}}{\gamma M_H K^{\frac{1}{\gamma}}} \left(\frac{M}{K}\right)^{1/\gamma-1} \frac{1}{K\gamma}\right], \\ &= \frac{M^{1/\gamma}}{\gamma M_H K^{\frac{1}{\gamma}}} \left[1 + \frac{1}{\gamma} - \frac{q}{\gamma}\left(\frac{M}{K}\right)^{1/\gamma}\right], \end{aligned} \tag{4.36}$$

which we rearrange to obtain

$$M_{\max} = Kq^{-\gamma}(1+\gamma)^{\gamma}. \tag{4.37}$$

By the assumption that a typical black hole has initial mass equal to the horizon mass, one has $M_{\max} = M_H(t_i)$. Then, by replacing K in 4.35 as per equation 4.27 (which also cancels the q-dependence) and making use of equation 4.31,

$$\frac{\mathrm{d}\Omega_{\mathrm{PBH}}(M,t_i)}{\mathrm{d}\ln M} = \left(\frac{M}{M_H}\right)^{\frac{1}{\gamma}} \left(\frac{1}{\gamma}+1\right) \beta(M_H) \exp\left((1+\gamma)\left(\frac{M}{M_H}\right)^{\frac{1}{\gamma}}\right). \tag{4.38}$$

By letting $\gamma \simeq 0.35$, one can integrate this equation as before using the Gamma function 4.21 to obtain

$$\begin{aligned} \Omega_{\mathrm{PBH}}(t_i) &\simeq (1+\gamma)^{-1}\Gamma(\gamma)\beta(M_H) \\ &\simeq 0.80\ \beta(M_H), \end{aligned} \tag{4.39}$$

where $\beta(M_H) = \Omega_{\mathrm{PBH}}(M_H)$, i.e. the density fraction in the nearly monochromatic case is equal to the total mass density of PBHs in the monochromatic case discussed in section 4.3. Figure 2 below clearly shows that the spectrum is characterised by a low-mass tail and a peak when $M = M_H$, hence the abundance of smaller mass PBHs is suppressed due to critical behaviour. The author [30] concluded that the difference between the monochromatic and almost-monochromatic case was practically negligible and the assumption that all PBHs had masses of order the horizon mass at formation was viable. Indeed, this assumption has been used frequently in the two decades since the scaling formula 4.27 was first applied to the PBH mass spectrum [32], [33].

However, more recently, Kühnel [34] has argued that this prevalent assumption is erroneous. He was motivated to investigate its validity by numerical calculations modelling the collapse of a relativistic fluid, corresponding to the continuum description of black hole formation in the early Universe, which indicated that the PBH mass distribution does not, in fact, peak at M_H [35]. Rather, the mass spectrum was suggested to have an extended feature and is not nearly-monochromatic. As such, the scaling relation cannot be simplified in the manner outlined above, i.e. by considering highly peaked spectra for which the 'bare' mass function in the neighbourhood of M_H is taken to be monochromatic [27]. Through a more careful application of the critical scaling formula, Kühnel argues that the effect on β is characterised by an appreciable shift, broadening and overall lowering of the mass contained in PBHs. In particular, he contends that neglecting the shift in β could have significant

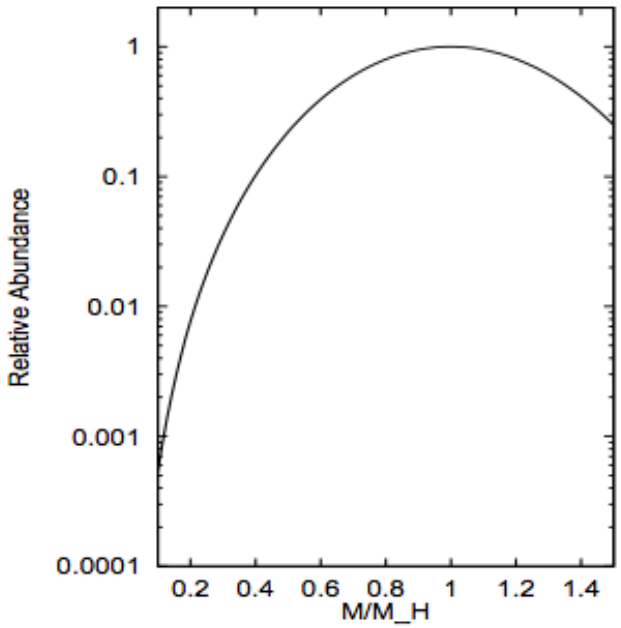

Figure 2. Spectrum of the relative abundance of primordial black holes (equation 4.38) as a function of the ratio of PBH mass to horizon mass at the time of formation, taken from [30].

consequences for observational constraints on certain models. For instance, if a model predicts a high abundance around a mass range wherein constraints are stringent (e.g. low mass constraints from galactic background observations) and there is a sharp transition to a much less constrained region, the shift of the power spectrum in light of these considerations may translate a loosely constrained region to a more highly constrained one, which could lead to mass ranges which were previously disregarded to be made potentially viable.

Kühnel demonstrates these effects on the mass spectrum due to critical collapse for numerous inflationary models which can produce PBHs in abundances of interest to its proposed role as dark matter. In the following section, two of these models are discussed in the context of their ability to permit PBH formation and the effects of critical collapse on each of their mass spectra in a certain range. Both models have an increased amplitude feature; that is, a spike at some small scale. Without the horizon mass assumption, each one-parameter family must be calculated (as opposed to just one in the nearly-monochromatic and monochromatic cases).

4.6 PBHs and inflation

Until now, we have considered the standard paradigm of slow roll inflation in which the curvature perturbation is generated by the vacuum fluctuation of the inflaton field [36]. If instead the curvature perturbation is generated after inflation, the only slow roll constraints are $\epsilon \ll 1$ and $(V/\epsilon)^{1/4} \ll 6.6 \times 10^{16}\text{GeV}$. The key ingredient for any model to produce PBHs is that it needs to generate curvature perturbations larger than some threshold value δ_c at an early time, which then collapse into black holes after horizon entry. Since the amplitude of the curvature perturbation power spectrum at the pivot scale ($k_* = 0.002\,\text{Mpc}^{-1}$ for the CMB measurement by WMAP or $k_* = 0.005\,\text{Mpc}^{-1}$ for Planck) is far too small to produce a notable abundance becomes large at an early time. For the case of a power spectrum which monotonically increases with decreasing K, the PBH abundance is largest for smallest M_H. The exact value of the threshold δ_c depends on the precise medium into which the perturbations enter. For a moderate number (3 or 4) of representative parameter sets, we subsequently investigate the effect of critical collapse and show how each of the spectra change [34].

4.6.1 Hybrid inflation

In hybrid inflation models, the bulk of the potential is generated by the displacement from the vacuum of some scalar 'waterfall field' distinct from the inflationary field. Inflation ends when the waterfall field is destabilised as the inflaton moves through some critical value. The flatness conditions of equations 3.15 and 3.17 are still satisfied in these models. Hybrid inflation is a two-field inflationary framework with the potential

$$V(\phi,\chi) = \Lambda\left[\left(1 + \frac{\chi^2}{M^2} + \frac{(\phi+\phi_c)}{\mu_1} - \frac{(\phi+\phi_c)^2}{\mu_2^2} + \frac{2\phi^2\chi^2}{M^2\phi_c^2}\right)\right], \tag{4.40}$$

where Λ is the cosmological constant (energy density of space), μ_1, μ_2 are mass parameters and M is the expectation value of the ϕ field when $V = 0$. The field ϕ_c is the critical value below which the waterfall field χ is destabilised, forcing the fields to reach one of the global minima located at $\phi = 0$, $\chi = \pm M$. The slope and the curvature of the potential at the critical point are controlled by the mass parameters μ_1 and μ_2 respectively. The end of hybrid inflation may be regarded as a phase transition which may leave behind topological defects as false vacuum remnants [37]. One can see a simplistic graph of this potential in figure 3 below.

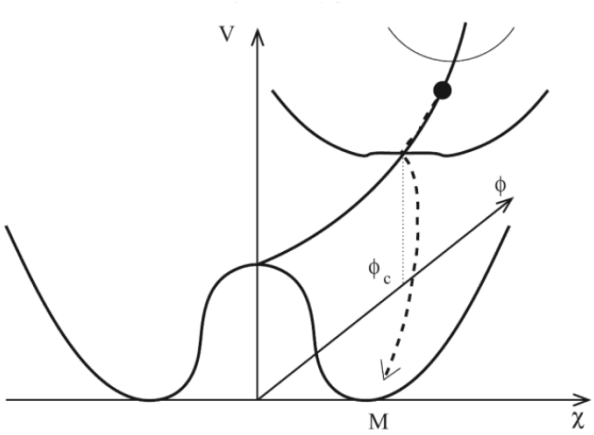

Figure 3. The hybrid inflation potential V as a function of auxiliary (or waterfall) field χ and inflaton field ϕ. The field rolls down the line $\chi = 0$ from large ϕ until it reaches ϕ_c, after which the $\chi = 0$ becomes unstable and the fields roll to their vacuum expectation values at $\phi = 0$, $\chi = \pm M$. Taken from [36].

We assume that μ_1 is sufficiently large compared to μ_2 for the slope along the valley to be constant over the range of scales from those relevant to CMB anisotropies down to scales that exit the Hubble radius at the critical density point. At $\phi = \phi_c$, the slow roll approximation is valid and the first and second Hubble-flow slow roll parameters are given by (using equation 2.12)

$$\begin{aligned} \epsilon_{1\phi_c} &= \frac{M_{Pl}^2}{2}\left(\frac{V'}{V}\right)^2 = \frac{M_{Pl}}{2\mu_1^2}, \\ \epsilon_{2\phi_c} &= 2M_{Pl}^2\left[\left(\frac{V'}{V}\right)^2 - \left(\frac{V''}{V}\right)\right] = 2M_{Pl}^2\left(\frac{1}{\mu_1^2} + \frac{2}{\mu_2^2}\right). \end{aligned} \tag{4.41}$$

One notices that $\epsilon_{1\phi_c} = \epsilon_v$ and $\epsilon_{2\phi_c}$ is a linear combination of ϵ_v and η_v, the original flatness parameters. The prime denotes differentiation with respect to the scalar field ϕ, as usual.

The period of interest is horizon-crossing and we denote parameters evaluated at this point by a star: $k_* = a(t_*)H(t_*)$, where $k_* = 0.05\text{Mpc}^{-1}$ is the pivot scale used by Planck. During this epoch, $\mu_1 \gg \mu_2$ and the spectral index n_s is dominated by the contribution from the second slow roll parameter of equation 4.41. The spectral index at horizon exit can thus be written

$$\begin{aligned} n_s &= 1 - 2\epsilon_{1*} - \epsilon_{2*}, \\ &\simeq 1 - \frac{4M_{Pl}^2}{\mu_2^2}. \end{aligned} \tag{4.42}$$

If the scalar spectral index is given by the best fit value from Planck [38], $n_s \simeq 0.9603$, one obtains

for the second mass parameter,

$$\mu_2 = \frac{2M_{Pl}}{\sqrt{1-n_s}} \simeq 10M_{Pl}. \tag{4.43}$$

The curvature power spectrum is also measured by Planck and is given at the pivot scale by

$$\begin{aligned} \mathcal{P}_\zeta(k_*) &= \frac{H_*^2}{8\pi^2 M_{Pl}^2 \epsilon_{1*}} \simeq \frac{\Lambda\mu_1^2}{12\pi^2 M_{Pl}^6}\left(\frac{k_*}{k_{\phi_c}}\right)^{n_s-1}, \\ &\simeq 2.21\times 10^9, \end{aligned} \tag{4.44}$$

where we have used the Friedmann equation in slow roll $H^2 \simeq V/3M_{Pl}^2$, equation 4.41 and the power-law approximation. The wavenumber ratio can be determined by solving the equations of motion for the two fields such that the amplitude of the power spectrum agrees with observations from Planck.

The large curvature perturbations required for the formation of PBHs are generated in the context of hybrid inflation with a so-called mild waterfall phase. The waterfall can be decomposed into two phases. During phase 1, inflation is driven by the inflaton only, so the terms with χ can be neglected. At some point, the χ terms become dominant and the field trajectories enter phase 2. The mildness condition implies that the inflation continues for up to 50 e-folds and can generate curvature perturbations on large scales that re-enter the horizon at later times. As such, they can accommodate the formation of PBHs with masses large enough (discussed in section 4) to constitute a significant portion of dark matter. Furthermore, the slope of the potential must be sufficiently small at the critical point ϕ_c for the final waterfall phase to be mild.

Clesse [38] considers the regime where inflation continues for 20 to 40 e-folds after crossing this point. We assume that the classical two-field dynamics from the critical point is valid given a tiny initial displacement from $\chi = 0$. We now briefly outline the analytical part of the calculation undertaken by Clesse to obtain the power spectrum in order to make sense of the argument made by Kühnel that critical collapse has the effect of lowering, broadening and shifting it.

$$\begin{aligned} \mathcal{N}_1 &= \frac{M\sqrt{k_1\phi_c\mu_1)}}{M_{Pl}^2}, \\ \mathcal{N}_2 &= \frac{M}{4M_{Pl}^2}\sqrt{\frac{\phi_c\mu_1}{k_2}}. \end{aligned} \tag{4.45}$$

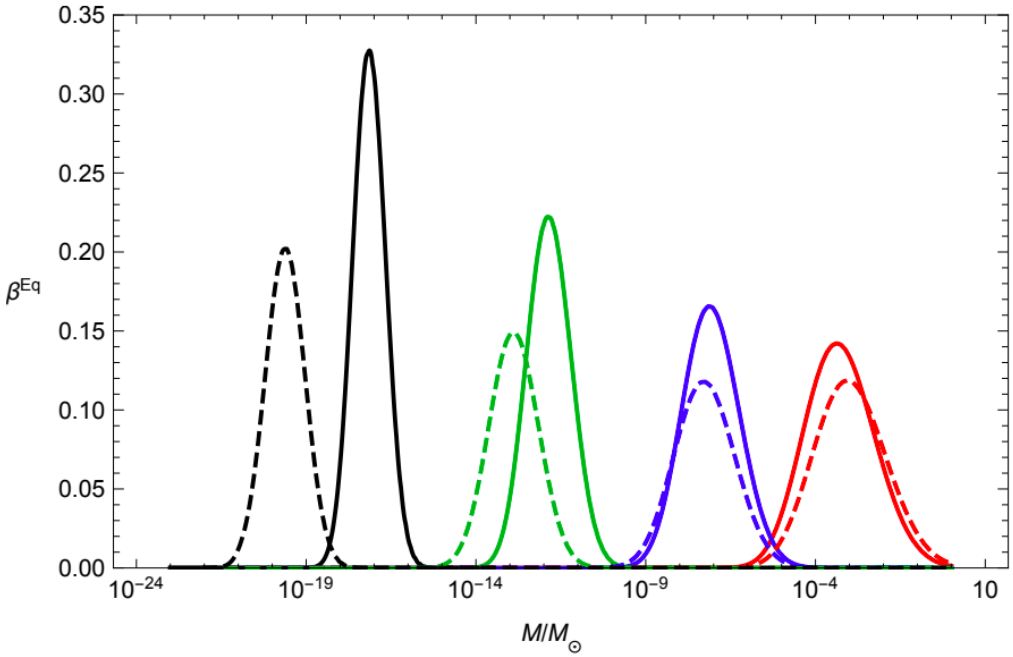

Figure 4. The relative energy density β in hybrid-inflation with the variance as per equation 4.46, at the time of matter-radiation equality as a function of $M/M_\odot$. The solid curves assume standard black-hole production with horizon mass, where the parameters are $\mu_1 = 3 \times 105\, M_{\rm Pl}$, $M = 0.1 M_{Pl}$ for all graphs, and individually (left to right) $\phi_c = 0.075 M_{Pl}$, $\delta_c = 1.64$ (black) $\phi_c = 0.125 M_{\rm Pl}$, $\phi_c = 0.1 M_{\rm Pl}$, $\delta_c = 1.63$ (green), $\phi_c = 0.1 M_{\rm Pl}$, $\delta_c = 1.54$ (blue), $\delta_c = 1.43$ (red). The dashed curves have the same respective parameters, but assume critical scaling according to equation 4.27 with $\gamma = 0.36$. Taken from [34].

The variance of the curvature perturbation is approximated by [34]

$$\sigma(k) \simeq \sqrt{\mathcal{P}_\zeta} \simeq \sqrt{\frac{\Lambda M^2 \mu_1 \phi_c}{192\pi^2 M_{Pl}^2 k^2 \chi_k^2}}. \tag{4.46}$$

By defining $\phi = \phi_c e^\xi$ and $\chi = \chi_0 e^\psi$, we can say that $|\xi| \ll 1$ during the waterfall phase (as long at the slow roll approximation is valid). One can therefore expand ϕ as $\phi \simeq \phi_c(1 + \xi + \mathcal{O}(\xi^2))$. We can use this approximation to evaluate the evolution equations for the scalar fields, which both have the form of equation 3.13. In terms of ξ and ψ, one obtains

$$3H\dot{\xi} \simeq -\frac{2\Lambda}{\mu_1^2}\left(1 + \frac{2\mu_1^2\phi^2}{M^2\phi_c^2}\right), \tag{4.47}$$

$$3H\dot{\psi} \simeq -\frac{4\Lambda}{M^2}\left(2\xi + \frac{\chi}{M^2}\right), \tag{4.48}$$

where the Friedmann equation $H^2 = \Lambda/3M_{Pl}^2$ was used. As previously described, at some stage the second term in the RHS of equation 3.81 exceeds 1 and the second phase of the waterfall begins. The durations of the two phases are given in terms of the number of e-folds,

One can obtain the trajectories ξ^2 by integrating the equations 4.47 and 4.48 for both phases respectively. For a given wavenumber k exiting the Hubble radius $|N_k|$ e-foldings before the end of inflation, the associated PBH mass (when assuming horizon-mass collapse) is given by

$$M_k = \frac{M_{Pl}}{\sqrt{\Lambda/3}} e^{-2N_k}. \tag{4.49}$$

The ratio $\beta = \rho_{\rm PBH}/\rho_{\rm tot}$ as a function of $M/M_\odot$ at the time of matter-radiation equality is shown in figure 4 above. This graph clearly shows the lowering, broadening and shifting of β^{Eq} over a range of density contrasts spanning the variance range $1.43 < \sigma_c < 1.64$.

4.6.2 Running-mass inflation

The running-mass model also provides a promising framework for the formation of PBHs which are sufficiently long-lived to serve as dark matter candidates. We follow the analysis conducted by Drees and Erfani [39] for PBHs which form in the radiation-dominated era after reheating is more or less complete. The reason for this is that the number density of PBHs formed during the reheating phase just after the end of inflation will be greatly reduced by the reheating itself. During the radiation era, $aH \propto a^{-1}$, and the expansion at constant entropy gives $\rho \propto g_*^{-1/3} aH$, where g_* is the number of relativistic degrees of freedom (dof) and the temperature and entropy dofs have been approximated as equal.

When scales enter the horizon, one can approximate the PBH mass in terms of the horizon mass by

$$M_{\rm PBH} = \gamma M_H = \gamma \frac{4\pi}{3H^3}\rho. \tag{4.50}$$

Inserting the expansion for ρ into equation 4.50 and evaluate at matter radiation equality (subscript terms with eq),

$$M_{\rm PBH} = \gamma M_{\rm eq} (k_{\rm eq} R)^2 \left(\frac{g_{*,eq}}{g_*}\right)^{1/3}. \tag{4.51}$$

In the early Universe, the effective relativistic dof g_* is expected to be of order 100, while $g_{*,eq} = 3.36$ and $k_{eq} = 0.07\,\Omega_m H^2$, where $\Omega_m h^2 = 0.1334$. The horizon mass at matter-radiation equality is

given by

$$M_{H,eq} = \frac{4\pi}{3}\rho_{\rm rad,eq}H_{\rm eq}^{-3} = \frac{4\pi}{3}\frac{\rho_{\rm rad,0}}{k_{\rm eq}^3 a_{\rm eq}}, \tag{4.52}$$

where $a_{eq}^{-1} = (1+z_{eq}) = 3146$ and (assuming 3 species of massless neutrinos), $\Omega_{\rm rad,0}h^2 = 4.17\times10^{-5}$ where $\Omega_{\rm rad,0} = \rho_{\rm rad,0}/\rho_0$. Substituting equation 4.52 into equation 4.51,

$$M_{\rm PBH} = \gamma\left(\frac{4\pi}{4}\frac{\rho_{\rm rad,eq}}{k_{\rm eq}^3 a_{\rm eq}}\right)(k_{\rm eq}R)^2\left(\frac{g_{*,\rm eq}}{g_*}\right)^{1/3}. \tag{4.53}$$

Evaluate this expression in terms of the numerical values given throughout and rearrange to make R the subject to obtain

$$\frac{R}{1\rm Mpc} = 5.54\times10^{-24}\gamma^{-1/2}\left(\frac{M_{\rm PBH}}{1g}\right)^{1/2}\left(\frac{g_*}{3.36}\right)^{1/6}. \tag{4.54}$$

Notice that $M_{\rm PBH} \propto R^2$. Recall that $M_{\rm PBH}$ is related to the horizon mass at the time when the comoving scale R again crossed into the horizon. Larger scales re-enter the horizon later, when the energy density is lower; this weakens the dependence of $M_{\rm PBH}$ on R. Moreover, the lightest black holes to form are those corresponding to a comoving scale that re-enters the horizon immediately after inflation.

The Gaussian window function in equation 4.7 strongly suppresses contributions with $k > 1/R$. At the same time, the factor k^4 in $\mathcal{P}_\Delta \propto \mathcal{P}_{\mathcal{R}_c}$ suppresses contributions to the integral in equation 4.7 from small k. As a result, this integral is dominated by a limited range of k-values near $1/R$. Over this limited range, one can assume (to good approximation) a power law primordial power spectrum with fixed power n_s,

$$\mathcal{P}_{\mathcal{R}_c}(k) = \mathcal{P}_{\mathcal{R}_c}(k_R)\left(\frac{k}{k_R}\right)^{n_s(R)-1}. \tag{4.55}$$

where $k_R = 1/R$. With this ansatz, the variance of the primordial density field at horizon crossing is given by (for $n_s(R) > -3$),

$$\sigma_\delta^2(R) = \frac{2(1+w)^2}{(5+3w)^2}\mathcal{P}_{\mathcal{R}_c}(k_R)\,\Gamma\left(\frac{n_s(R)+3}{2}\right). \tag{4.56}$$

This power $\mathcal{P}_{\mathcal{R}_c}$ is known accurately at CMB scales. For example, $\mathcal{P}_{\mathcal{R}_c}(k_0) = (2.43\pm0.11)\times10^{-9}$ at the 'COBE scale', $k_0 = 0.002\rm Mpc^{-1}$. In order to relate this to the scales relevant for PBH formation,

we parametrise the power spectrum as

$$\mathcal{P}_{\mathcal{R}_c}(k_R) = \mathcal{P}_{\mathcal{R}_c}(k_0)\left(\frac{k_R}{k_0}\right)^{n(R)-1}. \tag{4.57}$$

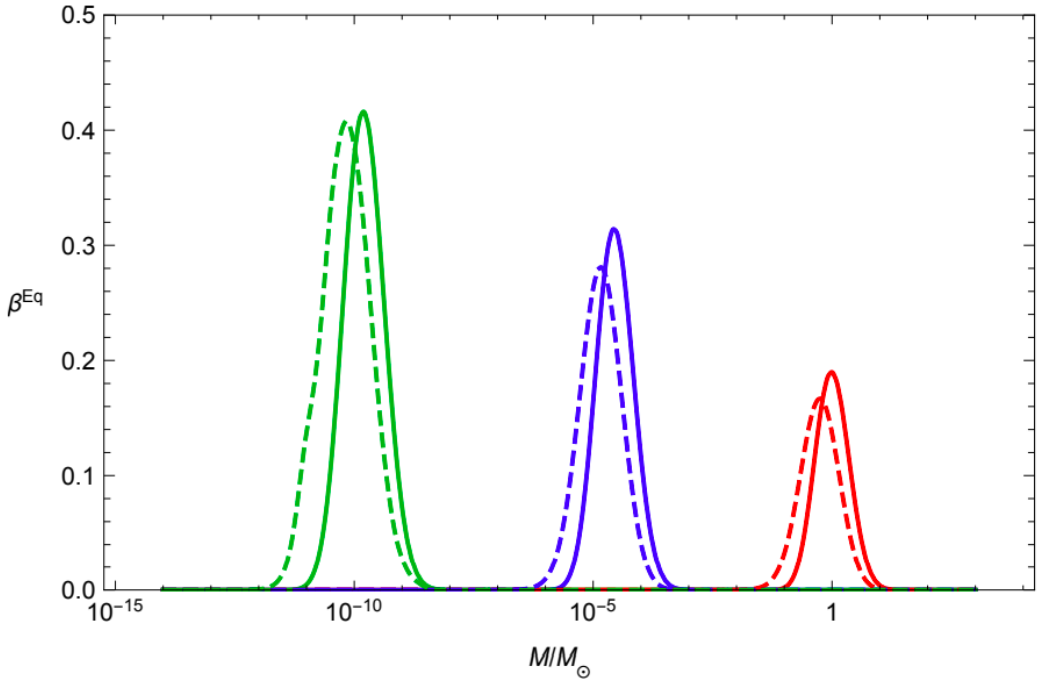

Figure 5. The relative energy density β in running-mass inflation with the variance as per equation 4.56, at the time of matter-radiation equality as a function of $M/M_\odot$. The solid curves assume standard black hole production with horizon mass, where the parameters are $a = 0.011$ for all graphs, and individually (left to right) $b = 0.006$, $c = -0.000519$ (green), $b = 0.011$, $c = -0.0010975$ (blue), and $b = 0.02$, $c = -0.00234$ (red). For all curves, the threshold δ_c has been set to 0.45. The dashed curves have the same respective parameters, but assume critical scaling according to equation 4.27 with $\gamma = 0.36$. Taken from [34].

We make a point of distinguishing between $n_s(R)$ and $n(R)$: n_s describes the slope of the power spectrum at scales $k \sim k_R = 1/R$ (as before), whereas $n(R)$ fixes the normalisation of the spectrum at $k_R \gg k_0$. These two powers are identical if the spectral index is strictly constant, i.e. if neither n nor n_s depend on R. However, in this case, CMB data imply that $n = n_s$ is close to unity. Equations 4.55 and 4.57 then give a very small variance, leading to essentially no PBH formation as f is highly dependent on the spectrum. Therefore, we conclude that significant PBH formation can only occur in

scenarios with a running spectral index. The spectral indices are given

$$n(k) = n_s(k_*) - \frac{1}{2!}a \ln \frac{k}{k_*} + \frac{1}{3!}b \ln^{\frac{k}{k_*}} - \frac{1}{4!}c \ln^3 \frac{k}{k_*} + ... \tag{4.58}$$

$$n_s(k) = n_s(k_*) - a \ln \frac{k}{k_*} + \frac{1}{2}b \ln^2 \frac{k}{k_*} - \frac{1}{6}c \ln^3 \frac{k}{k_*} + ... \tag{4.59}$$

The parameters a, b and c denote the running of the effective spectral index n_s and the running of the running and then the 'running-of-running-of-running', respectively. Recall that we are interested in $R \ll 1/k_0$, i.e. $\ln(k_0 R) < 0$ [34]. The relative energy density β at the time of matter-radiation equality is shown in figure 5. As expected, we observe a shift towards lower masses as well as a broadening with respect to the horizon-mass case. The associated areas are approximately cut in half.

However, there is a problem: if black holes are to form that can provide the CDM density to match with observation, the spectral index n must increase significantly between scales probed by the CMB. However, n must then decrease rapidly when going to slightly smaller length scales, since otherwise there would be overproduction of lighter PBHs. For example, BBNS requires $f(10^{13}\text{g}) \leq 2 \times 10^{-20}$, which is about 12 orders of magnitude below that predicted by keeping n(R) fixed at the value required for having 10^{15}g PBHs as CDM candidates [39]. The bounds on these very small primordial black holes are very severe [40], and should not be neglected.

4.7 Caveats concerning formation mechanisms

We have made important assumptions when describing the various theories of PBH formation outlined above which should be examined more closely.

Sphericity: Firstly, primordial black holes are assumed to form through spherically-symmetric gravitational collapse, as in the case for the standard case of black holes which form from stellar collapse. The critical scaling formula equation 4.27 describes the generation of a PBH mass spectrum at each instance of time at which over-densities re-enter the horizon. However, a realistic distribution of overdensities is likely to be non-spherical to such a degree that it may have appreciable consequences on the threshold value for PBH production. While overdensities can take a myriad of forms, it has been known for some time that assuming ellipsoidal collapse could account for certain discrepancies between theory and observation in the context of galactic halo formation [41]. The approximate threshold value

for ellipsoidal collapse was found to be

$$\delta_{ec} \simeq \delta_c + \kappa \left(\frac{\sigma^2}{\delta_c^2} \right)^{\gamma}. \tag{4.60}$$

where δ_c is the threshold for spherical collapse, σ^2 is the amplitude of the density power spectrum at a given scale, and κ and γ are constants (to be found numerically). Kühnel and Sandstad [24] asserted that this approximation holds true for ellipsoidal gravitational collapse in any environment, including PBH formation in the radiation-dominated era. They make a heuristic argument on the basis that the collapse may be approximated to the spherical collapse of a sphere with radius equal to the shortest axis of the ellipsoid (since the collapse is initiated on this axis) and the collapse along the longer axes follows, moving faster than linearly. They employ the expectation values for the shape of Gaussian-distributed overdensities (ellipticity and prolateness) and use these to give the mass and volume of the ellipsoidal region as a 'perturbation' of the sphere along the smallest axis. Furthermore, they assume that the ellipsoid is of uniform density and the density threshold is exceeded in the enclosed sphere. They subsequently find that $\gamma = 1/2$ and $\kappa = (9/\pi\sqrt{10})$ for this simplistic analysis.

To demonstrate the effect of ellipsoidal collapse on the mass spectrum, they apply their results to the relative energy density of PBHs at matter-radiation equality β^{Eq} in the running-mass model of formation, as described in the previous section. One can see below a plot (figure 6) of the mass functions in comparison with the mass function in the spherical collapse case, where the constants in equation 4.60 are given three different sets of values. The values for the dashed blue line ($\gamma = 0.47$ and $\kappa = 0.62$) are the numerical results found for ellipsoidal collapse in galactic halo formation [41]. The dashed green line corresponds to the values naïvely calculated for PBHs, as just outlined. One can immediately see the shift downwards in the spectrum in comparison with spherical collapse in all three scenarios. This makes sense, as an increase in the threshold value will cause a reduction in the number of black holes that can form.

Gaussianity: The second assumption worth discussing was also made in the analysis above; Gaussianity of the underlying density perturbation spectrum. Since PBHs form from the rare, large fluctuations in the extreme tail of the probability distribution function (PDF), any non-Gaussianity can significantly affect the abundance of PBHs and thus the viability of PBHs as dark matter candidates [42]. PBHs formed from non-Gaussian fluctuations lead to isocurvature modes that could be detected

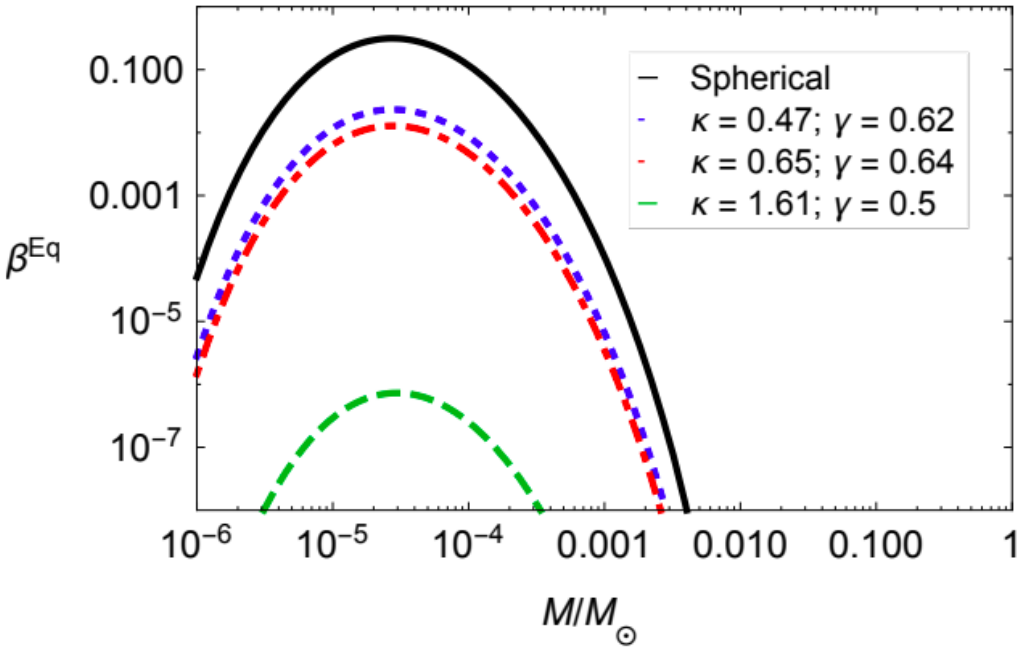

Figure 6. The relative energy density at the time of matter-radiation equality β^{Eq} as a function of $M/M_{\odot}$ of PBHs, formed due to spherical collapse (black solid line) and ellipsoidal collapse (three dashed lines) in the running-mass inflationary model. The spherical collapse model has scaling according to equation 4.27 with $k = 3.3$ and $\gamma = 0.36$ used to evaluate the black line above. The other three lines have scaling according to equation 4.60, with the values for the relevant constants given in the figure. Taken from [24].

in the CMB. In the hybrid inflation scenario, these modes would be too large and PBHs that significantly contribute to dark matter could no longer form in this model. For a realistic investigation of PBH formation in any inflationary model, it is paramount that effects from non-Gaussianties be accounted for going forward. However, non-Gaussianties have been shown to only have a perturbative effect in inflationary models with an inflection point in the potential and not drastically effect results [43].

Miscellaneous: There are several other more minor technical issues implicit in the treatment thus far asides from the potentially larger consequences non-sphericity and non-Gaussianity. We have used the Press-Schechter formalism as opposed to the theory of peaks to obtain the mass spectrum from density fluctuations. There has been some debate over the differences in the results from each method. However, the authors of [33] conclude that the discrepancy is dwarfed by the uncertainty in the value of the threshold overdensity for PBH formation. As such, until more stringent constraints

are found from inflationary models (or observation), both approaches can still be used. However, it has been claimed that peaks theory can better address certain issues, such as the overcounting of low-mass PBHs which are embedded in larger PBHs (so-called cloud-in-cloud problem) [44].

Related to this issue, and also scrutinised in [33], is the question of which power spectrum to use; the curvature power spectrum $\mathcal{P}_\zeta$ or the density power spectrum $\mathcal{P}_\delta$. The authors of [33] show that if one considers a scale-invariant power spectrum, the variance of the comoving curvature perturbation $\mathcal{R}_c$ diverges, which leads them to conclude that, in general, the density perturbation is safer to work with. However, in this paper and in the literature more broadly, both spectra are employed for their benefits in specific calculations; curvature perturbations are preferred in the context of inflationary models, whilst density perturbations are used for discussions of critical collapse.

5 The Cosmic Role of PBHs

We have focused our discussion of PBHs hitherto on their formation from theoretical models and their ability to constitute dark matter based on expected abundances and mass ranges from these models. We now review the constraints placed on the PBH mass function $fM = \rho(M)/\rho_{\rm CDM}$ from observation in this same context, but also extending the discussion to their possible role as seeds of super-massive black holes in the centre of galaxies (SMBHs). While these two functions are essentially independent of one another, there exist some mass ranges for which they could both provide the dark matter and play an active role in structure formation.

As we have seen, the formation mass of primordial black holes can be approximated as the particle horizon mass at the time of their formation t_i, which is the mass corresponding to a Schwarzschild radius of ct

$$M_H(t_i) \simeq \frac{c^3 t}{G} \simeq 10^{15} \left(\frac{t_i}{10^{-23}}\right) \text{g}. \tag{5.1}$$

As such, PBHs could span a substantial mass range, depending on the era during which they formed: those formed at Planck time 10^{-43}s would have mass 10^{-5}g, $t_i = 1$s produces a mass range around $10^5 M_\odot$, whilst black holes forming now could never be smaller than about one solar mass.

5.1 PBHs as dark matter

The constraints outlined in this section are usually applied on the assumption that the PBH mass function is nearly monochromatic ($\Delta M \equiv M$). However, as discussed in section 4.4, this is not the most realistic scenario. In the context of the dark matter problem, this is a double-edged sword. On the one hand, it means that the total PBH density may be sufficient to explain the dark matter, even if the density in any particular mass band is small within the observational bounds. On the other hand, even if PBHs can provide all the dark matter at some mass-scale without violating constraints, the extended mass function may still violate the constraints at some other scale (even if f is low there).

One can treat constraints on the extended mass function as a sequence of flat constraints, i.e. split the curves into a sequence of monochromatic mass functions called bins. Then, if $f < a$ over the range of the bin, $M_{\rm min}$ to $M_{\rm max}$, then one integrates $\mathrm{d}f_{\rm exp}/\,\mathrm{d}M$ over this range, where $f_{\rm exp}$ is the expected PBH mass fraction. If the f in the narrow band is quite curved, then approximate a as $q_{\rm max}$ where $q_{\rm max}$ is the maximum value o f between these masses, chosen so that it is close to the minimum of maximum fraction allowed by the constraint, $f_{\rm max}$, and comparable to the integrated

mass function $f_{\rm exp}$ in this region. Then move to the next bin, $M_3 \lesssim M_1$ to $M_4 \geq M_2$, and repeat the process. This involved procedure has been criticised [45] and more elegant approaches have been taken [46]. However, at the time of writing, this imperfect methodology was used to produce the most comprehensive study of the constraints and as such is a useful benchmark for further investigation and worth discussing.

There is a subtle interpretation intersecting constraints for the extended mass function. If two constraints meet at $M = M_{\rm meet}$, there can be a fraction $f_{\rm meet} = f(M_{\rm meet}$ in PBHs both below and above $M_{\rm meet}$, making the combined constraint $f < 2f_{\rm meet}$ in the appropriate range, unless some other stronger constraint applies there. Hence for a limit which is independent of the PBH formation mechanism, all the constraints in the relevant mass range must sum up to $f < 1$. Unless one invokes an extended mass function with multiple maxima, all mass ranges could be excluded in principle. However, there are currently still windows where the model parameters are insufficiently known to exclude PBHs from providing all the dark matter. Carr et al. [28] outline four such mass windows, however not all are equally likely. In the latter two sections of this chapter, the most viable windows are discussed; the intermediate and sublunar mass ranges. The other two ranges are subatomic and Planck-mass relic black holes. The former is implausible since the range of masses is so narrow, and the latter is essentially unverifiable since the relics are too small (10^{-33}cm) to be detected non-gravitationally.

5.1.1 An overview of constraints

Evaporation constraints: Hawking's seminal discovery that black holes emit radiation due to the process of pair creation and annihilation at the event horizon [15] has important consequences for our discussion as it immediately places a lower bound on the mass and thus the time of formation. Black holes radiate thermally with a temperature measured in kelvins of

$$T = \frac{\hbar c^3}{8\pi G M k_{\rm B}} \simeq 10^{-7} \left(\frac{M}{M_\odot}\right)^{-1} K, \tag{5.2}$$

where $k_{\rm B}$ is Boltzmann's constant, $\hbar$ is the reduced Planck's constant and other variables are as defined previously. We can find the time taken for a black hole to evaporate from the blackbody power law

$$P = \sigma A T^4 \tag{5.3}$$

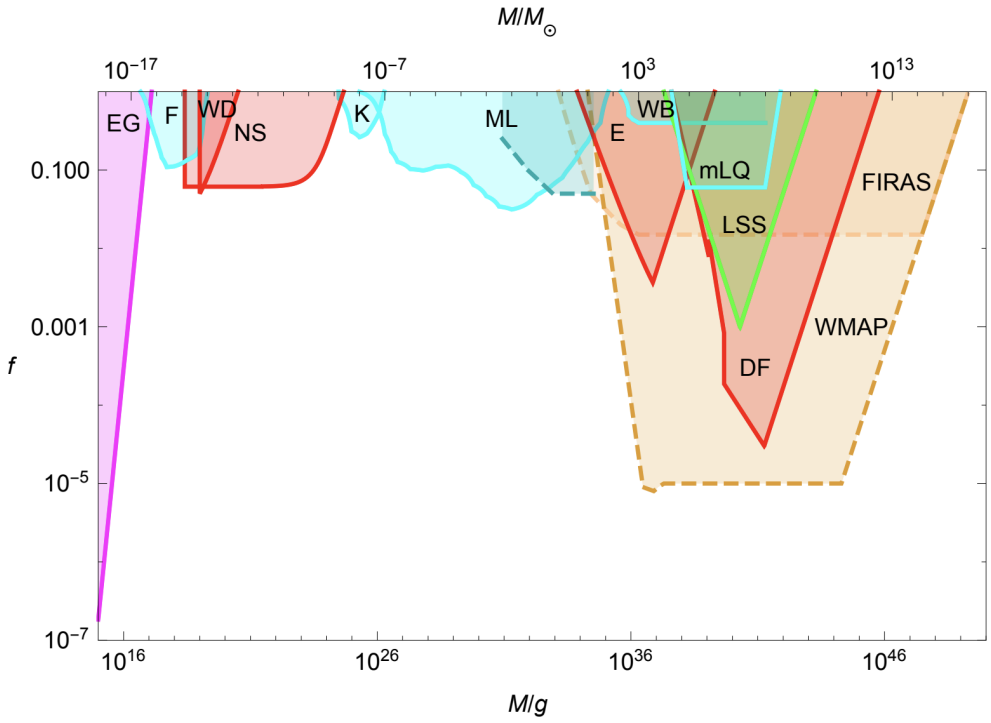

Figure 7. A graph of constraints on *f(M)* outlined in this section: evaporation (magenta), dynamical (red), lensing (cyan), large-scale structure (green) and accretion (yellow/orange). From left to right, the specific sources are extragalactic γ-rays from evaporation (EG), femtolensing of γ-ray bursts (F), white-dwarf explosions (WD), neutron-star capture (NS), Kepler microlensing of stars (K), MACHO/EROS/OGLE microlensing of stars (ML) and quasar microlensing (broken line) (ML), survival of a star cluster in Eridanus II (E), wide-binary disruption (WB), dynamical friction on halo objects (DF), millilensing of quasars (mLQ), generation of large-scale structure through Poisson fluctuations (LSS), and accretion effects (WMAP, FIRAS). Only the strongest constraint is included in each mass range, but the accretion limits are shown with broken lines since they are are highly model-dependent. Most constraints cut off at high M due to large-mass dynamical constraints. Taken from [28].

where σ is the Stefan-Boltzmann constant, A is the surface area $A = 4\pi r_s^2$ and T is the temperature. Given that the power of the radiation is the rate of energy loss from the black hole, one can write $P = -c^2 dM/dt$. Then, equating this with equation 5.3 and integrating from M at $t = 0$ to $M = 0$ at $t = \tau$, one obtains the lifetime of a black hole in years

$$\tau(M) \simeq \frac{\hbar c^4}{G^2 M^3} \simeq 10^{64} \left(\frac{M}{M_\odot}\right)^3 \text{yrs.} \tag{5.4}$$

Since the lifetime of the Universe is 1.38×10^{10} years, $(M/M_\odot)^3 \simeq 1.38 \times 10^{-54}$ and $(M/M_\odot) \simeq 1.11 \times 10^{-18}$. Given that $M_\odot \simeq 2 \times 10^{30}$kg, only black holes smaller than about 10^{12} kg would have

evaporated by the present epoch, so equation 5.1 suggests that this effect is only significant for black holes which formed before 10^{-23}s. There are strong constraints on $M_* \simeq 5 \times 10^{14}$g (black holes which are evaporating at the present epoch) from observations of the extragalactic γ-ray background (EGB). Towards the end of their lifetimes, the rate of photon and neutrino emission from black holes increases rapidly and they are said to explode, releasing about 10^{30}erg in the last 0.1 s [15]. This radiation contributes to the Galactic γ-ray background observed today if PBHs with mass $M > M_*$ evaporating at present are clustered inside galactic halos (as expected). In order to calculate the Galactic γ-ray background, one requires the instantaneous emission as a function of the black hole mass M. Only black holes with $M > M_*$ are relevant. Using units where $8\pi G = 1$, we can set the temperature of a black hole to be $T = 1/M$. For $M > 2M_*$, one can neglect any change in the mass of the black hole due to Hawking radiation (as this introduces complications pertaining to quark and gluon jet emission). The instantaneous emission rate for photons of energy E from each PBH is given by

$$\frac{\mathrm{d}N^\gamma}{\mathrm{d}E} = \frac{1}{2\pi^2}\frac{E^2\sigma(M,E)}{E^{ME}-1} \propto \begin{cases} E^3M^3 & \text{for } E < M^{-1}, \\ E^2M^2e^{-EM} & \text{for } E > M^{-1}. \end{cases} \tag{5.5}$$

where $\sigma(M, E)$ is the absorption cross-section for photons. This peaks at $E \sim M^{-1}$ with a value independent of M. The number of background photons per unit energy per unit volume from all the PBHs is determined by integrating over the mass function

$$\mathcal{E}(E) = \int_{M_{\min}}^{M_{\max}} \mathrm{d}M \frac{\mathrm{d}n}{\mathrm{d}M}\frac{\mathrm{d}N^\gamma(m,E)}{\mathrm{d}E} \tag{5.6}$$

where $M_{\min}$ and $M_{\max}$ specify the mass limits. For a monochromatic mass function $M_{\min} = M_{\max} = M$ and energy density fraction

$$f(M) = M^2\frac{\mathrm{d}n}{\mathrm{d}M}\frac{1}{\rho_{\mathrm{CDM}}}, \tag{5.7}$$

one obtains

$$\mathcal{E} \propto f(M) \times \begin{cases} E^3M^2 & \text{for } E < M^{-1}, \\ E^2Me^{-EM} & \text{for } E > M^{-1}. \end{cases} \tag{5.8}$$

The associated intensity is

$$I(E) \equiv \frac{cE\mathcal{E}}{4\pi} \propto f(M) \times \begin{cases} E^4 M^2 & \text{for } E < M^{-1}, \\ E^3 M e^{-EM} & \text{for } E > M^{-1}, \end{cases} \tag{5.9}$$

with units $s^{-1}sr^{-1}cm^{-2}$. This peaks at $E \sim M^{-1}$ with value $I^{\max} \propto f(M)M^{-2}$. The observed extragalactic instensity is $I^{\rm obs} \propto E^{-(1+\epsilon)} \propto M^{1+\epsilon}$, where ϵ lies between 0.1 [47] and 0.4 [48]. Hence, putting $I^{\max} < I^{\rm obs}$ gives

$$f(M) \lesssim 2 \times 10^{-8} \left(\frac{M}{M_*}\right)^{3+\epsilon} \text{for} M > M_* = 5 \times 10^{14}\text{g}. \tag{5.10}$$

The Galactic γ-ray background constraint could give a stronger limit but this requires the mass function to be extended and depends sensitively on its form.

MICROLENSING CONSTRAINTS: Gravitational lensing is a phenomenon predicted by general relativity which involves the deflection, distortion or magnification of light from a source (star, quasar, galaxy) by an intervening object along the line of sight of an observer. This object is said to act as a 'lens' as it bends the light travelling from the source of interest, although the mechanism by which this occurs is gravitation and not the change in the density of the medium as in optical lensing. Microlensing is a specific kind of lensing in which the mass of the lens object is too small for its gravitational effect to deflect the light rays from the background source enough to be measured easily. However, as the lens passes across the light source, one can measure the change in the apparent brightness of this object over a few weeks. The increased brightness is caused by the contribution from the slightly smeared image (corresponding to image separations on the order of micro-arc-seconds) of the background star, and peaks when the two objects are directly aligned in the observer's line of sight, forming a so-called 'Einstein ring'. The intensity and length of the light curve can be used to study the lens object, which could be objects of astrophysical interest such as a brown dwarf [4], neutron star or a (primordial) black hole. These dim objects are collectively referred to as massive compact halo objects (MACHOs) and form one class of likely dark matter candidates, the other being WIMPs (weakly interacting massive particles) [49]. Mircolensing events are relatively rare and notoriously

[4] Brown dwarfs are very dim astronomical bodies which are unable to sustain hydrogen fusion in their cores and instead may fuse deuterium. They belong to a class of *substellar* objects for this reason.

difficult to predict. Hence, they are largely found through surveys of vast regions of the sky with a high number of source stars densely packed together, such as the Large and Small Magellanic Clouds[5], the nearby Andromeda galaxy and the central bulge of the Milky Way [50]. The presence of dark matter in galactic halos is inferred through observations of their effects on gravitational lensing. In the early 1990s, several teams of astronomers called MACHO, EROS and OGLE began large projects using wide-field telescopes to search for microlensing events [49]. The best targets for dark matter searches are the Large and Small Magellanic clouds (henceforth referred to as the LMC and SMC respectively), since the line of sight from earth to these satellite galaxies of the Milky Way passes through the Galactic halo.

Microlensing observations of stars in the Large and Small Magellanic Clouds probe the fraction of the Galactic halo in massive compact halo objects (MACHOs) of a certain mass range [51]. The optical depth of the halo towards LMC and SMC, defined as the probability that any given star is amplified by at least 1.34 at a given time, is related to the fraction f by

$$\tau_{\rm L}^{(\rm SMC)} = 1.4\tau_{\rm L}^{(\rm SMC)} = 6.6 \times 10^{-7} f, \tag{5.11}$$

for the S halo model [52]. Although the initial motivation for microlensing surveys was to search for brown dwarfs with $0.02M_\odot < M < 0.08M_\odot$, the possibility that the halo is dominated by these objects was soon ruled out by the MACHO experiment [53]. However, MACHO observed 17 events and claimed that these were consistent compact objects of $M \sim 0.5M_\odot$ contributing 20 % of the halo mass [52]. This raised the possibility that some of the halo dark matter could be PBHs formed at the QCD phase transition [6] [54], [55]. However, later studies suggested that the halo contribution of $M \sim 0.5M_\odot$ PBHs could be at most 10% [56]. The EROS experiment obtained more stringent constraints by arguing that some of the MACHO events were due to self-lensing or halo clumpiness [57] and excluded $6 \times 10^{-8}M_\odot < M < 15M_\odot$ MACHOs from dominating the halo. Combining the earlier MACHO [58] results with the EROS-I and EROS-II results extended the upper bound to $30M_\odot$

[5]The Magellanic Clouds are two irregular dwarf galaxies visible in the Southern Celestial Hemisphere. They are members of the Local Group and orbit the Milky Way.

[6]The cosmological QCD phase transition, which happened between 10^{-5} and 10^{-4} seconds after the Big Bang, accounts for confinement of quarks and gluons to within hadrons.

[57]. The constraints from MACHO and EROS about a decade ago may be summarised as

$$f(M) < \begin{cases} 1 & 6 \times 10^{-8} M_\odot < M < 30 M_\odot, \\ 0.1 & 10^{-6} M_\odot < M < 1 M_\odot, \\ 0.04 & 10^{-3} M_\odot < M < 0.1 M_\odot. \end{cases} \tag{5.12}$$

Similar limits were obtained by the POINT-AGAPE collaboration, which detected 6 microlensing events in a survey of the Andromeda galaxy [59]. Since then, further limits have come from the OGLE experiment. The OGLE II data [60] yielded somewhat weaker constraints, but data from OGLE-III [61] and OGLE-IV gave stronger results for the high mass range;

$$f(M) < \begin{cases} 0.02 & 6 \times 0.1 M_\odot < M < 20 M_\odot, \\ 0.09 & 0.04 M_\odot < M < 1 M_\odot, \\ 0.06 & 0.1 M_\odot < M < 0.4 M_\odot. \end{cases} \tag{5.13}$$

It is important to note that these limits depend on some unidentified detections being attributed to self-lensing [7]. Later (comparable) constraints combining EROS and OGLE data were presented in [63]. Recently, Kepler data has improved the limits considerably in the low mass range [64]

$$f(M) < 0.3 \text{ for } (2 \times 10^{-9} M_\odot < M < 10^{-7} M_\odot) \tag{5.14}$$

Millilensing (image separation on the order of milli-arc-seconds) is caused by slightly larger objects such as small satellite galaxies as well as as intermediate mass black holes, so it is still of relevance for studying PBHs of this size. Unlike microlensing, it is not a transient event. The millilensing of compact radio sources [65] gives a limit which can be approximated as

$$f(M) < \begin{cases} (M/2 \times 10^4 M_\odot)^{-2} & M < 10^5 M_\odot, \\ 0.06 & 10^5 M_\odot < M < 10^8 M_\odot, \\ (M/4 \times 10^8 M_\odot)^2 & M < 10^8 M_\odot. \end{cases} \tag{5.15}$$

[7] Self-lensing is the effect due to galaxies at low redshift that source background emission also acting as lenses for the emission from higher redshift galaxies [62].

Dynamical constraints: The effects of PBH collisions on astronomical objects have been the subject of long-standing interest [66]. For example, Zhilyaev [67] has suggested that collisions with stars could produce γ-ray bursts and Khriplovich et al.[68] have examined whether terrestrial collisions could be detected acoustically. Gravitational wave observatories in space (e-LISA) might detect the dynamical effects of PBHs in the mass-range $10^{14} - 10^{20}$g by measuring the gravitational impulse induced by any nearby passing PBH [69], [70]. It has been suggested [71] that halo PBHs could be captured and swallowed by stars in the Galactic disc [8]. The stars would eventually be accreted by the holes, producing a lot of radiation and a population of subsolar black holes which could only be of primordial origin. They argue that every disc star would contain a black hole if the dark matter were in PBHs smaller than 3×10^{26}g and the following analytic argument [40] gives the form of the constraint. Since the time-scale on which a star captures a PBH scales as $\tau_{\rm cap} \propto n_{\rm PBH}^{-1} \propto Mf(M)^{-1}$, requiring this to exceed the age of the Galactic disc implies

$$f < (M/3 \times 10^{26})\text{g}, \tag{5.16}$$

which corresponds to a lower limit on the mass of objects providing the dark matter. A similar analysis of the collisions of PBHs with main-sequence stars, red-giant cores, white dwarfs and neutron stars [72] suggests that collisions are too rare for $M > 10^{20}$g or produce too little power to be detectable for $M < 10^{20}$g. However, in a related argument, the authors of [73] have constrained PBHs as dark matter candidates by considering their capture by white dwarfs and neutron stars [74]. The survival of these objects implies a limit which can be approximated as

$$f(M) < \frac{M}{4.7 \times 10^{24} g}\left[1 - \exp\left(-\frac{M}{2.9 \times 10^{23}\text{g}}\right)\right]^{-1} \quad (2.5 \times 10^{18}\text{g} < M < 10^{25}\text{g}). \tag{5.17}$$

This is similar to equation 5.16 at the high-mass end, the upper cut-off at 10^{25}g corresponding to the condition $f = 1$. There is also a lower cut-off at 2×10^{18}g because PBHs lighter than this will not have time to consume the neutron stars during the age of the Universe. This argument assumes that there is dark matter at the centres of globular clusters and is sensitive to the dark matter density there (taken to be 10^4 GeV cm^{-3}). The authors of [75] have argued that this excludes PBHs from providing the dark matter throughout the sublunar mass window, although this has been disputed [76], [77]. In fact,

[8] A galactic disc is a component of disc galaxies, such as spiral galaxies and lenticular galaxies, which consists of stars and gas. The galactic disc of the Milky Way is notable for its spiral arms.

dark matter density is limited to much lower values than assumed above for particular globular clusters [78], [79]. Binary star systems with wide separation are vulnerable to disruption from encounters with MACHOs [80], [81]. Observations of wide binaries in the Galaxy therefore constrain the abundance of halo PBHs. By comparing the results of simulations with observations, the authors of [82] originally ruled out MACHOs with $M > 43M_\odot$ from providing the dark matter. However, careful analysis by Quinn [83] of the radial velocities of these binaries found that the widest-separation one was spurious, so that the constraint became

$$f(M) < \begin{cases} (M/500M_\odot)^{-1} & 500M_\odot < M \lesssim 10^3 M_\odot, \\ 0.04 & 10^3 M_\odot \lesssim M < 10^8 M_\odot. \end{cases} \tag{5.18}$$

It flattens off above $10^3 M_\odot$ because the encounters are non-impulsive there. The narrow mass window between the microlensing lower bound and the wide-binary upper bound is therefore shrinking and may even have been eliminated altogether.

A variety of dynamical constraints come into play at higher mass scales. These have been studied by Carr and Sakellariadou [66] and apply providing there is at least one PBH per galactic halo. This corresponds to the so-called "incredulity limit" condition

$$f(M) > (M/M_{\rm halo}),\ M_{\rm halo} \simeq 3 \times 10^{12} M_\odot. \tag{5.19}$$

An argument similar to the binary disruption one shows that the survival of globular clusters against tidal disruption by passing PBHs gives a limit

$$f(M) < \begin{cases} (M/3 \times 10^4 M_\odot)^{-1} & 3 \times 10^4 M_\odot < M < 10^6 M_\odot, \\ 0.03 & 10^6 M_\odot < M < 10^{11} M_\odot, \\ (M/M_{\rm halo}) & M > 10^{11} M_\odot. \end{cases} \tag{5.20}$$

However, this depends sensitively on the mass and the radius of the cluster. The limit flattens off above $10^6 M_\odot$ because the encounter becomes non-impulsive. The upper limit of $3 \times 10^4 M_\odot$ on the mass of objects dominating the halo is consistent with the numerical calculations of Moore [84]. In a related limit, Brandt [85] claims that a mass above $5M_\odot$ is excluded by the fact that a star cluster

near the centre of the dwarf galaxy Eridanus II has not been disrupted by halo objects. His constraint can be written as

$$f(M) \lesssim \begin{cases} (M/3.7M_\odot)^{-1}/[1.1 - 0.1 \ln M/M_\odot & M < M < 10^3 M_\odot, \\ (M/10^6 M_\odot) & M > M < 10^3 M_\odot, \end{cases} \tag{5.21}$$

where the density of the dark matter at the centre of the Galaxy is taken to be $0.1 M_\odot \mathrm{pc}^{-3}$, the velocity dispersion there is taken to be 5km s^{-1}, and the age of the star cluster is taken to be 3 Gyr. The second expression in 5.21 was not included in [85] but is the incredulity limit, corresponding to having one black hole for the dwarf galaxy.

Halo objects will overheat the stars in the Galactic disc unless one has [66]

$$f(M) < \begin{cases} (M/3 \times 10^6 M_\odot)^{-1} & M < 3 \times 10^9 M_\odot, \\ (M/M_{\rm halo}) & M > 3 \times 10^9 M_\odot, \end{cases} \tag{5.22}$$

where the lower expression is the incredulity limit. The upper limit of $3 \times 10^6 M_\odot$ agrees with the more precise calculations by Lacey and Ostriker [86], although they argued that black holes with $2 \times 10^6 M_\odot$ could explain some features of disc heating. Constraint 5.22 bottoms out at $M \sim 3 \times 10^9 M_\odot$ with a value $f \sim 10^{-3}$. These disc-heating limits are smaller than others in this mass range.

Another limit in this mass range arises because halo objects will be dragged into the nucleus of our own Galaxy by the dynamical friction of the spheroid stars and halo objects themselves (if they have an extended mass function), which leads to an excessive nuclear mass unless

$$f(M) < \begin{cases} (M/3 \times 10^4 M_\odot)^{-10/7} (\mathrm{r}_c/2\mathrm{kpc})^2 & M < 5 \times 10^5 M_\odot, \\ (M/4 \times 10^4 M_\odot)^{-2} (\mathrm{r}_c/2\mathrm{kpc})^2 & (5 \times 10^5 M_\odot \ll M < 2 \times 10^6 (\mathrm{r}_c/2\mathrm{kpc}) M_\odot), \\ (M/0.1 M_\odot)^{-1/2} & (2 \times 10^6 (\mathrm{r}_c/2\mathrm{kpc}) M_\odot < M < 10^7 M_\odot, \\ (M/M_{\rm halo} & M > 10^7 M_\odot. \end{cases} \tag{5.23}$$

The last expression is the incredulity limit and the first three correspond to the drag being dominated by spheroid stars (low M), halo objects (high M) and some combination of the two (intermediate M). The limit bottoms out at $M \sim 10^7 M_\odot$ with a value $f \sim 10^{-5}$ but is sensitive to the halo core radius

r_c. Moreover, there is a caveat here in that holes drifting into the nucleus might be ejected by the slingshot mechanism[9] if there is already a binary black there [87]. This possibility was explored by Xu and Ostriker [88], who obtained an upper limit $3 \times 10^6 M_\odot$.

Each of these dynamical constraints is subject to certain conditions but it is worth noting that they all correspond to an upper limit on the mass of the objects which dominate in the halo in the range $500 - 2 \times 10^4 M_\odot$, the binary disruption limit being the strongest. This is particularly relevant for constructing models in which the dark matter is postulated to compromise intermediate-sized black holes (IMBHs). Apart from the Galactic disc and elliptical galaxy heating arguments of [86], it must be stressed that none of these dynamical effects gives *positive evidence* for MACHOs. Furthermore, none of them requires the MACHOs to be PBHs. Indeed, they could equally well be clusters of smaller objects [88], [89] or Ultra-Compact Mini-Halos (UCMHs)[10] [91]. This is pertinent in light of the claim by [92] that PBHs could form in tight clusters, giving a local overdensity well in excess of that provided by the halo concentration alone. It is also important to note that the UCMH constraints on the density perturbations may by stronger than the PBH limits in the higher mass range [91]. This is relevant if one wants to consider the effect of an extended mass function.

Large-scale Structure Constraints: Sufficiently large PBHs could have important consequences for large-scale structure formation because of the Poisson fluctuations (the expected relative fluctuations in a random sample of size N are $\delta N/N \propto 1/\sqrt{N}$ in their number density). This effect was first pointed out be Mészáros [93] and subsequently studies by various authors [94]. In particular, [95] used observations of the Lyman-α forest[11] to obtain an upper limit of about $10^4 M_\odot$ on the mass of any PBHs which provide the dark matter. Since Poisson fluctuations in the number density of PBHs on a mass-scale $M_{\mathrm{Ly}\alpha} \sim 10^{10} M_\odot$ grows between the redshift of CDM domination ($z_{eq} \sim 4000$) and the redshift at which Lyman-α clouds are observed ($z_{\mathrm{Ly}\alpha}$) by a factor $z_{eq}/z_{\mathrm{Ly}\alpha} \sim 10^3$, the clouds will bind too early unless

$$f(M) < \begin{cases} (M/10^4 M_\odot)^{-1} (M_{\mathrm{Ly}\alpha}/10^{10} M_\odot) & M < 10^7 M_\odot, \\ (M/10^{10} M_\odot)(M_{\mathrm{Ly}\alpha}/10^{10} M_\odot)^{-1} & M > 10^7 M_\odot. \end{cases} \tag{5.24}$$

[9] In few body systems, one can speed up the orbit of one of the bodies through gravitational interactions in the system.

[10] UCMHs are expected to form at early times in regions with $\delta\rho/\rho \geq 10^{-3}$, and they are theorised to possess an extremely compact $\rho \propto r^{-9/4}$ radial density profile, which enhances their observable signatures [90].

[11] The Lyman-alpha forest is a series of absorption lines in the spectra of distant galaxies and quasars arising from the Lyman-alpha electron transition of the neutral hydrogen atom.

The lower expression corresponds to having at least one PBH per Lyman-α mass, so the limit bottoms out at $M \sim 10^7 M_\odot$ with a value $f \sim 0.001$. The data from SDSS are more extensive [96], so the limiting mass may now be reduced. A similar effect can allow clusters of large PBHs to evolve into the supermassive black holes in the galactic nuclei [97]; if one replaces $M_{\mathrm{L}t\alpha}$ with $10^8 M_\odot$ and $(z_{\mathrm{Ly}\alpha})$ with 10 in the above analysis, the limiting mass in equation 5.24 is reduced to $600 M_\odot$.

Accretion Constraints: The growth of PBHs in the radiation era is strongly constrained by relativistic hydrodynamical considerations and the known deuterium abundance in subsequent eras [98], and consequently there is little growth during this time. In the period after decoupling, there could be larger growth and one can apply a Bondi-Hoyle-Lyttleton model of accretion (see A) to investigate the growth of PBHs [99]. The associated accretion and emmission of radiation could have a substantial effect on the thermal history of the Universe, as detailed in Ricotti *et al.* [100] who studied the effects of accreting PBHs on the ionisation and temperature evolution of the Universe. The emitted X-rays would produce measurable effects in the spectrum and anisotropies of the CMB. Using FIRAS[12] data to constrain the former and WMAP data to constrain the latter, they improve upon the constrains on *f(M)* by several orders of magnitude for $M > 1 M_\odot$. The WMAP limit can be approximated as

$$f(M) < \begin{cases} (M/30M_\odot)^{-2} & (30M_\odot < M \lesssim 10^4 M_\odot), \\ 10^{-5} & (10^4 M_\odot \lesssim M < 10^{11} M_\odot), \\ M/M_{l=100} & (M > 10^{11} M_\odot), \end{cases} \tag{5.25}$$

where the last expression corresponds to having one PBH on the scale associated with CMB anisotropies. For $l = 100$ modes, this is $M_{l=100} \approx 10^{16} M_\odot$. The FIRAS limit can be approximated as

$$f(M) < \begin{cases} (M/1M_\odot)^{-2} & (1M_\odot < M \lesssim 10^3 M_\odot), \\ 0.015 & (10^3 M_\odot \lesssim M < 10^{14} M_\odot), \\ M/M_{l=100} & (M > 10^{14} M_\odot), \end{cases} \tag{5.26}$$

These limits are dependent on the assumptions of BHL accretion and are therefore not as secure as dynamical constraints. In particular, there is dependence on the fraction of time PBHs spend

[12] FIRAS stands for Far-InfraRed Absolute Spectrophotometer and is used to measure the spectrum of the CMB.

accreting near the Eddington limit[13] called f_{duty}. Observations from active galactic nuclei suggest that $f_{duty} \approx 0.03$, however the nature of the feedback mechanisms for PBHs are poorly understood, and as a result f_{duty} in Riccotti's paper cannot be estimated to good accuracy [100].

5.1.2 Intermediate-mass range

The most significant constraints on the intermediate-mass range (roughly between $M_\odot < M < 10^3 M_\odot$) are dynamical and are shown in figure 8; EROS[101], Wide-binary [102] and Eridanus II[85]. Other constraints have been excluded for reasons of uncertainty, overlap and model-dependency. The constrain can be written as

$$f(M) \lesssim \frac{0.5\left(1+\frac{0.046 M_\odot \mathrm{pc}^{-3}}{\rho}\right)\left(\frac{10M_\odot}{M}\right)\left(\left(\frac{\sigma}{10\mathrm{km\ s}^{-1}}\right)\right.}{\left(1+0.1\ln\left[\frac{10M_\odot}{M}\left(\frac{\sigma}{10\mathrm{km\ s}^{-1}}\right)^2\right]\right)}, \tag{5.27}$$

where ρ is the density and σ is the velocity dispersion of the dark matter at the centre of the galaxy. This reduces to equation 5.21 for $\rho = 0.1 M_\odot \mathrm{pc}^{-3}$ and $\sigma = 5\mathrm{km\ s}^{-1}$. The constraints 5.21 assume and a star cluster age of 3 Gyr. However, it could be as old as 12 Gyr [103], in which case the equations must be modified and yield tighter constraints [85].

As can be seen from figure 8, the least restrictive Eridanus II[14] constraint, corresponding to $\rho = 0.01 M_\odot \mathrm{pc}^{-3}$ and $\sigma = 10\mathrm{km\ s}^{-1}$, admits a monochromatic function containing all the dark matter at $M \approx 30 M_\odot$. As observations of the dwarf galaxy and wide binaries improve, this gap may be filled. However, a monochromatic mass function is not very physical. A model-independent way of assessing the more realistic extended mass function case is to consider where the different constraints cross. For $\rho = 0.1 M_\odot \mathrm{pc}^{-3}$, $\sigma = 5\mathrm{km\ s}^{-1}$ (red solid curve), the Eridanus II and microlensing constraints cross at $M \approx 10 M_\odot$ and $f \approx 0.4$. This means that 40% of the dark matter can be contained in PBHs with $M < 10 M_\odot$, thereby evading the microlensing bounds, and another 40% in PBHs with $M > 10 M_\odot$, thereby evading the Eridanus II constraints. Hence the Eridanus II and microlensing constraints together exclude PBHs from having more than 80% of the dark matter in this intermediate-mass range. The slightly less restrictive Eridanus II constraint with $\rho = 0.1 M_\odot \mathrm{pc}^{-3}$, $\sigma = 10\mathrm{km\ s}^{-1}$ (red

[13] The Eddington limit is the maximum mass a body can achieve when there is balance between the force of radiation acting outward and the gravitational force acting inward. At the Eddington mass limit, the outward pressure of the body's radiation balances the inward gravitational force.

[14] Eridanus II is a low-surface brightness dwarf galaxy in the constellation Eridanus. Eridanus II was independently discovered by two groups in 2015. It contains a centrally located globular cluster; and is the smallest, least luminous galaxy known to contain a globular cluster. Eridanus II is significant because the widely accepted ΛCDM cosmology predicts the existence of many more dwarf galaxies than have yet been observed.

dashed line) crosses the microlensing constraints at $M \approx 20M_\odot$ and $f \approx 0.5$, marginally allowing the dark matter to be in PBHs in this range. However, in this case the extended mass function has to be perfectly tuned to fit beneath the bounds, which is unlikely. On the other hand, for $\rho = 0.01M_\odot \mathrm{pc}^{-3}$, $\sigma = 5\mathrm{km\ s}^{-1}$ (red dot-dashed curve) and $\rho = 0.01M_\odot \mathrm{pc}^{-3}$, $\sigma = 10\mathrm{km\ s}^{-1}$ (red dotted line), a mass function which provides all the dark matter is certainly possible.

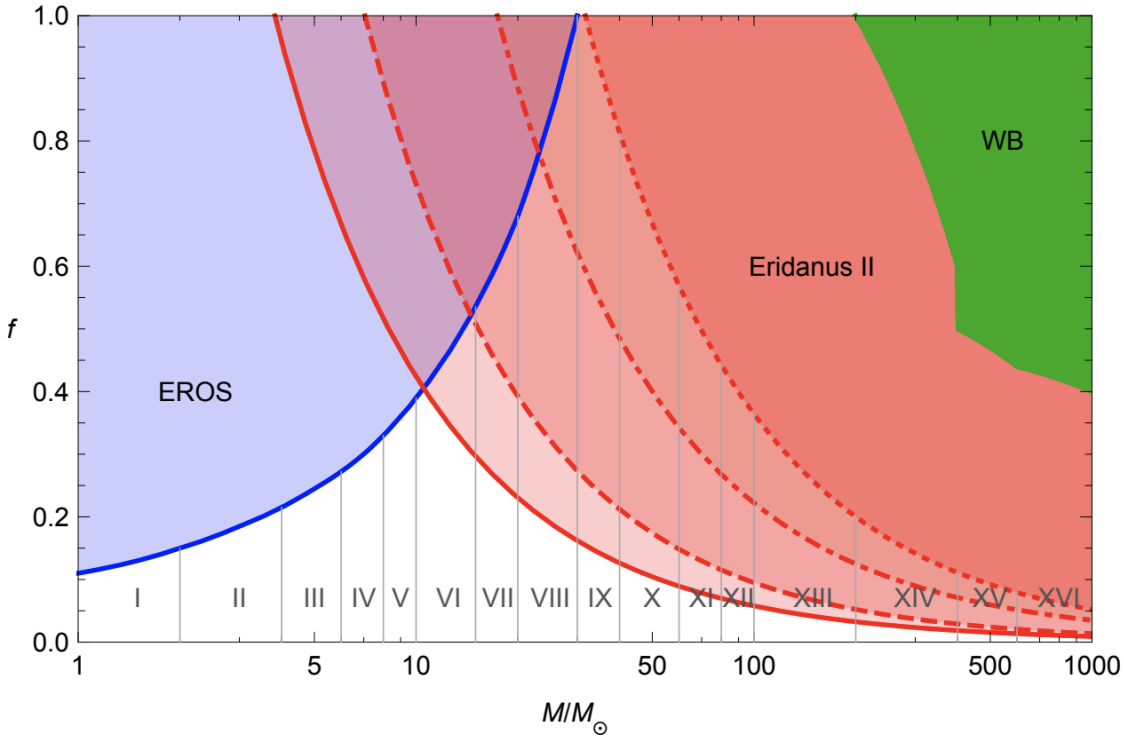

Figure 8. Constraints on the dark matter fraction of primordial black holes in the intermediate-mass range $M_\odot < M < 10^3 M_\odot$. Excluded regions are shaded. EROS constraints are taken from [101] and are depicted in blue. Wide-binary (WB) constraints [102] correspond to the green region in the plot. The latest constraints from the survival of the star cluster near the core of Eridanus II [85] are shown in the red-shaded areas. For all red curves we assume a cluster age of 3 Gyr. The various constraints are due to different choices of values for the velocity dispersion σ and the dark matter density in the centre of the galaxy ρ. Taken from [28].

From these and other constraints, an extended mass function contributing an equal density at all mass scales can also be excluded. Even without including the Eridanus II constraints, if such a function extends to the range of microlensing observations, the most restrictive range for these indicates that the mass function cannot make up more than 4% of the dark matter over the two orders of magnitude from $10^{-3}M_\odot$ to $0.1M_\odot$. To get the total dark matter in PBHs, one would then need 50 orders of magnitude, whereas the widest possible range, ignoring all other observations, would be from $10^{-15}M_\odot$

to $10^{17} M_\odot$, which is only 32 orders of magnitude. In practice, the upper limit may be considerably tighter for both observational and theoretical reasons. Hence some bumpy feature is needed to provide the dark matter without violating the constraints. If the strongest Eridanus II constraints is taken seriously, this bumpy feature cannot be confined to the $30 M_\odot$ region. Instead, the bump must either be located at a lower mass or, if restrictive bounds from neutron-star capture [73] and star formation [74] can be trusted, a (camel-like) feature with at least two bumps in the appropriate regions might be necessary to put all the dark matter in PBHs [28].

The suggestion that the dark matter could comprise PBHs has attracted much attention in recent years as a result of the LIGO/Virgo detections [104]. To date, 10 events have been observed with black hole masses in the range $8 - 51 M_\odot$. After the first detection, Bird et al.[105] claimed that the expected merger was compatible with the range obtained by the LIGO analysis and this was supported by other studies [106], [107]. On the other hand, Sasaki et al.[108] argued that the lower limit on the merger rate would be in tension with the CMB distortion constraints if the PBHs provided all the dark matter, although one might avoid these constraints if the LIGO/Virgo back holes derive from the accretion and merger of smaller PBHs [107]. Raidal et al. [109] have studied the production and merging of PBH binaries for an extended mass function and possible PBH clustering. They show that PBHs can explain the LIGO/Virgo events without violating any current constraints if they have a lognormal mass function. Subsequent work [110] has studied the formation and disruption of PBH binaries in more detail, using both analytical and numerical calculations for a general mass function. If PBHs make up just 10% of the dark matter, the analytic estimates are reliable and indicate that the constraint from the observed LIGO/Virgo rate is strongest in the mass range $2 - 160 M_\odot$, albeit weakened because of the suppression of mergers. Their general conclusion is that the LIGO/Virgo events can result from the mergers of PBHs but that such objects cannot provide all the dark matter unless the PBHs have an extended mass function.

The intermediate-mass range is arguably the most popular amongst cosmologists as it has the potential to explain multiple open problems. Silk [111] has proposed that intermediate-mass PBHs (IMPBHs) could be the answer to many dwarf galaxy[15] anomalies. IMPBHs may have been common in early dwarf galaxies, mostly passive today but active in their gas-rich past. They could suppress the number of luminous dwarfs, generate cores in dwarfs by dynamical heating, form ultra-faint dwarfs

[15] A dwarf galaxy is a small galaxy composed of 1000 up to several billion stars, as compared to the Milky Way's 200–400 billion stars.

and trigger star formation in dwarfs via the active galactic nucleus (AGN). They could also reduce the baryon fraction in Milky-Way type galaxies, produce ultra-diffuse galaxies and explain ultra-luminous X-ray sources in the outskirts of galaxies. Perhaps the most effectual function of IMPBHs would be as seeds of the supermassive black holes we see at the centre of galaxies today. More discussion of this will follow in section 5.2.

5.1.3 Sublunar-mass range

The sublunar-mass range lies between $10^{20}\text{g} < M < 10^{24}\text{g}$ (or with $M_\odot = 1.99 \times 10^{33}\text{g}$, between $10^{-14}M_\odot < M < 10^{-10}M_\odot$). Figure 9 shows the constraints on the mass function from GRB femtolensing and Kepler microlensing. It also shows the neutron-star capture constraint, but is reliant on the uncertain assumption that there is dark matter in globular clusters [16]. If the NS constraint is omitted, PBHs could provide all of the dark matter at 10^{20}g and $4 \times 10^{24}\text{g}$, where $f = 1$. However, the inclusion of the NS constraint [73] could significantly alter this scenario, depending on the dark matter density in the core of globular clusters.

The three lines in figure 9 correspond to $\rho_{\text{DM}} = 4 \times 10^2$ GeV cm^{-3} (solid), $\rho_{\text{DM}} = 2 \times 10^3$ GeV cm^{-3} (broken) and $\rho_{\text{DM}} = 10^4$ GeV cm^{-3} (dotted). In all of these cases, PBHs are excluded from providing all the dark matter at the lower mass end, where the NS and femtolensing bounds meet. So if the NS bounds are believed, only the window at the upper end is allowed. For the highest dark-matter density, $\rho_{\text{DM}} = 10^4$ GeV cm^{-3}, the NS constraint intersects the Kepler constraint at $f_{\text{meet}} \approx 0.35$, so PBHs cannot provide all the dark matter, whatever the shape of the mass function. For $\rho_{\text{DM}} = 2 \times 10^3$ GeV cm^{-3} which is suggested by some numerical models [73], the constraints cross at $f_{\text{meet}} \approx 0.75$, so a monochromatic mass function cannot give all the dark matter but an extended one could allow a fraction $2f_{\text{meet}} \approx 1.5$. Indeed, if one applies critical collapse to an initially monochromatic mass function, one evades the constraints in the mass range $1 - 2 \times 10^{24}$ g. For the lowest dark-matter density shown, $\rho_{\text{DM}} = 4 \times 10^2$ GeV cm^{-3}, even a monochromatic mass function is allowed, so it is important to stress that the density is known to be as low as 1GeV cm^{-3} for some globular clusters [112]. Indeed, according to [73], dark-matter densities below 120GeV cm^{-3} always lead to constraints above $f = 1$.

The sublunar-mass range between has received a peak in interest due to the upcoming LISA mission

[16] A globular cluster is a spherical collection of stars that orbits a galactic core. Globular clusters are very tightly bound by gravity, which gives them their spherical shapes, and relatively high stellar densities toward their centres.

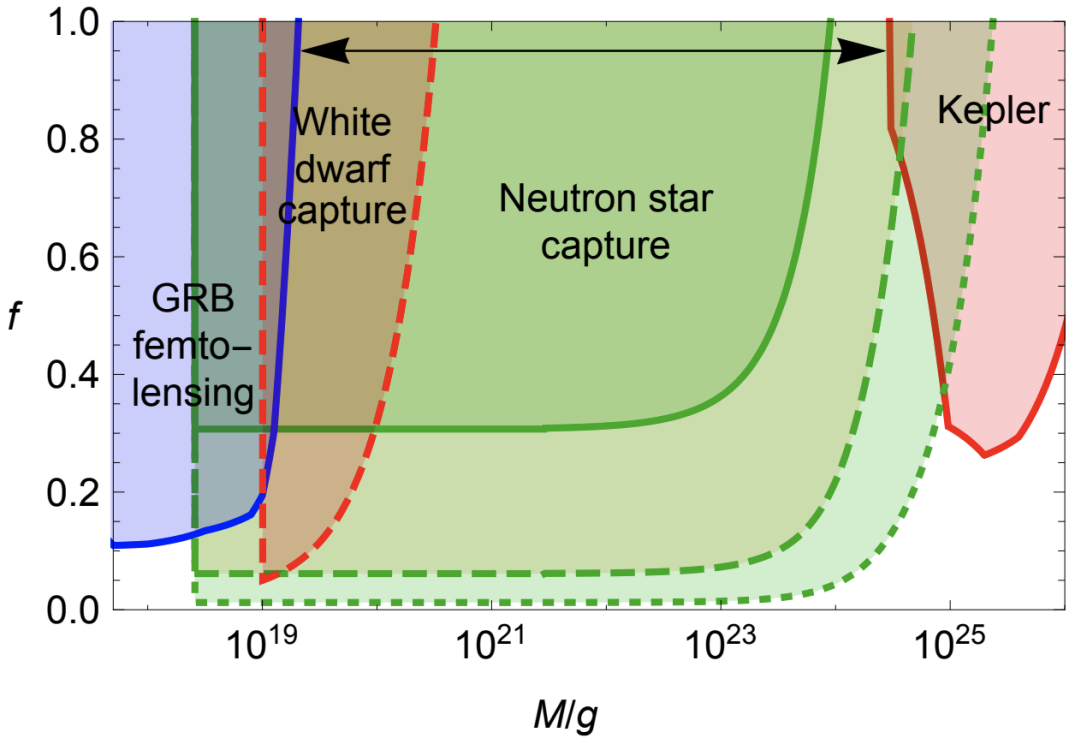

Figure 9. Constraints on the dark matter fraction of primordial black holes in the sublunar-mass range $10^{20}\text{g} < M < 10^{24}\text{g}$. The constraints in blue are the femtolensing of GRBs from [113], while the limits from neutron-star capture (in green) are taken from [73]. The red-shaded region to the right-hand side of the plot denotes microlensing constraints from the Kepler survey [114], while the red-shaded region to the plot's left-hand side shows constraints from white-dwarf explosions [115]. Taken from [28].

[116]. LISA (Laser Interferometer Space Antenna) will be the first space-situated gravitational wave observatory, due to be launched in the 2030s. If sublunar-mass PBHs are generated by enhanced scalar perturbations produced during inflation, their formation is accompanied by the generation of non-Gaussian gravitational waves with a frequency peaking within the range sensitive to LISA, irrespective of the value of f_{NL} (non-linear evolution of non-Gaussian perturbations) [117]. These PBHs could potentially provide all of the dark matter [118].

5.2 PBHs as seeds for structure formation

The hypothesis for cold dark matter (CDM) structure formation begins with density perturbations in the Universe that grow linearly until they reach a critical density, after which they would stop expanding and collapse to form gravitationally bound dark matter halos. These halos would continue to grow in mass (and size), either through accretion of material from their immediate neighbourhood

or by merging with other halos. Numerical simulations of CDM structure formation proceed as follows: a small volume with small perturbations initially expands with the expansion of the Universe. As time proceeds, small-scale perturbations grow and collapse to form small halos. At a later stage, these small halos merge to form a single virialized dark matter halo with an ellipsoidal shape. The fact that the dark matter is cold compared to the baryonic matter allows the dark matter to form these initial, gravitationally bound clumps with some subhalo structures. Once these subhalos formed, their gravitational interaction with baryonic matter is enough to overcome the thermal energy, and allow it to collapse into the first stars and galaxies.

PBHs could be a source of fluctuations which then grow and bind overdense regions. There are two possible mechanisms behind this perturbative effect; the seed effect and the Poisson effect. The former produces an initial density fluctuation via the gravitational Coulomb effect of a single black hole. The latter involves the $\sqrt{N}$ fluctuation in the number of black holes generating an initial density fluctuation. A PBH of mass m growing by gravitational instability to bind regions of mass M produces initial density fluctuations δ_i

$$\delta_i \approx \begin{cases} m/M & \text{seed effect} \\ \sqrt{\frac{fm}{M}} & \text{Poisson effect} \end{cases} \tag{5.28}$$

where f is the fraction of the dark matter in PBHs and M excludes the radiation content. If PBHs provide the dark matter, $f \approx 1$ and the Poisson effect dominates for all M but we also consider scenarios with $f \ll 1$. The Poisson effect then dominates for $M > m/f$ and the seed effect for $M < m/f$. This interplay between the two effects can be seen in figure 10. One can also compare the seed and Poisson fluctuations with the primordial density fluctuations implied by the CDM model. At the time of matter-radiation equality, $t_{\rm eq} \sim 10^4$ yrs, when the PBH fluctuations started to grow, the primoridal fluctuations have the form

$$\delta_{\rm eq} \propto \begin{cases} M^{-1/3} & M < M_{\rm eq} \\ M^{-2/3} & M > M_{\rm eq} \end{cases} \tag{5.29}$$

where $M_{\rm eq} \sim 10^{16} M_\odot$ is the horizon mass at $t_{\rm eq}$. There is generally a mass $M_{\rm CDM}$ below which the PBH fluctuation dominates, due either to the seed effect for $f \ll 1$ or the Poisson effect for $f \approx 1$, so this produces extra power on small scales. However, in the mass range $M < M_{\rm eq}$ relevant to the present

considerations, the CDM fluctuations fall off slower than both the Poisson and seed fluctuations, so they dominate for sufficiently large M. In the mass range $M > M_{\rm eq}$, the CDM fluctuations fall off slower than the seed fluctuation but faster than the Poisson fluctuation, so the latter could dominate again on very large scales, with CDM only dominating over some intermediate range of M.

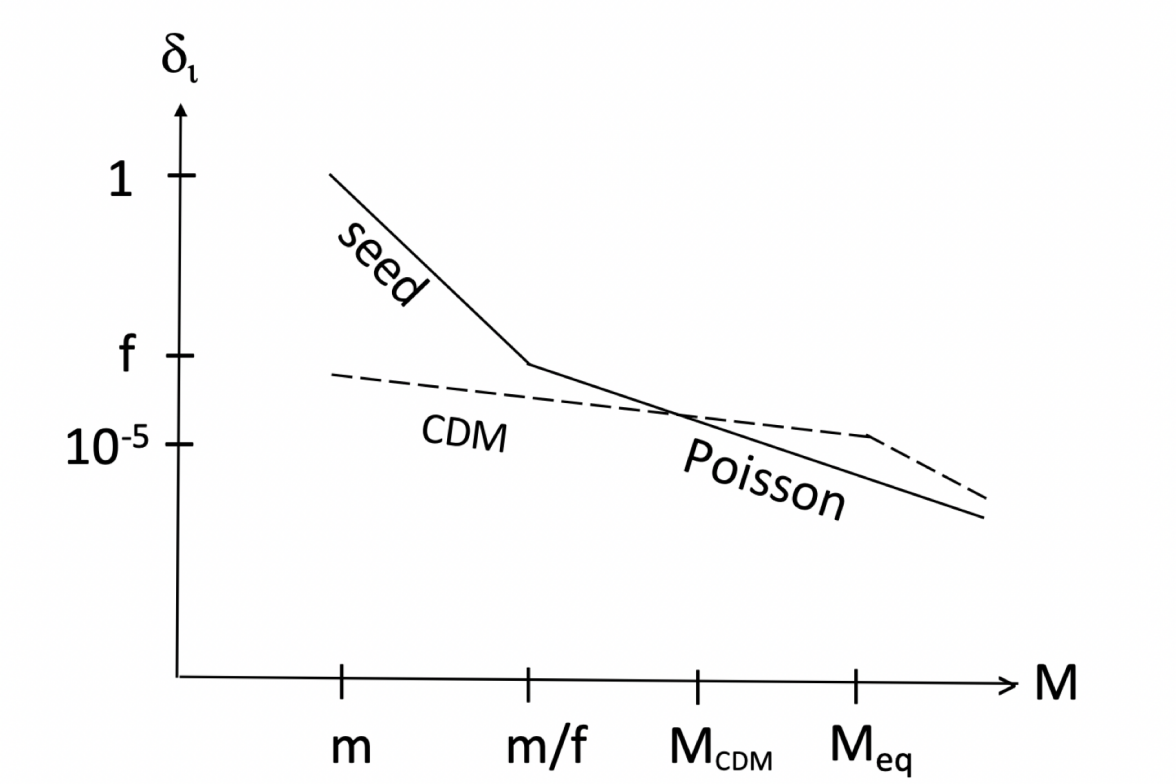

Figure 10. Form of initial fluctuations δ_i as a function of M for the seed and Poisson effects for monochromatic f. The seed effect dominates at small M if f is small but the Poisson effect always dominates for $f \approx 1$. $M_{\rm eq}$ is the horizon mass at matter-radiation equality and $M_{\rm CDM}$ is the mass below which PBH fluctuation dominate over primoridial density fluctuations implied by the CDM model. Taken from [119]

Of course, this is assuming a monochromatic mass function for the PBHs, which as previously discussed is not physical. An extended mass function may cause the seed and Poisson effects to operate on different scales. This requires a more considered approach and numerical calculations [119].

5.3 PBHs as seeds for supermassive black holes

There is clear evidence that supermassive black holes (SMBHs) with masses between $10^5 - 10^{10} M_\odot$ reside in the centre of most galaxies, including our own [120], [121]. Observations of quasars[17] suggest that these were already in place at very early times ($z > 6$) and so may be primoridial in origin. This includes the recent discovery of quasars powered by black holes of mass $1.2 \times 10^{10} M_\odot$ at $z = 6.3$ [123] and $8 \times 10^8 M_\odot$ at $z = 7.5$ [124]. The standard view is that SMBHs formed through dynamical processes in galactic nuclei after galaxy formation [125]. However, the evidence for this is inconclusive so it is still worth considering the possibility that SMBHs may form before galaxies.

There are three possible scenarios for pre-galaxy formation PBHs. The first is that the PBHs themselves were supermassive and could help generate galaxies through the seed or Poisson effect in line with 'seed' theories of galaxy formation [126]. This would naturally explain the direct relationship between black hole and galaxy mass. Additionally, it could provide an early mode of galaxy formation that may be important for the reionisation of the Universe. Recent observational and theoretical progress has led to the conclusion that the limit of hydrogen-ionising photons is dominated by low-mass star-forming galaxies, with little contribution from Pop III stars and quasars [127]. The reionization history of the Universe therefore critically depends on the number density of low-mass galaxies at high redshift.

The second scenario is that PBHs in the intermediate-mass range grew through Eddington-limited accretion. This was first suggested by Bean and Magueijo [128] who employed the theory of quintessence to grow the black holes. Since most accretion occurs after decoupling, it may be difficult to observationally distinguish between black holes of primordial and non-primordial origin. Recent results from numerical simulations suggest that the growth rate of early Universe direct-collapse black holes is not fast enough to produce the magnitude of SMBHs we observe today [129]. Beckmann [99] uses an adaptive-mesh refinement code to simulate the growth of black holes in mini-halos (not primordial) accreting via the Bondi-Hoyle-Lyttleton model (see appendix A), although they do not limit accretion by the Eddington rate. They found that accretion onto the black hole is driven by surrounding cloud structure, independent of the black hole seed mass. Black hole mass growth predominantly occurs when infalling dense clumps trigger instabilities in the accretion disc surrounding the black

[17] A massive and remote celestial object which emits exceptionally large amounts of energy, and typically has a starlike image in a telescope. It has been suggested that quasars contain black holes and may represent a stage in the evolution of some galaxies [122]

hole, fuelling intense but short-lived accretion episodes. There may be some hope yet for PBHs to achieve a sufficient growth, but the models must be tried and tested further to improve accuracy and reliability.

The third possibility is that the PBHs had a more modest mass and generated the SMBHs in galactic nuclei through the seed or Poisson effect. For example, to produce a SMBH with $M \sim 10^8 M_\odot$ by $z \sim 4$, one considers the discussion in section 5.2 and uses the fact that matter-radiation equality corresponds to a redshift $z_{\rm eq} \approx 4000$ and an overdense region binds when $\delta_i \approx 1$ to write down the mass binding at redshift z_B,

$$M \approx \begin{cases} 4000 m z_B^{-1} & \text{seed effect} \\ 10^7 f m z_B^{-2} & \text{Poisson effect.} \end{cases} \tag{5.30}$$

Using this equation, we see that we require $m \sim 10^5 M_\odot$ for the seed effect or $m \sim 10^2 M_\odot$ for the Poisson effect. However, the largest SMBHs have a mass $\sim 10^{10} M_\odot$ [130], so in this case we would require $m \sim 10^7 M_\odot$ for the seed effect or $m \sim 10^4 M_\odot$ for the Poisson effect. However, one still has to explain how the gravitationally bound region around an IMPBH or a bound cluster of intermediate mass PBHs can evolve to a single SMBH. Accretion and merging could be important and only some fraction of the bound region may end up in the central black hole.

6 Summary and Outlook

In the introduction, fundamental concepts from cosmology were derived, such as the FLRW metric and how it evolves according to the Einstein equations, and the equations which link together key cosmological parameters (the Friedmann, fluid and acceleration equations). The history and properties of dark matter were briefly covered along with a motivation for its existence from calculating the mass density parameter of a galaxy cluster, following the reasoning of Fritz Zwicky. The difference between black holes of stellar and primordial origin was outlined, as was the tentative beginnings of the field in the 60s and 70s based on the work of Novikov, Zel'dovich, Hawking and Carr.

In the following chapter, a timeline of the evolution of the Universe is provided to contextualise our discussion. The horizon problem and inflation are explained and the slow roll parameters are stated. The Boltzmann equations for photons and CDM is derived, as are the Boltzmann equations in the radiation-dominated early Universe. These equations provide a way of dealing with the coupling of the initial fluctuations in the radiation with each other and with the metric. They form the groundwork

on which the next chapter is based: cosmological perturbation theory. In this chapter, the scalar field driving inflation was split into a homogeneous part and a perturbation and both parts are discussed in some detail. The power spectrum of fluctuations due to inflation Ψ was derived in detail. The final section covered the derivation of the curvature power spectrum of initial fluctuations.

As the Universe evolves, these primordial fluctuations produce overdensities which accumulate matter and eventually form structures through gravitational instability. In chapter 4, the matter power spectrum was derived and used to find an expression for the fraction of the Universe which exceeds the threshold density for PBH formation when they were first forming. The Press-Schechter formalism was employed here but its shortcomings were discussed in the last section of this chapter. These calculations were done under the assumption that the PBH mass at formation is uniform (monochromatic mass function), yet this is probably naive. A more likely scenario is that the mass function is extended. These two functions were compared in section 4.4. We then considered a nearly-monochromatic mass function in the critical collapse model of formation and discussed its practicality. Two alternative models of inflation which are conducive to PBH formation (and also to their possible role as dark matter) were investigated; hybrid inflation and running-mass inflation. Finally, some assumptions concerning PBH formation mechanisms were critiqued, the primary issues being the sphericity and gaussianity assumptions.

The final chapter covered the role of PBHs in cosmology; namely, providing some or all of the dark matter and seeding black holes and structure formation. An overview of observational constraints on the monochromatic PBH mass spectrum was provided, with the broad categories of evaporation, dynamical, lensing, large-scale structure and accretion. The adjustments required for constraints on an extended mass spectrum were discussed. The intermediate-mass and sublunar-mass ranges were given particular attention in the context of the dark matter problem due to recent discoveries and research developments. The potential of PBHs to drive structure formation via the seed and Poisson effects was considered, as was the possibility that PBHs grew into the supermassive black holes we observe in the centre of galaxies today.

It is undeniable that primordial black holes have gained significant interest over the past five or so years. A good representation of this is the exponential increase in the number of citations of Carr and Hawking's seminal paper on primordial black holes since its publication in 1974 [19], as shown in figure 11. The number of citations peaked last year and is very high this year also. This invigorated interest

can be largely attributed to the observations of black hole mergers and the detection of gravitational waves made by LIGO, which first occurred in 2015 [131]. The black holes observed by LIGO since then have generally been larger than expected, with the largest being an enormous $150M_{\odot}$ post-merger [132], which has raised discussion of alternative formation mechanisms to stellar collapse [133], [134], [135] and suggestions that these black holes are of primordial origin [136], [108], [105]. In addition, there is a possibility that PBHs may be detected from the stochastic gravitational wave background [137] by the space-based observatory LISA, due to be launched in the 2030s [138].

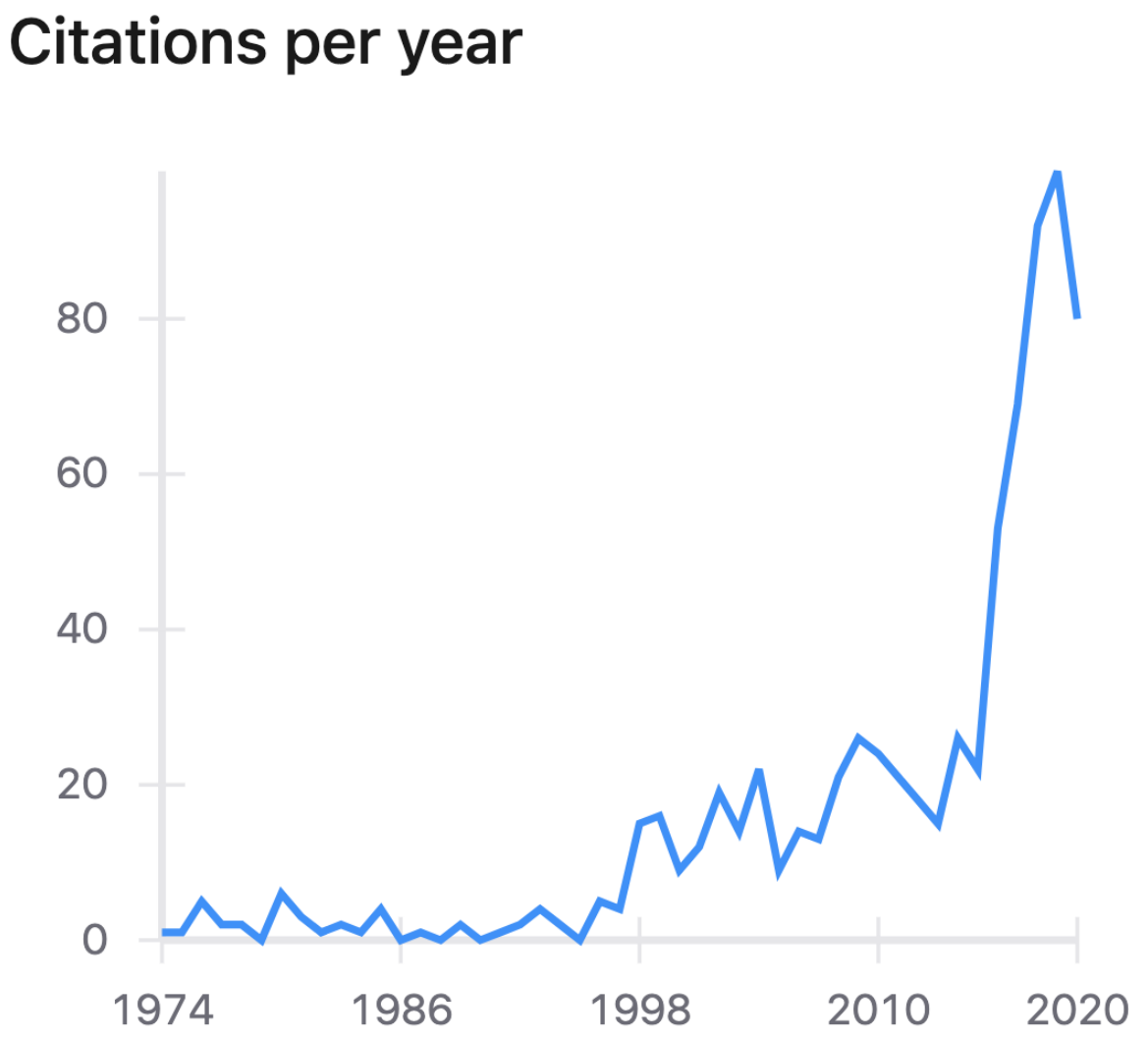

Figure 11. The number of citations per year of Carr and Hawking's 1974 seminal paper [19] which instigated the study of primordial black holes. Taken from [139].

However, understanding the theory behind early Universe black hole formation and evolution will play a crucial role in detection. There is much work to be done on models of black hole growth, not just for primordial black holes, but also black holes from Pop III stars [129] and direct collapse in dark matter halos [99]. Data from these simulations can be fed into the upcoming James Webb Space Telescope to try and detect such early Universe black holes [140]. Improving these simulations will pave the way for more sophisticated models of PBH growth in the future and detecting early Universe black holes would be a significant step forward towards elucidating whether or not there exist black holes of primordial origin.

A Bondi-Hoyle-Lyttleton Accretion Model

There can be some confusion around the terms 'Bondi accretion', 'Bondi-Hoyle-Lyttleton model' and the 'Hoyle-Lyttleton accretion rate'. This appendix will elucidate the meaning of these terms, how they're related and the differences between them. We follow the approach taken in [141].

Hoyle and Lyttleton [142] considered accretion by a star moving at a steady speed through an infinite gas cloud. The gravity of the star focuses the flow into a wake which it then accretes. Their logic was as follows. Consider a streamline with impact parameter ξ. If this follows a ballistic orbit with negligible pressure, then one can apply conventional orbit mechanics from Newton's second law of motion and the law of gravitation for the first equation and conservation of angular momentum for the second,

$$\ddot{r} - r\dot{\theta}^2 = -\frac{GM}{r^2}, \tag{A.1}$$

$$r^2\dot{\theta} = \chi\nu_\infty, \tag{A.2}$$

in radial and polar directions respectively, where m, M, r, v_∞ and G are the mass of the particle, the mass of the gravitating object, the radial distance of the particle from the object, the velocity of the particle far upstream, and the gravitational constant, respectively. See figure 12 for details of the setup. Setting $h = \xi\nu_\infty$ and making the substitution $u = 1/r$, we may rewrite the first equation as

$$\frac{\mathrm{d}^2u}{\mathrm{d}\theta} + u = \frac{GM}{h^2}. \tag{A.3}$$

The general solution to this ODE is $u = A\cos\theta + B\sin\theta + C$ for arbitrary constants A, B and C.

Substitution of this general solution immediately shows that $C = GM/h^2$. The values of A and B are fixed by boundary conditions that $u \to 0$ ($r \to \infty$) as $\theta \to \pi$, and that

$$\dot{r} = -h\frac{\mathrm{d}u}{\mathrm{d}\theta} \to -\nu_\infty \text{ as } \theta \to \pi. \tag{A.4}$$

These conditions will be satisfied by

$$u = \frac{GM}{h^2}(1 + \cos\theta) - \frac{\nu_\infty}{h}\sin\theta. \tag{A.5}$$

Now consider when the flow encounters the $\theta = 0$ axis. As a first approximation, the θ velocity will go to zero at this point. The radial velocity will be ν_∞ and the radius of the streamline will be given by

$$\frac{1}{r} = \frac{2GM}{h^2}. \tag{A.6}$$

Assuming that material will be accreted if it is bound to the star, we have

$$\frac{1}{2}\nu_\infty^2 - \frac{GM}{r} < 0, \tag{A.7}$$

or

$$\chi < \chi_{\mathrm{HL}} = \frac{2GM}{\nu_\infty^2}, \tag{A.8}$$

which defines the critical impact parameter, known as the Hoyle-Lyttleton radius. Material with an impact parameter smaller than this value will be accreted. the mass flux is therefore

$$\dot{M}_{\mathrm{HL}} = \pi\chi_{\mathrm{HL}}^2\nu_\infty\rho_\infty = \frac{4\pi G^2M^2\rho_\infty}{\nu_\infty^3}, \tag{A.9}$$

which is the *Hoyle-Lyttleton accretion rate*.

The Hoyle-Lyttleton analysis contains no fluid effects, which makes it suitable for analytic solution. This was performed by [143], who derived the following solution for the flow field

$$\nu_r = -\sqrt{\nu_\infty^2 + \frac{2GM}{r} - \frac{\chi^2\nu_\infty^2}{r^2}}, \tag{A.10}$$

$$\nu_\theta = \frac{\chi\nu_\infty}{r}, \tag{A.11}$$

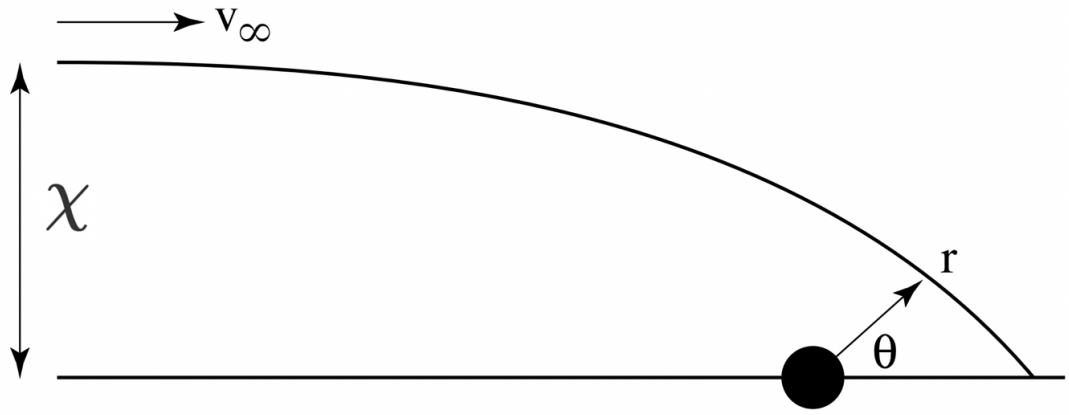

Figure 12. Diagram of Bondi-Hoyle-Lyttleton accretion geometry [141]. χ is the impact parameter, r is the radius and θ is the angle between the object trajectory and the axis.

$$r = \frac{\chi^2 \nu_\infty^2}{GM(1+\cos\theta) + \chi\nu_\infty^2 \sin\theta}, \tag{A.12}$$

$$\rho = \frac{\rho_\infty \chi^2}{r\sin\theta(2\chi - r\sin\theta)}. \tag{A.13}$$

The first three equations follow (through further calculations) from the orbit solution provided above. The equation for the density is less straightforward and involves the steady state gas continuity under conditions of axial symmetry.

Equation A.5 can be rewritten in the form

$$r = \frac{r_0}{1 + e\cos(\theta - \theta_0)}, \tag{A.14}$$

where e is the eccentricity of the orbit, r_0 is the semi-latus rectum. For an ellipse, this the distance L measured from a focus such that

$$\frac{1}{L} = \frac{1}{2}\left(\frac{1}{r_+} + \frac{1}{r_-}\right), \tag{A.15}$$

where $r_+ = a(1+e)$ and $r_- = a(1-e)$ are the apoapsis and periapsis respectively, and e is the ellipse's eccentricity. θ_0 is the periastron angle, which is the angle from the body's ascending node to

its periapsis. These quantities may be expressed as

$$\theta_0 = tan^{-1}\left(\frac{\chi\nu_\infty^2}{GM}\right), \tag{A.16}$$

$$e = \sqrt{1 + \frac{\chi^2\nu_\infty^4}{G^2M^2}}, \tag{A.17}$$

$$r_0 = \frac{\chi^2\nu_\infty^2}{GM}. \tag{A.18}$$

Note that these equations do not follow material down to the accretor. Accretion is assumed to occur through an infinitely thin, infinite dense column on the $\theta = 0$ axis. This is not physically consistent with the ballistic assumption, since it would not be possible to radiate away the thermal energy released as the material loses its θ velocity. Even with a finite size for the accretion column, a significant trapping of thermal energy would still be expected. For now we shall neglect this effect.

Bondi and Hoyle [144] extended this analysis to include the accretion column (the wake following the point mass on the $\theta = 0$ axis). We will now follow their reasoning, and show that this suggests that the accretion rate could be as little as half the value suggested in equation A.9.

From the orbit equations, we know that the material encounters the $\theta = 0$ axis at

$$r = \frac{\chi^2\nu_\infty^2}{2GM}. \tag{A.19}$$

This means that the mass flux arriving in the distance r to $r + \mathrm{d}r$ is given by

$$2\pi\chi\,\mathrm{d}\chi \cdot \rho_\infty\nu_\infty = \frac{2\pi GM\rho_\infty}{\nu_\infty}\,\mathrm{d}r = \Lambda\,\mathrm{d}r, \tag{A.20}$$

which defines Λ. Note that it is independent of r. The transverse momemtum flux in the same interval is given by

$$\Lambda \cdot \nu_\theta(\theta = 0) \cdot \frac{1}{2\pi s}, \tag{A.21}$$

which is the mass flux, multiplied by the transverse velocity, divided over the approximate area of the wake. Applying the orbit equations once more, and noting that a momentum flux is the same as a pressure, we find

$$P_s \approx \frac{\Lambda}{2\pi s}\sqrt{\frac{2GM}{r}}, \tag{A.22}$$

as an estimate of the pressure in the wake. The longitudinal pressure force is therefore

$$\mathrm{d}(\pi s^2 P_s) = \Lambda\sqrt{\frac{GM}{2}}\,\mathrm{d}\left(\frac{s}{\sqrt{r}}\right). \tag{A.23}$$

Material will take a time of about r/ν_∞ to fall onto the accretor from the point it encounters the axis. This means that we can use the accretion rate to estimate the mass per unit length of the wake, m, as

$$m \approx \Lambda\frac{GM}{\nu_\infty^3}, \tag{A.24}$$

which makes the gravitational force per unit length

$$F_{\mathrm{grav}} = \frac{GMm\,\mathrm{d}r}{r^2} \approx \Lambda\frac{G^2M^2}{\nu_\infty^3}\cdot\frac{\mathrm{d}r}{r^2}. \tag{A.25}$$

For accreting material, we must have $r \sim GM\nu_i nfty^{-2}$. If we also assume that the wake is thin ($s \ll r$) and roughly conical ($\mathrm{d}s/s \approx \mathrm{d}r/r$, then taking the ratio of the pressure and gravitational forces, we find that pressure force is much less than the gravitational force. We can therefore neglect the gas pressure in the wake.

The mass per unit length of the wake, m, was introduced above. If we assume the mean velocity in the wake is ν, we can write two conservation laws, for mass and momentum:

$$\frac{\mathrm{d}}{\mathrm{d}r}(m\nu) = \Lambda, \tag{A.26}$$

$$\frac{\mathrm{d}}{\mathrm{d}r}(m\nu^2) = \Lambda\nu_\infty - \frac{GMm}{r^2}. \tag{A.27}$$

Recall that $\Lambda\nu_\infty$ is the momentum supply into the wake, since $r = \nu_\infty$ on axis for all streamlines. We can reduce these equations by introducing dimensionless variables for m, r and v,

$$\nu = \nu_\infty v, \tag{A.28}$$

$$r = \frac{GM}{\nu_\infty^2}\xi, \tag{A.29}$$

$$m = \frac{\Lambda GM}{\nu_\infty^3}\mu, \tag{A.30}$$

where $\xi = 2$ corresponds to material arriving from the streamline characterised by $\chi_{\rm HL}$. Substituting these definitions into equations A.26 and A.27, we obtain

$$\frac{\mathrm{d}}{\mathrm{d}\xi}(\mu v) = 1, \tag{A.31}$$

$$\frac{\mathrm{d}}{\mathrm{d}\xi}(\mu n^2) = 1 - \mu\xi^{-2}. \tag{A.32}$$

We shall now analyse the behaviour of these equations. We can integrate equation A.31 to yield

$$\mu v = \xi - \alpha, \tag{A.33}$$

for some constant α. Since μ is a scaled mass (and hence always positive), we see that the scaled velocity (ν) changes sign when $\xi = \alpha$. That is, α is the stagnation point. Material for $\xi < \alpha$ will accrete, so knowing α will tell us the accretion rate (since the accretion rate will be Lambda r_0 where r_0 is the value of r corresponding to α). By writing $\mu \cdot v^2 = \mu v \cdot \nu$, we can use equation A.33 to rewrite equation A.32 as

$$v\frac{\mathrm{d}v}{\mathrm{d}\xi} = \frac{v(1-v)}{\xi - \alpha} - \frac{1}{\xi^2}. \tag{A.34}$$

This has not obviously improved matters, but we can now study the general behaviour of the function, without trying to solve it. First we need some boundary conditions. These are as follows: $v \to 1$ as $\xi \to \infty$, which means that $\nu \to \nu_\infty$ at large radii; $v = 0$ at $\xi = \alpha$ is the stagnation point; and $\mathrm{d}v/\,\mathrm{d}\xi > 0$ everywhere. Hence, the velocity must be a monotonic function. This is physically reasonable, if we are to avoid unusual flow patterns. The first two conditions can be satisfied for any value of alpha. Fortunately, the third implies as restriction. We now manipulate the equations algebraically to achieve the desired result.

Firstly, substitute $\psi = \alpha^{-1}\xi$. Equation A.34 then reads

$$v\frac{\mathrm{d}v}{\mathrm{d}\xi} = \frac{v(v-1)}{\psi - 1} - \frac{1}{\alpha\psi^2}. \tag{A.35}$$

Now, suppose the derivative is zero. This leads to the condition

$$v^2 - v + \frac{1}{\alpha\psi^2}(x-1) = 0, \tag{A.36}$$

or, with the application of the quadratic roots formula,

$$v = \frac{1}{2} \pm \sqrt{\frac{1}{4} - \frac{1}{\alpha\psi^2}(x-1)}. \tag{A.37}$$

Since v ultimately represents a physical quantity (the velocity), it's obviously desirable that it remain real. We therefore need to look at when the discriminant can become zero. This is another quadratic equation, leading to

$$\psi = \frac{2}{\alpha}(1 \pm \sqrt{1-\alpha}), \tag{A.38}$$

hence, $\alpha = 1$ must be a point of significance. Its value must be determined by numerical analysis or computations and depends on the nature of the fluid in question. Bondi and Hoyle asserted that if $\alpha > 2$ ($\alpha = 2$ is the solution of Hoyle and Lyttleton), then the wake would become unstable to perturbations which preserve axial symmetry. Subsequent numerical simulations and analytic work have shown that Bondi-Hoyle-Lyttleton flow is far from stable.

Bondi [145] studied herically symmetric accretion onto a point mass. The analysis [146] shows that a Bondi radius may be defined as

$$r_B = \frac{GM}{c_s^2(r_B)}. \tag{A.39}$$

Flow outside this radius is subsonic, and the density is almost uniform. Within it, the gas becomes supersonic and moves towards a freefall solution. The similarities between equations A.8 and A.39 led Bondi to propose an interpolation formula:

$$\dot{M} = \frac{2\pi G^2 M^2 \rho_\infty}{(c_\infty^2 + \nu_\infty^2)^{3/2}} \tag{A.40}$$

This is often known as the *Bondi-Hoyle accretion rate*. Based on numerical calculations, sometimes an extra factor appears in this equation. Nomenclature in this field can be a little confused. When papers refer to 'Bondi-Hoyle accretion rates', they may mean equation A.9 or A.40. However, it is useful to bear in mind the distinctions made here. When there is gas pressure, it is useful to talk about 'Bondi-Hoyle accretion' and use M_{BH} and χ_{BH}, in the sense defined by equation A.40.'Bondi-Hoyle-Lyttleton' accretion refers to the problem in more general terms.

References

[1] A. R. Liddle and D. H. Lyth, *Cosmological inflation and large-scale structure*. Cambridge University Press, 2000.

[2] A. Liddle, *An Introduction to Modern Cosmology*. Wiley, 2015.

[3] C. L. Bennett, D. Larson, J. L. Weiland, N. Jarosik, G. Hinshaw, N. Odegard et al., *Nine-year wilkinson microwave anisotropy probe (wmap) observations: Final maps and results*, *The Astrophysical Journal Supplement Series* **208** (2013) 20.

[4] B. Ryden, *Introduction to Cosmology*. Addison-Wesley, 2003.

[5] F. Zwicky, *On the Masses of Nebulae and of Clusters of Nebulae*, *apj* **86** (1937) 217.

[6] A. Del Popolo and M. Le Delliou, *Small scale problems of the ΛCDM model: a short review*, *Galaxies* **5** (2017) 17 [1606.07790].

[7] E. of Encylopaedia Britannica, "Gravitational lens." https://www.britannica.com/science/gravitational-lens, June, 2017.

[8] M. E. Peskin, *Supersymmetric dark matter in the harsh light of the Large Hadron Collider*, *Proc. Nat. Acad. Sci.* **112** (2014) 12256.

[9] D. Hooper and S. Profumo, *Dark Matter and Collider Phenomenology of Universal Extra Dimensions*, *Phys. Rept.* **453** (2007) 29 [hep-ph/0701197].

[10] G. Arcadi, M. Dutra, P. Ghosh, M. Lindner, Y. Mambrini, M. Pierre et al., *The waning of the WIMP? A review of models, searches, and constraints*, *Eur. Phys. J. C* **78** (2018) 203 [1703.07364].

[11] P. Konar, K. Kong, K. T. Matchev and M. Perelstein, *Shedding Light on the Dark Sector with Direct WIMP Production*, *New J. Phys.* **11** (2009) 105004 [0902.2000].

[12] A. Dar, *Dark matter and big bang nucleosynthesis*, *Astrophys. J.* **449** (1995) 550 [astro-ph/9504082].

[13] L. M. Griffiths, A. Melchiorri and J. Silk, *CMB constraints on a baryonic dark matter dominated universe*, *Astrophys. J. Lett.* **553** (2001) L5 [astro-ph/0101413].

[14] A. Hewish, S. Bell, J. Pilkington, P. Scott and R. Collins, *Observation of a rapidly pulsating radio source*, *Nature* **217** (1968) 709.

[15] S. W. Hawking, *Black hole explosions?*, *nat* **248** (1974) 30.

[16] S. Hawking, *Gravitationally collapsed objects of very low mass*, *Mon. Not. Roy. Astron. Soc.* **152** (1971) 75.

[17] Y. B. Zel'dovich and I. D. Novikov, *The Hypothesis of Cores Retarded during Expansion and the Hot Cosmological Model*, *sovast* **10** (1967) 602.

[18] I. D. Novikov, A. G. Polnarev, A. A. Starobinskii and I. B. Zeldovich, *Primordial black holes*, *aap* **80** (1979) 104.

[19] B. J. Carr and S. Hawking, *Black holes in the early Universe*, *Mon. Not. Roy. Astron. Soc.* **168** (1974) 399.

[20] F. Azhar and J. Butterfield, *Scientific Realism and Primordial Cosmology*, 1606.04071.

[21] S. Dodelson, *Modern Cosmology*. Academic Press, Amsterdam, 2003.

[22] H. V. Peiris, *Cosmology part two: the perturbed universe*, *UCL Department of Physics and Astronomy* (2018) .

[23] M. Lachieze-Rey, *Cosmology: A first course*. Cambridge University Press, 1995.

[24] F. Kuhnel and M. Sandstad, *On ellipsoidal collapse and primordial black-hole formation*, 2016.

[25] A. M. Green, A. R. Liddle, K. A. Malik and M. Sasaki, *New calculation of the mass fraction of primordial black holes*, *Physical Review D* **70** (2004) .

[26] L. Abbott and S.-Y. Pi, *Inflationary cosmology*. World Scientific Publishing Co.Pte,Ltd., 1986.

[27] B. Carr, F. Kuhnel and M. Sandstad, *Primordial Black Holes as Dark Matter*, *Phys. Rev.* **D94** (2016) 083504 [1607.06077].

[28] B. Carr, K. Kohri, Y. Sendouda and J. Yokoyama, *Constraints on primordial black holes from the galactic gamma-ray background*, *Physical Review D* **94** (2016) .

[29] M. W. Choptuik, *Universality and scaling in gravitational collapse of a massless scalar field*, *Phys. Rev. Lett.* **70** (1993) 9.

[30] J. Yokoyama, *Cosmological constraints on primordial black holes produced in the near-critical gravitational collapse*, *Physical Review D* **58** (1998) .

[31] J. C. Niemeyer and K. Jedamzik, *Near-critical gravitational collapse and the initial mass function of primordial black holes*, *Physical Review Letters* **80** (1998) 5481–5484.

[32] T. Kawaguchi, M. Kawasaki, T. Takayama, M. Yamaguchi and J. Yokoyama, *Formation of intermediate-mass black holes as primordial black holes in the inflationary cosmology with running spectral index*, *Mon. Not. Roy. Astron. Soc.* **388** (2008) 1426 [0711.3886].

[33] S. Young, C. T. Byrnes and M. Sasaki, *Calculating the mass fraction of primordial black holes*, *JCAP* **1407** (2014) 045 [1405.7023].

[34] F. Kühnel, C. Rampf and M. Sandstad, *Effects of critical collapse on primordial black-hole mass spectra*, *The European Physical Journal C* **76** (2016) .

[35] I. Musco and J. C. Miller, *Primordial black hole formation in the early universe: critical behaviour and self-similarity*, *Classical and Quantum Gravity* **30** (2013) 145009.

[36] D. H. Lyth and A. R. Liddle, *The primordial density perturbation: Cosmology, inflation and the origin of structure*. Cambridge, UK: Cambridge Univ. Pr. (2009) 497 p, 2009.

[37] M. Sakellariadou, *Production of Topological Defects at the End of Inflation*, vol. 738. Springer, 10, 2007, $10.1007/978-3-540-74353-8_10$.

[38] S. Clesse and J. García-Bellido, *Massive Primordial Black Holes from Hybrid Inflation as Dark Matter and the seeds of Galaxies*, *Phys. Rev.* **D92** (2015) 023524 [1501.07565].

[39] M. Drees and E. Erfani, *Running-mass inflation model and primordial black holes*, *Journal of Cosmology and Astroparticle Physics* **2011** (2011) 005–005.

[40] B. J. Carr, K. Kohri, Y. Sendouda and J. Yokoyama, *New cosmological constraints on primordial black holes*, *Phys. Rev.* **D81** (2010) 104019 [0912.5297].

[41] R. K. Sheth, H. J. Mo and G. Tormen, *Ellipsoidal collapse and an improved model for the number and spatial distribution of dark matter haloes*, *mnras* **323** (2001) 1 [astro-ph/9907024].

[42] S. Young and C. T. Byrnes, *Primordial black holes in non-gaussian regimes*, *Journal of Cosmology and Astroparticle Physics* **2013** (2013) 052–052.

[43] V. Atal and C. Germani, *The role of non-gaussianities in Primordial Black Hole formation*, *Phys. Dark Univ.* **24** (2019) 100275 [1811.07857].

[44] K. Jedamzik, *The cloud-in-cloud problem in the press-schechter formalism of hierarchical structure formation*, *The Astrophysical Journal* **448** (1995) 1.

[45] A. M. Green, *Microlensing and dynamical constraints on primordial black hole dark matter with an extended mass function*, *Phys. Rev. D* **94** (2016) 063530.

[46] F. Kühnel and K. Freese, *Constraints on Primordial Black Holes with Extended Mass Functions*, *Phys. Rev. D* **95** (2017) 083508 [1701.07223].

[47] P. Sreekumar, D. L. Bertsch, B. L. Dingus, J. A. Esposito, C. E. Fichtel, R. C. Hartman et al., *EGRET observations of the extragalactic gamma-ray emission*, *The Astrophysical Journal* **494** (1998) 523.

[48] A. W. Strong, I. V. Moskalenko and O. Reimer, *A new determination of the extragalactic diffuse gamma-ray background from egret data*, *The Astrophysical Journal* **613** (2004) 956–961.

[49] P. Murdin, *Encyclopedia of astronomy and astrophysics*. NASA, 2001.

[50] S. Mao, *Astrophysical applications of gravitational microlensing*, *Research in Astronomy and Astrophysics* **12** (2012) 947–972.

[51] B. Paczynski, *Gravitational Microlensing at Large Optical Depth*, *APJ* **301** (1986) 503.

[52] C. Alcock, R. A. Allsman, D. R. Alves, T. S. Axelrod, A. C. Becker, D. P. Bennett et al., *The macho project: Microlensing results from 5.7 years of large magellanic cloud observations*, *The Astrophysical Journal* **542** (2000) 281–307.

[53] É. Aubourg, *Eros microlensing results: Not enough machos in the galactic halo*, in *Sources and Detection of Dark Matter and Dark Energy in the Universe*, D. B. Cline, ed., (Berlin, Heidelberg), pp. 168–176, Springer Berlin Heidelberg, 2001.

[54] K. Jedamzik, *Primordial black hole formation during the qcd epoch*, *Phys. Rev. D* **55** (1997) R5871.

[55] C. Schmid, D. J. Schwarz and P. Widerin, *Peaks above the harrison-zel'dovich spectrum due to the quark-gluon to hadron transition*, *Phys. Rev. Lett.* **78** (1997) 791.

[56] C. Hamadache, L. Le Guillou, P. Tisserand, C. Afonso, J. N. Albert, J. Andersen et al., *Galactic Bulge microlensing optical depth from EROS-2*, *aap* **454** (2006) 185 [astro-ph/0601510].

[57] EROS-2 collaboration, *Limits on the Macho Content of the Galactic Halo from the EROS-2 Survey of the Magellanic Clouds*, *Astron. Astrophys.* **469** (2007) 387 [astro-ph/0607207].

[58] C. Alcock, R. A. Allsman, D. R. Alves, T. S. Axelrod, A. C. Becker, D. P. Bennett et al., *MACHO Project Limits on Black Hole Dark Matter in the 1-30 solar mass Range*, *The Astrophysical Journal* **550** (2001) L169.

[59] S. Calchi Novati, S. Paulin-Henriksson, J. An, P. Baillon, V. Belokurov, B. J. Carr et al., *Point-agape pixel lensing survey of m31*, *Astronomy & Astrophysics* **443** (2005) 911–928.

[60] L. Wyrzykowski et al., *The OGLE View of Microlensing towards the Magellanic Clouds. I. A Trickle of Events in the OGLE-II LMC data*, *Mon. Not. Roy. Astron. Soc.* **397** (2009) 1228 [0905.2044].

[61] L. Wyrzykowski et al., *The OGLE View of Microlensing towards the Magellanic Clouds. IV. OGLE-III*

SMC Data and Final Conclusions on MACHOs, *Mon. Not. Roy. Astron. Soc.* **416** (2011) 2949 [1106.2925].

[62] E. Schaan, S. Ferraro and D. N. Spergel, *Weak lensing of intensity mapping: The cosmic infrared background*, *Phys. Rev. D* **97** (2018) 123539.

[63] S. Calchi Novati, S. Mirzoyan, P. Jetzer and G. Scarpetta, *Microlensing towards the smc: a new analysis of ogle and eros results*, *Monthly Notices of the Royal Astronomical Society* **435** (2013) 1582–1597.

[64] K. Griest, A. M. Cieplak and M. J. Lehner, *Experimental Limits on Primordial Black Hole Dark Matter from the first 2 years of Kepler Data*, *Astrophys. J.* **786** (2014) 158 [1307.5798].

[65] R. J. Nemiroff, G. F. Marani, J. P. Norris and J. T. Bonnell, *Limits on the cosmological abundance of supermassive compact objects from a millilensing search in gamma-ray burst data*, *Phys. Rev. Lett.* **86** (2001) 580 [astro-ph/0101488].

[66] B. J. Carr and M. Sakellariadou, *Dynamical Constraints on Dark Matter in Compact Objects*, *APJ* **516** (1999) 195.

[67] B. Zhilyaev, *Gamma-Ray Bursts as Manifestation of Collisions of Primordial Black Holes with Stars*, *Bull. Crim. Astrophys. Observ.* **103** (2007) 58 [0706.0930].

[68] I. B. Khriplovich, A. A. Pomeransky, N. Produit and G. Y. Ruban, *Passage of small black hole through the earth. is it detectable?*, 2008.

[69] A. Adams and J. Bloom, *Direct detection of dark matter with space-based laser interferometers*, astro-ph/0405266.

[70] N. Seto and A. Cooray, *Search for small-mass black-hole dark matter with space-based gravitational wave detectors*, *Physical Review D* **70** (2004) .

[71] M. Roncadelli, A. Treves and R. Turolla, *Primordial black holes are again on the limelight*, 2009.

[72] M. A. Abramowicz, J. K. Becker, P. L. Biermann, A. Garzilli, F. Johansson and L. Qian, *No observational constraints from hypothetical collisions of hypothetical dark halo primordial black holes with galactic objects*, *The Astrophysical Journal* **705** (2009) 659–669.

[73] F. Capela, M. Pshirkov and P. Tinyakov, *Constraints on primordial black holes as dark matter candidates from capture by neutron stars*, *Physical Review D* **87** (2013) .

[74] F. Capela, M. Pshirkov and P. Tinyakov, *Constraints on primordial black holes as dark matter*

candidates from star formation, *Physical Review D* **87** (2013) .

[75] P. Pani and A. Loeb, *Tidal capture of a primordial black hole by a neutron star: implications for constraints on dark matter*, *Journal of Cosmology and Astroparticle Physics* **2014** (2014) 026–026.

[76] F. Capela, M. Pshirkov and P. Tinyakov, *A comment on "exclusion of the remaining mass window for primordial black holes ...", arxiv:1401.3025*, 2014.

[77] G. Defillon, E. Granet, P. Tinyakov and M. H. Tytgat, *Tidal capture of primordial black holes by neutron stars*, *Physical Review D* **90** (2014) .

[78] R. Ibata, C. Nipoti, A. Sollima, M. Bellazzini, S. C. Chapman and E. Dalessandro, *Do globular clusters possess dark matter haloes? a case study in ngc 2419*, *Monthly Notices of the Royal Astronomical Society* **428** (2012) 3648–3659.

[79] J. D. Bradford, M. Geha, R. R. Muñoz, F. A. Santana, J. D. Simon, P. Côté et al., *Structure and dynamics of the globular cluster palomar 13*, *The Astrophysical Journal* **743** (2011) 167.

[80] J. N. Bahcall, P. Hut and S. Tremaine, *Maximum mass of objects that constitute unseen disk material*, *APJ* **290** (1985) 15.

[81] M. D. Weinberg, S. L. Shapiro and I. Wasserman, *The Dynamical Fate of Wide Binaries in the Solar Neighborhood*, *APJ* **312** (1987) 367.

[82] J. Yoo, J. Chaname and A. Gould, *The end of the macho era: Limits on halo dark matter from stellar halo wide binaries*, *The Astrophysical Journal* **601** (2004) 311–318.

[83] D. P. Quinn, M. I. Wilkinson, M. J. Irwin, J. Marshall, A. Koch and V. Belokurov, *On the reported death of the macho era*, *Monthly Notices of the Royal Astronomical Society: Letters* **396** (2009) L11–L15.

[84] B. Moore, *An upper limit to the mass of black holes in the halo of the galaxy*, *The Astrophysical Journal* **413** (1993) L93.

[85] T. D. Brandt, *Constraints on macho dark matter from compact stellar systems in ultra-faint dwarf galaxies*, *The Astrophysical Journal* **824** (2016) L31.

[86] C. G. Lacey and J. P. Ostriker, *Massive black holes in galactic halos ?*, *APJ* **299** (1985) 633.

[87] P. Hut and M. J. Rees, *Constraints on massive black holes as dark matter candidates.*, *mnras* **259** (1992) 27P.

[88] G. Xu and J. P. Ostriker, *Dynamics of Massive Black Holes as a Possible Candidate of Galactic Dark Matter*, *apj* **437** (1994) 184.

[89] B. J. Carr and C. G. Lacey, *Dark Clusters in Galactic Halos?*, *apj* **316** (1987) 23.

[90] M. S. Delos, A. L. Erickcek, A. P. Bailey and M. A. Alvarez, *Are ultracompact minihalos really ultracompact?*, *Physical Review D* **97** (2018) .

[91] T. Bringmann, P. Scott and Y. Akrami, *Improved constraints on the primordial power spectrum at small scales from ultracompact minihalos*, *Physical Review D* **85** (2012) .

[92] V. Dokuchaev, Y. Eroshenko and S. Rubin, *Quasars formation around clusters of primordial black holes*, *Grav. Cosmol.* **11** (2005) 99 [astro-ph/0412418].

[93] P. Meszaros, *Primeval black holes and galaxy formation.*, *aap* **38** (1975) 5.

[94] B. J. Carr, *The statistical clustering of primordial black holes.*, *aap* **56** (1977) 377.

[95] N. Afshordi, P. McDonald and D. N. Spergel, *Primordial black holes as dark matter: The power spectrum and evaporation of early structures*, *The Astrophysical Journal* **594** (2003) L71–L74.

[96] SDSS collaboration, *The Linear theory power spectrum from the Lyman-alpha forest in the Sloan Digital Sky Survey*, *Astrophys. J.* **635** (2005) 761 [astro-ph/0407377].

[97] N. Düchting, *Supermassive black holes from primordial black hole seeds*, *Physical Review D* **70** (2004) .

[98] G. V. Bicknell and R. N. Henriksen, *Formation of primordial black holes.*, *apj* **232** (1979) 670.

[99] R. Beckmann, J. Devriendt and A. Slyz, *Zooming in on supermassive black holes: how resolving their gas cloud host renders their accretion episodic*, *Monthly Notices of the Royal Astronomical Society* **483** (2019) 3488.

[100] M. Ricotti, J. P. Ostriker and K. J. Mack, *Effect of Primordial Black Holes on the Cosmic Microwave Background and Cosmological Parameter Estimates*, *Astrophys. J.* **680** (2008) 829 [0709.0524].

[101] EROS-2 collaboration, *Limits on the Macho Content of the Galactic Halo from the EROS-2 Survey of the Magellanic Clouds*, *Astron. Astrophys.* **469** (2007) 387 [astro-ph/0607207].

[102] J. Yoo, J. Chaname and A. Gould, *The end of the MACHO era: limits on halo dark matter from stellar halo wide binaries*, *Astrophys. J.* **601** (2004) 311 [astro-ph/0307437].

[103] D. Crnojević, D. J. Sand, D. Zaritsky, K. Spekkens, B. Willman and J. R. Hargis, *Deep imaging of eridanus ii and its lone star cluster*, *The Astrophysical Journal* **824** (2016) L14.

[104] LIGO Scientific Collaboration and Virgo Collaboration collaboration, *Observation of gravitational waves from a binary black hole merger*, *Phys. Rev. Lett.* **116** (2016) 061102.

[105] S. Bird, I. Cholis, J. B. Muñoz, Y. Ali-Haïmoud, M. Kamionkowski, E. D. Kovetz et al., *Did LIGO detect dark matter?*, *Phys. Rev. Lett.* **116** (2016) 201301 [1603.00464].

[106] S. Blinnikov, A. Dolgov, N. Porayko and K. Postnov, *Solving puzzles of GW150914 by primordial black holes*, *JCAP* **11** (2016) 036 [1611.00541].

[107] S. Clesse and J. García-Bellido, *The clustering of massive Primordial Black Holes as Dark Matter: measuring their mass distribution with Advanced LIGO*, *Phys. Dark Univ.* **15** (2017) 142 [1603.05234].

[108] M. Sasaki, T. Suyama, T. Tanaka and S. Yokoyama, *Primordial Black Hole Scenario for the Gravitational-Wave Event GW150914*, *Phys. Rev. Lett.* **117** (2016) 061101 [1603.08338].

[109] M. Raidal, V. Vaskonen and H. Veermäe, *Gravitational Waves from Primordial Black Hole Mergers*, *JCAP* **09** (2017) 037 [1707.01480].

[110] M. Raidal, C. Spethmann, V. Vaskonen and H. Veermäe, *Formation and Evolution of Primordial Black Hole Binaries in the Early Universe*, *JCAP* **02** (2019) 018 [1812.01930].

[111] J. Silk, *Feedback by massive black holes in gas-rich dwarf galaxies*, *The Astrophysical Journal* **839** (2017) L13.

[112] E. C. Fortes, O. D. Miranda, F. W. Stecker and C. A. Wuensche, *What Could be the Observational Signature of Dark Matter in Globular Clusters?*, *JCAP* **08** (2020) 010 [1912.12262].

[113] A. Barnacka, J.-F. Glicenstein and R. Moderski, *New constraints on primordial black holes abundance from femtolensing of gamma-ray bursts*, *Phys. Rev. D* **86** (2012) 043001.

[114] K. Griest, A. M. Cieplak and M. J. Lehner, *Experimental Limits on Primordial Black Hole Dark Matter from the First 2 yr of Kepler Data*, *Astrophys. J.* **786** (2014) 158 [1307.5798].

[115] P. W. Graham, R. Janish, V. Narayan, S. Rajendran and P. Riggins, *White Dwarfs as Dark Matter Detectors*, *Phys. Rev. D* **98** (2018) 115027 [1805.07381].

[116] B. Carr and F. Kuhnel, *Primordial Black Holes as Dark Matter: Recent Developments*, 2006.02838.

[117] R.-g. Cai, S. Pi and M. Sasaki, *Gravitational Waves Induced by non-Gaussian Scalar Perturbations*, *Phys. Rev. Lett.* **122** (2019) 201101 [1810.11000].

[118] N. Bartolo, V. De Luca, G. Franciolini, M. Peloso, D. Racco and A. Riotto, *Testing primordial black holes as dark matter with lisa*, *Phys. Rev. D* **99** (2019) 103521.

[119] B. Carr and J. Silk, *Primordial Black Holes as Generators of Cosmic Structures*, *Mon. Not. Roy. Astron. Soc.* **478** (2018) 3756 [1801.00672].

[120] J. Kormendy and K. Gebhardt, *Supermassive black holes in nuclei of galaxies*, *AIP Conf. Proc.* **586** (2001) 363 [astro-ph/0105230].

[121] J. Magorrian, S. Tremaine, D. Richstone, R. Bender, G. Bower, A. Dressler et al., *The Demography of Massive Dark Objects in Galaxy Centers*, *aj* **115** (1998) 2285 [astro-ph/9708072].

[122] E. of Encylopaedia Britannica, "Quasar." https://www.britannica.com/science/quasar, June, 2017.

[123] X.-B. Wu, F. Wang, X. Fan, W. Yi, W. Zuo, F. Bian et al., *An ultraluminous quasar with a twelve-billion-solar-mass black hole at redshift 6.30*, *nat* **518** (2015) 512 [1502.07418].

[124] E. Banados et al., *An 800-million-solar-mass black hole in a significantly neutral Universe at redshift 7.5*, *Nature* **553** (2018) 473 [1712.01860].

[125] M. J. Rees, *Black Hole Models for Active Galactic Nuclei*, *araa* **22** (1984) 471.

[126] J. E. Gunn and I. Gott, J. Richard, *On the Infall of Matter Into Clusters of Galaxies and Some Effects on Their Evolution*, *apj* **176** (1972) 1.

[127] J. Chevallard, J. Silk, T. Nishimichi, M. Habouzit, G. A. Mamon and S. Peirani, *Effect of primordial non-Gaussianities on the far-UV luminosity function of high-redshift galaxies: implications for cosmic reionization*, *Mon. Not. Roy. Astron. Soc.* **446** (2015) 3235 [1410.7768].

[128] R. Bean and J. Magueijo, *Could supermassive black holes be quintessential primordial black holes?*, *Phys. Rev. D* **66** (2002) 063505 [astro-ph/0204486].

[129] B. D. Smith, J. A. Regan, T. P. Downes, M. L. Norman, B. W. O'Shea and J. H. Wise, *The growth of black holes from population iii remnants in the renaissance simulations*, *Monthly Notices of the Royal Astronomical Society* **480** (2018) 3762–3773.

[130] J. Walsh, R. Bosch, K. Gebhardt, A. Yıldırım, D. Richstone, K. Gültekin et al., *A 5 x 10 9 m solar mass black hole in ngc 1277 from adaptive optics spectroscopy*, *The Astrophysical Journal* **817** (2016) 2.

[131] LIGO Scientific Collaboration and Virgo Collaboration collaboration, *Observation of gravitational waves from a binary black hole merger*, *Phys. Rev. Lett.* **116** (2016) 061102.

[132] LIGO Scientific Collaboration and Virgo Collaboration collaboration, *Gw190521: A binary black hole merger with a total mass of 150 solar masses*, *Phys. Rev. Lett.* **125** (2020) 101102.

[133] V. De Luca, V. Desjacques, G. Franciolini, P. Pani and A. Riotto, *The GW190521 Mass Gap Event and the Primordial Black Hole Scenario*, 2009.01728.

[134] Y.-Z. Wang, S.-P. Tang, Y.-F. Liang, M.-Z. Han, X. Li, Z.-P. Jin et al., *GW190521 and the GWTC-1 Events: Implication on the Black Hole Mass Function of Coalescing Binary Black Hole Systems*, 2009.03854.

[135] M. Fishbach, D. E. Holz and B. Farr, *Are LIGO's Black Holes Made From Smaller Black Holes?*, *Astrophys. J. Lett.* **840** (2017) L24 [1703.06869].

[136] M. Tkachev, S. Pilipenko and G. Yepes, *Dark Matter Simulations with Primordial Black Holes in the Early Universe*, 2009.07813.

[137] Y.-F. Wang, Q.-G. Huang, T. G. Li and S. Liao, *Searching for primordial black holes with stochastic gravitational-wave background in the space-based detector frequency band*, *Phys. Rev. D* **101** (2020) 063019 [1910.07397].

[138] "Lisamission.org."

[139] Sep, 2020.

[140] P. Natarajan, F. Pacucci, A. Ferrara, B. Agarwal, A. Ricarte, E. Zackrisson et al., *Unveiling the First Black Holes With JWST:Multi-wavelength Spectral Predictions*, *Astrophys. J.* **838** (2017) 117 [1610.05312].

[141] R. G. Edgar, *A Review of Bondi-Hoyle-Lyttleton accretion*, *New Astron. Rev.* **48** (2004) 843 [astro-ph/0406166].

[142] F. Hoyle and R. A. Lyttleton, *The effect of interstellar matter on climatic variation*, *Proceedings of the Cambridge Philosophical Society* **35** (1939) 405.

[143] G. S. Bisnovatyi-Kogan, Y. M. Kazhdan, A. A. Klypin, A. E. Lutskii and N. I. Shakura, *Accretion onto a rapidly moving gravitating center*, *sovast* **23** (1979) 201.

[144] H. Bondi and F. Hoyle, *On the mechanism of accretion by stars*, *mnras* **104** (1944) 273.

[145] H. Bondi, *On spherically symmetrical accretion*, *mnras* **112** (1952) 195.

[146] J. Frank, A. King and D. J. Raine, *Accretion Power in Astrophysics: Third Edition*. NASA, 2002.